NPS ARCHIVE
1960
RORIE, C.

A TRANSIENT RESPONSE ANALYSIS OF A MULTI-LOOP COMPUTATION SERVOMECHANISM IN THE SUBROC MK 75, ATTACK ANALYZER

CONRAD J. RORIE

DUDLEY KNOX LIBRARY
NAVAL POSTGRADUATE SCHOOL
MONTEREY CA 93943-5101

Library
U. S. Naval Postgraduate School
Monterey, California

A TRANSIENT RESPONSE ANALYSIS OF A MULTI-LOOP COMPUTATION SERVOMECHANISM IN THE SUBROC MK 75, ATTACK ANALYZER

Conrad J. Rorie

A TRANSIENT RESPONSE ANALYSIS OF A MULTI-LOOP COMPUTATION SERVOMECHANISM IN THE SUBROC MK 75, ATTACK ANALYZER

By

Conrad J. Rorie
//
Lieutenant, United States Navy

Submitted in partial fulfillment of
the requirements for the degree of:

Master of Science
in
Electrical Engineering

United States Naval Postgraduate School
Monterey, California

1960

NPS Archive
1960
Rorie, C.

Thesis
R73

Library
U. S. Naval Postgraduate School
Monterey, California

DUDLEY KNOX LIBRARY
NAVAL POSTGRADUATE SCHOOL
MONTEREY CA

A TRANSIENT RESPONSE ANALYSIS OF A MULTI-LOOP COMPUTATION SERVOMECHANISM IN THE SUBROC MK 75, ATTACK ANALYZER

By

Conrad J. Rorie

This work is accepted as fulfilling the thesis requirements for the degree of:

Master of Science
in
Electrical Engineering

from the

United States Naval Postgraduate School

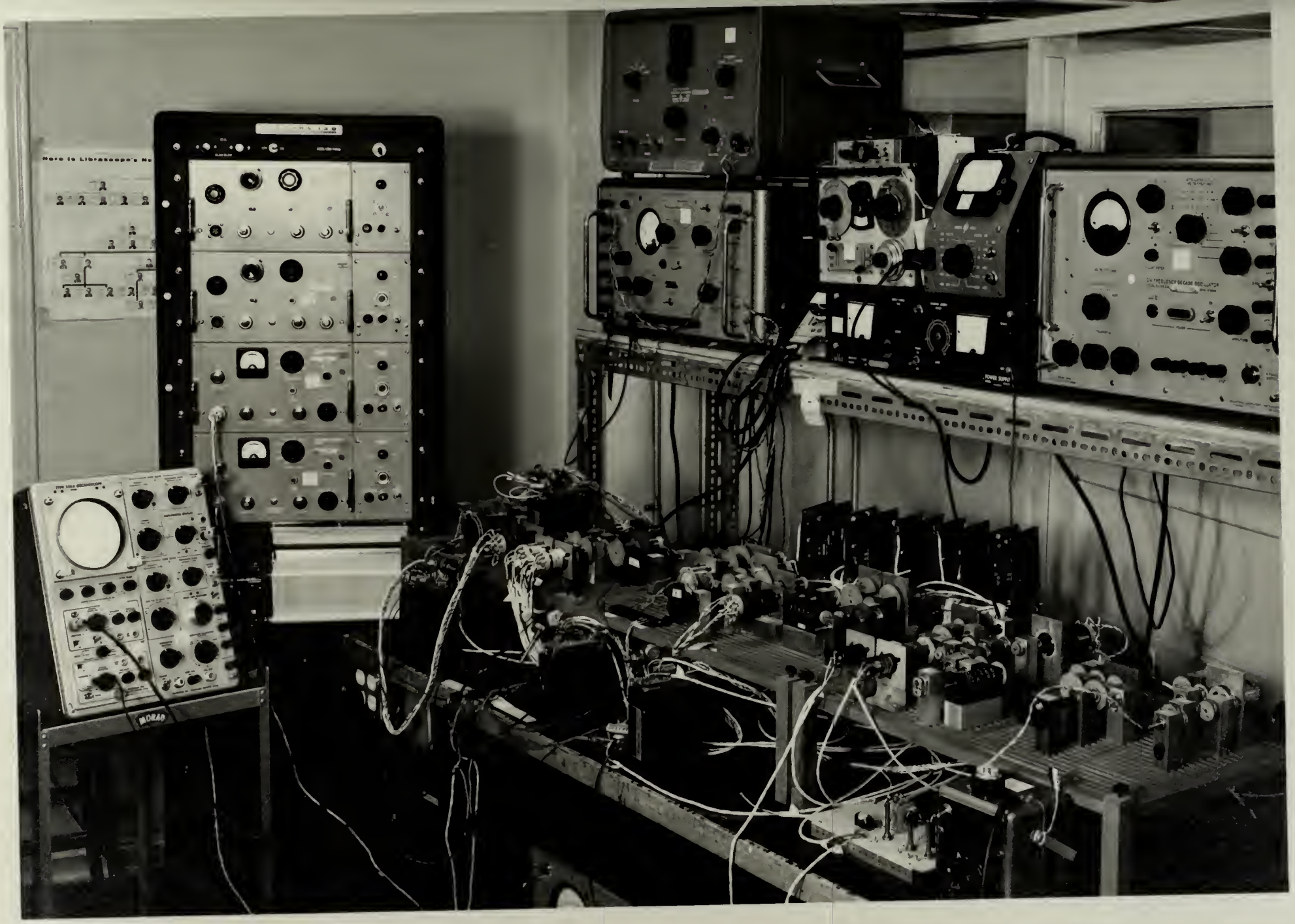

ABSTRACT

The multi-loop Lead Angle servo loop is utilized as a analog computing loop that mechanizes the range-bearing torpedo fire control equation. This thesis applies several new servo analysis techniques, developes system component transfer functions, analyzes individual loops, and examines qualitative stability and response of the overall system. No response or error criteria was specified. Based on the author's experience and advice from submariners a minimum error criteria is derived. This thesis preposes several modifications of the origional system in order to improve performance, points out several difficiencies, and recommends areas of further study.

The writer wishes to express his appreciation for the courtesies and cooperation extended to him by the personnel he had the pleasure of working with at the Librascope Division of General Precision, Incorporated at Glendale, California.

The author also expresses his appreciation for the advice and encouragement received from Lt. Charles Pollak and especially Dr. Marvin Pastel, faculty advisor.

TABLE OF CONTENTS

	Page
Certificate of Approval	i
Abstract	ii
Table of Contents	iii
List of Illustrations	v
Table of Symbols and Abbreviations	vii
Section	
I. Summary	1
II. Introduction	3
2.1 The Gyro Lead Angle Computing Loop	3
2.2 Objectives of Analysis	20
2.3 Period of Time Allowed for Analysis	20
III. Review or Introduction to Some Recent Development in Servo Analysis Techniques	21
3.1 Determinantal Method of Analysis	21
3.2 Determination of Composite Open Loop Transfer Function and Velocity Constant for Multiloop Systems	27
3.3 Root Locus Gain Versus Real Roots	29
IV. Derivation of Transfer Function of Components and Minimum Velocity Constant Requirement	34
4.1 Servo Amplifier	34
4.2 Integral Network	36
4.3 Derivation of Theoretical Minimum Kv Requirement	43
V. Mathematical Analysis of the System and Comparison with Observed Data	46
5.1 Analysis of Individual Loops	46
5.2 Qualitative Stability and Performance Analysis of Overall System	68

5.3 Discussion of Analysis and Observed Data 79

a. Individual Loop 79

b. Overall System 81

VI. Conclusions and Recommendations 90

6.1 Individual Loop 90

6.2 Complete System 90

VII. Recommendations for Further Investigation 92

Bibliography 93

Appendix I Induction Resolver 94

LIST OF ILLUSTRATIONS

Figures		Page
1.	Fire Control Problem	7
2.	Isolation Amplifier	10
3.	Enabling Run Servo Loop	12
4.	Lead Angle, Bb6 Servo Loop	14
5.	Total Run to Burst	15
6.	Gyro Angle Order	19
7.	Standard Block Diagram	22
8.	Example of Use of Standard Block Diagram	25
9.	Computation of Root Locus Gain on the S-Plane	30
10.	Plot of Root Locus Gain Versus Real Roots	31
11.	Input Network to Servo Amplifier	35
12.	Equivalent Circuit of Input Network to Servo Amplifier	34
13.	Integral - Damping Network	37
14.	Equivalent Circuit of Integral - Damping Network	36
15.	Frequency Response of Integral - Damping Network	38
16.	Root Locus of Individual Loop as a Second Order System	41
17.	Magnitude ($\frac{e_o}{e_i}$) Versus Angular Frequency from Frequency Analysis of Individual Loop	42
18.	Closed Loop Equivalent Circuit of Individual Loop	46
19.	Equivalent Circuit of Input and Feedback Vernistats	47
20.	Equivalent Circuit of Amplifier and Integral - Damping Network	48
21.	Reduced Block Diagram of Individual Loop	51
22.	Plot of R_7 Versus Root Locus Gain and Z_R Zero Due to Tachometer Feedback	54
23.	R_7 Versus K_v (Individual Loop)	55
24.	Root Locus Plot for Individual Loop With Unity, Integral - Damping and Tachometer Feedback	58

Figures Page

25. Root Locus Gain Versus Real Roots of Individual Loop with Unity, Integral-Damping, and Tachometer Feedback 59

26. Predicted Response of Individual Loop Using Optimum Values of Input Resistance for Individual Loop with Unity, Integral-Damping, and Tachometer Feedback 61

27. Measured Response of Individual Loop Using Optimum Values of Input Resistance with Unity, Integral-Damping, and Tachometer Feedback 62

28. Root Locus Plot for Individual Loop with Unity and Tachometer Feedback 63

29. Root Locus Gain Versus Real Roots of Individual Loop with Unity and Tachometer Feedback 64

30. Predicted Response, to a Unit Step Input, of the Individual Loop with Unity and Tachometer Feedback 66

31. Measured Response, to a Unit Step Input, of the Individual Loop with Unity and Tachometer Feedback 67

32. Root Locus Plot of Individual Loop with Unity and Integral-Damping Feedback 69

33. Root Locus Gain Versus Real Roots of Individual Loop with Unity and Integral-Damping Feedback 70

34. Predicted Response, to a Step Input, of the Individual Loop with Unity and Integral-Damping Feedback 71

35. Measured Response, to a Step Input, of the Individual Loop with Unity and Integral-Damping Feedback 72

36. Functional Block Diagram 73

37. Standard Block Diagram of Overall System 75

38. Bodie Plot of Overall Closed Loop System 80

39. Measured Response of Overall System to a Step Input 83

40. Measured Response of Overall System to a Ramp Input 84

41. Measured Error of Overall System to a Step Input 85

42. Measured Error of Overall System to a Ramp Input 86

43. Standard Block Diagram with Compensation Necessary to Produce a Type One System 87

TABLE OF SYMBOLS AND ABBREVIATIONS

Symbol	Name	Definition
B	Relative Target Bearing	When used alone, B denotes the relative bearing to the present position of the target and is measured in the Master own ship horizon system.
B-Bg	Missile Azimuth	The difference between Relative Target Bearing and Relative Tube Bearing, measured in the horizontal plane of the own ship horizon system.
Bb6	Torpedo Lead Angle	The angle formed by the intersection of the line from own ship's present position to target's present position with the line from torpedo's pseudo or real position to target's future position. Positive angles are measured clockwise from the line connecting own ship and target, i.e., the present relative bearing line. Prior to event 4, and for all Preset problems, point 4 is the pseudo position. For Wire Guided problems, after event 4, the dead reckoned torpedo position is used.
e(Bb6)	Error in Bb6	
Bg	Relative Tube Bearing	Relative bearing of the torpedo tube measured in an own ship horizon system.
Bms	Torpedo Angle	Angle between the horizontal projection of the missile or torpedo speed vector and the present bearing line from own ship to the missile or torpedo, measured in the horizontal plane of a missile or torpedo horizon system.

Symbol	Name	Definition
Bts	Target Angle	Angle between the target speed vector and the present bearing line from own ship to target, measured in the target horizon system.
Co	Own Ship Course	Course of own ship measured in the Master system.
Cm	Torpedo Course	Course of the torpedo or missile measured in the horizontal plane of a north oriented horizon system at The torpedo or missile.
j(Cm)	Computed Correction to Torpedo Course	
Cm4	Torpedo Course at Event 4	The course of the torpedo measured in the horizontal plane of a north oriented horizon system at point 4.
Cmo4	Relative Torpedo Course at Event 4	The course of the torpedo measured in the horizontal plane of an own ship oriented horizon system at point 4.
Ct	Target Course	Course of the target measured in the target north oriented horizon system.
DBy	Bearing Rate	The time rate of change of true target bearing.
DCo	Own Ship Turning Rate	The rate of change of own ship course with respect to real time.
DCt	Target Turning Rate	The rate of change of target course with respect to time.
DMho	Own Ship Speed	The time rate of change of the distance traversed by own ship, measured in the horizontal plane of the Master own ship horizon system.

Symbol	Name	Definition
DMht	Target Speed	The time rate of change of the distance traversed by the target, measured in the horizontal plane of the target horizon system.
f	Frequency, cycles per second	
Fc	Closed loop transfer function	
Fo	Open loop transfer function	
G	Gyro Angle	Angle between vertical plane thru line of fire and vertical plane thru desired missile centerline measured in horizontal plane. (When used alone only.)
e(G)	Error in Gyro Angle	
sq(G)	Angular Spread	A manual correction to gyro angle to initiate an angular spread of torpedo paths.
G6	Gyro Angle at Event 6	The torpedo gyro angle at event 6.
Hm	Length of Torpedo Path	Actual distance traveled by torpedo from own ship to target.
c(Hm)	Computed Length of Torpedo Path	
ec(Hm)	Error in Computed Length of Torpedo Path	
q(Hm)	Run to Burst Command	Manual correction to torpedo path length.
sj(Hm)	Correction to Torpedo Path Length	A bias added to torpedo path length to compensate for torpedo acceleration to required speed.

Symbol	Name	Definition
sq(Hm)	Enabling Run Offset	Correction used to shift enabling point along the torpedo track.
Hm26	Total Run to Burst	The total theoretical length of the torpedo path from event 2 to event 6. (Obsolete symbol Hmt)
Hm6	Distance from Torpedo to Point 6	The straight line distance from the torpedo's present position to point 6.
Hm7	Remaining Run to Burst	The total distance the torpedo must run from its present position to its bursting position (point 7).
Hvm	Torpedo Run Depth	Vertical distance the torpedo is set to run below the surface of the water.
Hvmg	Depth Difference	Vertical distance between the torpedo tube and the missile or torpedo. (Hvm - Hvg)
H_{27}	Distance from event 2 to event 7	
H67	Linear Spread Along Target Track	The distance along the target track between the future target position (point 6) and the advance point (point7).
j		
Ly2	Latitude of Firing	The latitude of own ship at the time of fire.
Lyo	Latitude of Own Ship	
Lyp	Latitude of Proofing	The latitude at which the torpedo was proofed.
Lyt	Latitude of Target	
k	One Thousand ohms	
K	Gain	

Symbol	Name	Definition
Mho	Own Ship Horizontal Motion	The horizontal distance made good by own ship during a given interval of time.
Pdn	Athwartship Parallax Displacement	The component, in the deck reference plane and perpendicular to own ship centerline, of the total distance from the origin of the Master system to the origin of the weapon system. (The center of the torpedo gyro or the missile platform.) Pdn is measured in the Master own ship deck system.
Pdo	Centerline Parallax Displacement	The component, along own ship centerline, of the total distance from the origin of the Master system to the origin of the weapon system. (The center of the torpedo gyro or the missile platform.) Pdo is measured in the Master own ship deck system.
$r_1, r_2 \ldots$	Roots of equation	
R	Present Slant Range	R, when used alone, is the present distance between own ship and target, measured along a straight line in the Master system.
j(R)	Computed Correction to Range	
Rh	Horizontal Range	The present horizontal range from own ship to the target's present position as seen by radar or as computed from sonar data, measured in the Master system.
c(Rh)	Computed Horizontal Range	
j(Rh)	Horizontal Range Correction	Computed correction to horizontal range.
Rh2	Horizontal Range to Target at Event 2	The range, measured in the Master system, from own ship to target at time of fire (event 2).

Symbol	Name	Definition
Rh3	Horizontal Range to Reach Point	The range, measured in the Master system, from own ship present position to the torpedo reach point, point 3.
t	Time	
α	$F/2J$	
β	$\sqrt{K/J}$	
ϵ	Base of Natural Logarithm	
ε	Error	
θ	Angular displacement, radians	
θ_i	System Input	
θ_o	System Output	
Tf	Time of Flight	
ω	Angular Velocity, radians per second	
J	Time Constant	
μf	Microfarads	
T26	Time of Travel	The total time from time of fire (event2) to time of torpedo burst (event 6).
T_x	Time to Event x in Fig. 1.	
Um	Torpedo or Missile Speed	The speed of the torpedo or missile with respect to the medium through which it is moving. The time rate of change of the distance over which it is moving.
j(Um)	Correction to Torpedo Speed	A computed correction to torpedo speed.

Symbol	Name	Definition
Y_m	Torpedo Turn Radius	The mean radius of curvature of the path taken by the torpedo (essentially circular) in traveling from the reach point (point 3) to the gyro involute point (point 4).
P_2	Target Half-Length	Distance from the stern of the target to the middle of the target (MOT).

I. SUMMARY

An analysis of individual loops was conducted and a representative loop was selected and presented herein. The individual loop as designed will operate satisfactorily; however, using optimum settings of input and feedback resistances determined in section 5.1 the response can be improved 37.5 per cent over the best response obtained by trial and error, using settling time as a criteria. A further improvement was obtained by eliminating the integral-damping network; however, considerable noise was incountered which would not show up in the output but would cause gear wear in the chain near the servo motor. By changing capacitors C-3 and C-4 in figure 14 to .25 microfarads instead of the presently installed 1 microfarad, the same response could be obtained without the undesirable performance at steady state. The overall improvement in response using the resistances determined and the change in the capacitance was 54.2 per cent.

The overall system was considered but because of the non-linear nature of the resolver in the circuit exact response could not be predicted in the time allowed for analysis. Linearizing assumptions were made and a stability analysis was performed. It was found that the system was highly stable with a gain margin of 24 db and a phase margin of 72 degrees. During the analysis it was discovered that the system was type zero which has an infinite steady state error to a ramp input. Within the area of expected performance of the system this error did not appear to be significant; however, if large ramp inputs are incountered or long computing times the error can become significant. The system is easily compensated to become type one by an additional amplifier-motor loop.

If it is desired to use the system as designed it appears that by careful scaling that the error can be reduced significantly without further compensation.

II. INTRODUCTION

2.1 The Gyro Lead Angle Computing Loop

The gyro lead angle computing circuit functions as a part of the Attack Director, Mk 75. It is considered advantageous to familiarize the reader with the overall system prior to discussing the specific circuit analyzed.

The Attack Director, Mk 75 performs as a torpedo data computer and position keeper. Continuous inputs of range and bearing information are supplied from various selected data powers.

As a position keeper the Attack Director generates range and bearing of target position for transmission to sonar via the Analyzer Console, [illegible] from the most recent values of target course, speed, range, and bear[illegible] r generates range and bearing of apparent target position for direct transmission to sonar, from the most recent values of automatically or manually inserted inputs of target course and speed.

As an angle solver the Attack Director computes gyro angle, enabling run, and torpedo running depth for electrically set torpedoes.

Required information for the control of wire guided torpedoes is supplied. Corrections to torpedo course and run to burst, and a continuous [illegible] of the wire is accomplished on the director.

[illegible] bearings of own ship and target ship are orientated to a line representing the bearing line to a target. Torpedo inputs are displayed on counters prior to time of fire for wire guided and preset torpedoes. Torpedo position is displayed after time of fire for the wire guided problems.

The Attack Director, Mk 75 functions in both automatic and display modes.

The specific loop which is the subject of this analysis is a multi-loop, electro-mechanical servo-mechanism. The loop is composed of eight individual loops, which are interdependent in the operation of the Attack Director, Mk 75. Listed below are the element loops of the compensation of lead angle loop and their physical location in the director:

1. Gyro Angle - located in the Angle Solver Section
2. Enabling Run - located in the Angle Solver Section
3. Torpedo Lead Angle - located in the Position Keeper Display Section
4. Relative Target Bearing - located in the Position Keeper Display Section of the Attack Director
5. Relative Tube Bearing - located in the Ballistic Computer Section
6. Weapon Time to Burst - located in the Ballistic Computer Section of the Attack Director
7. Target Speed - located in the Position Keeper Display Section
8. Target Angle - located in the Position Keeper Display Section

The computation of the lead angle loop is a sequential computation loop. This loop has four possible mechanical inputs and five possible electrical inputs. The outputs from this loop are three dial readings. These readings are valid only when the loop has reached a steady state condition.

In order to explain the operation of the computation of lead angle loop several assumptions were made. Initial conditions are such that Gyro Angle $[G]$, Torpedo Lead Angle $[B_{66}]$, Enabling Run $[C(Hm)]$, and

Weapon Time to Burst $[T_{26}]$, are initially at some particular value. Another condition is that electric power to all loops is not applied until such time as the computation begins.

Another assumption made is that all electrical inputs are constants with the exception of the following variables.

1. Ym' Sin Bb6
2. Cos Bts (Dmht -K1 . T26)
3. Ym' Cos Bb6
4. Sin Bts (Dmht . K1 . T26)

With the above in mind let us consider the solution to the problem:

The firing of a preset torpedo requires solving for a predetermined point of impact between torpedo and the target, noted as point 6. The torpedo input requirements are: run to the enabling point, c(Hm); the gyro angle order, G; run depth, Hvm; and a 26 Volt mark signal when $0° < I < 180°$, for automatic horizontal search.

Computations are made to resolve into mutually perpendicular components the final vector (leg) of the torpedo run to the target. This is the straight line connecting event 4 with event 6. The components are ΣY, which is parallel to the line of sight (LOS) and ΣX, which is perpendicular to it, (reference figure 1).

The quantities ΣX and ΣY are predicted by two isolation amplifiers summing the applicable inputs. These two amplifiers are the start of a sequential computation. The amplifier inputs involve the parallax quantities of the tube, Pdo and Pdn, the reach of the torpedo Rh3, the torpedo turn radius Ym', the relative Target Bearing B, corrected for Relative Tube Bearing Bg, the Torpedo Lead Angle Bb6, the Target Angle Bts, target speed times

the total run time of the torpedo (DMht . T26), and a linear spread H67, quantity if present. These quantities are related to ΣX and ΣY by the following equations.

$$X = \sin B\ (Pdo + Rh3 \cos Bg - Ym' \sin Bg)$$
$$- \cos B\ (Pdn + Rh3 \sin Bg - Ym' \cos Bg)$$
$$+ Ym' \cos Bb6 + \sin Bts\ (DMht \cdot K_1 \cdot T26 + H67)$$
$$Y = Rh - \cos B(Pdo + Rh3 \cos Bg - Ym' \cos Bg)$$
$$- \sin B\ (Pdn + Rh3 \sin Bg - Ym' \cos Bg)$$
$$- Ym' \sin Bb6 - \cos Bts\ (DMht \cdot K_1 \cdot T\ 26 + H67)$$

The quantities ΣX and ΣY are inputs to the two stator windings of a resolver. A servo loop positions the mechanical input of the resolver until one of the rotor outputs approaches null. The output of the other rotor is the vector sum of ΣX and ΣY Hm6. The shaft position of the servo loop is an angle equal to the $\tan^{-1} \frac{\Sigma X}{\Sigma Y}$ = Bb6, the torpedo lead angle (reference figure 1).

A perturbation, which includes a compensation for drift and gyro uncaging time, is summed with the null signal e(Bb6) from the resolver in an isolation amplifier. The generation of this perturbation will be explained later. The output of this isolation amplifier is sent to a variable gain amplifier, VGA, which divides this signal by the other output of the lead angle resolver.

The output of this amplifier is the error in Bb6.

$$e(Bb6) = \left\{(\Sigma X \cos Bb6 - \Sigma Y \sin Bb6) + \left[\frac{Dcm}{2} T_{26} (\sin \angle yp - \sin \angle y_2) - Oco\ Td\right] e(Hm)\right\} \div Hm6$$

NOTE :

[ ] =) PARALLEL LINES

• =) NOT USED IN W/G PROBLEM

LEGEND:

ΣY = Rh -

1. Pdo Cos B
2. Pdn Sin B
3. Rh3 Cos (B-Bg)
4. Ym' Sin (B Bg)
5. Ym' Sin Bb6
6. DMht·T26·Cos Bts
- • H67 Cos Bts

ΣX =

- A Pdo Sin B
- B Pdn Cos B
- C Rh3 Sin (B-Bg)
- D Ym' Cos (B Bg)
- E Ym' Cos Bb6
- F DMht T26 Sin Bts
- • G H67 Sin Bts

N

N

ORIGIN OF MASTER SYSTEM

OWN SHIP

S

S

TARGET

Bb6

Σ X

Σ Y

Rh2

H=46

Bts

2P2

C.

PRESET TORPEDO GEOMETRY

FIG 1

This error is computed by the relation $\theta = \frac{s}{r}$ where θ is the error in Bb6, s is an error in the difference in length of a particular component of Σ X and Σ Y and the perturbation mentioned above, and r is the vector sum of Σ X and Σ Y, Hm6.

The vector sum of Σ X and Σ Y is the length of torpedo travel from point 4 to point 6. This signal is sent another isolation amplifier, whose function will be explained later. The shaft position of torpedo lead angle (Bb6) is displayed on the outer dial of the "Target Group" and "Own Ship Group" dial display in the Position Keeper Display Section.

The Bb6 shaft position is added to the target angle (Bts) by a mechanical differential (Bb6 + Bts = I). The output of this differential positions a limit cam, which operates a micro switch. The normally closed position of the microswitch gives a right turn mark signal to the torpedo for automatic horizontal search, NC, $0 < I < 180$. The normally open position provides no mark signal and therefore, aleft turn is in order. This turn signal is available as a preset torpedo function that is activated at the enabling point.

The Bb6 loop also positions a two speed control transmitter synchro system. These CX's send an electrical analog signal proportional to the Torpedo Lead Angle, Bb6, to a two apeed control differential transmitter synchro system that is mechaically referenced with the Relative Target Bearing, B. These CDX's add the two functions and yield Relative Torpedo Course, Cmo4. The CDX's then send this signal to the Own Ship's course module. The Cmo4 signal also references a two apeed control differential transmitter synchro system that is mechanically referenced with Relative Tube Bearing, Bg. The output of the relative tube bearing CDX's reference

a two speed CDX system on the Angular Spread module sq (G). This module is located on the firing panel. The output of these CDX's reference a two speed control transformer system on the Gyro Angle Order module, G. These CT's are the feedback element for the loop. The equation involved here is: $[G = C_{mo4} - B_g + S_q(G)]$.

Each of the terms on the right side of the above equation for G have been added by the use of two speed synchro systems (CDX). This signal references the gyro angle module feedback CT's. These CT's have a shaft position proportional to Gyro Angle, G, and an output, which through a servo amplifier and motor, positions the gyro angle order shaft.

The gyro angle order gear train positions the wiper on a DC potentiometer (pot). This G pot is referenced with π times torpedo right turn radius, πY_{m_r} and π times torpedo left turn radius, πY_{m_l} . The center tap of the pot is grounded. The voltage from the pot is positive for both right and left turns, but it is not of the same magnitude. The voltage output at the wiper position of this pot is then proportional to the wiper position, a function of G, and the reference voltage. The analog signal is then the product of these two inputs; hence the arc distance traveled about the gyro angle, Ym' . G $.\frac{\pi}{180^\circ}$. This signal is sent to an isolation amplifier, figure 2. Other inputs to this amplifier are: The distance to the reach point, Rh3, from the ballistic constants network; the vector sum, $[\Sigma$ X sin Bb6 + Σ Y cos Bb6 = Hm6$]$, from the lead angle resolver previously discussed; and a correction for torpedo run depth Hvm, and own ship depth Hvo, $Hvm_{g_{Rh3}}$, from the ballistic constants network.

The output of this amplifier is proportional to Hm26. This voltage is sent to an impedance matching transformer in the input network of a servo

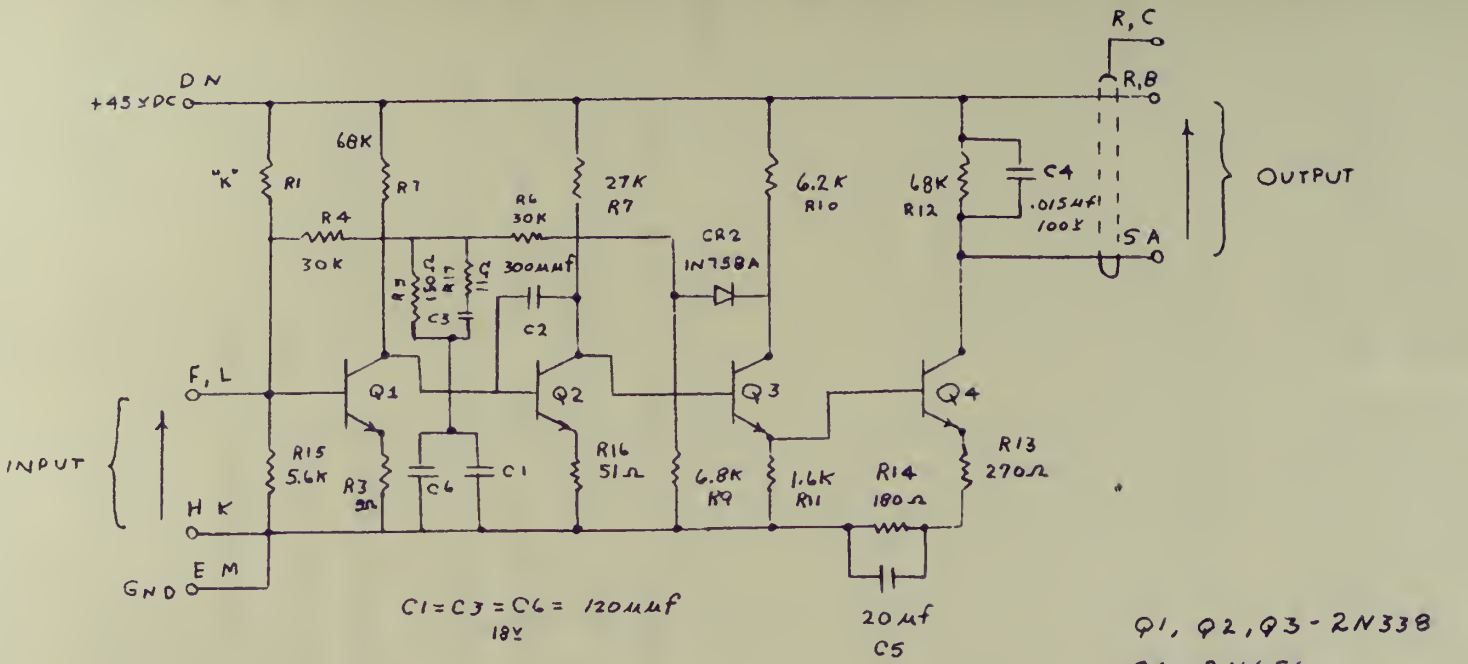

FIGURE 2

ISOLATION AMPLIFIER SCHEMATIC

amplifier. The output of this network is the output of the feedback vernistat Hm26 on the Enabling Run servo module. The amplifier drives the servo motor until the two inputs are equal in magnitude and 180 out of phase. The motor has then driven out a mechanical analog position proportional to Hm26. This shaft position may be added to or subtracted from manually by a hand crank input labeled Enabling Run Offset, sq(Hm). This is accomplished by the use of a mechanical differential. The amount of offset is recorded on a counter for display.

The Enabling Run module visually displays computed Enabling Run, c(Hm), which is the summation of Hm26 and the offset sq(Hm). One vernistat on this loop sends a voltage proportional to the computed Enabling Run c(Hm), to the Run to Burst module as a reference source for a vernistat feedback loop. This particular total run to burst, [Hm26 w/g - NR = c(Hm) w/g + q(Hm)] , is used only in the wire guided solution and will not be discussed here.

A separate cam for each weapon on the computed Enabling Run shaft, c(Hm) figure 3, sends a within limit signal to the gyro angle limit cam. If the gyro limit cams are within limits, then they send a signal to the depth stratum limit cams. The run depth cam, then sends a signal to the within limit circuitry in the weapon monitor unit.

The Enabling Run module position six one speed control transformers that send an analog error signal, ec(Hm), to a servo motor in the torpedo. There is a control transmitter, mechanically linked to a servo motor in each torpedo. This CX feeds a follow-up signal oc(Hm) back to the CT's in the Enabling Run module to complete the servo loop.

The second vernistat in the Enabling Run module is referenced with the

NOTES:

1. * THERE ARE INDIVIDUAL CT'S FOR EACH TUBE.
2. Δ THERE ARE INDIVIDUAL CAMS FOR EACH TYPE OF WEAPON.

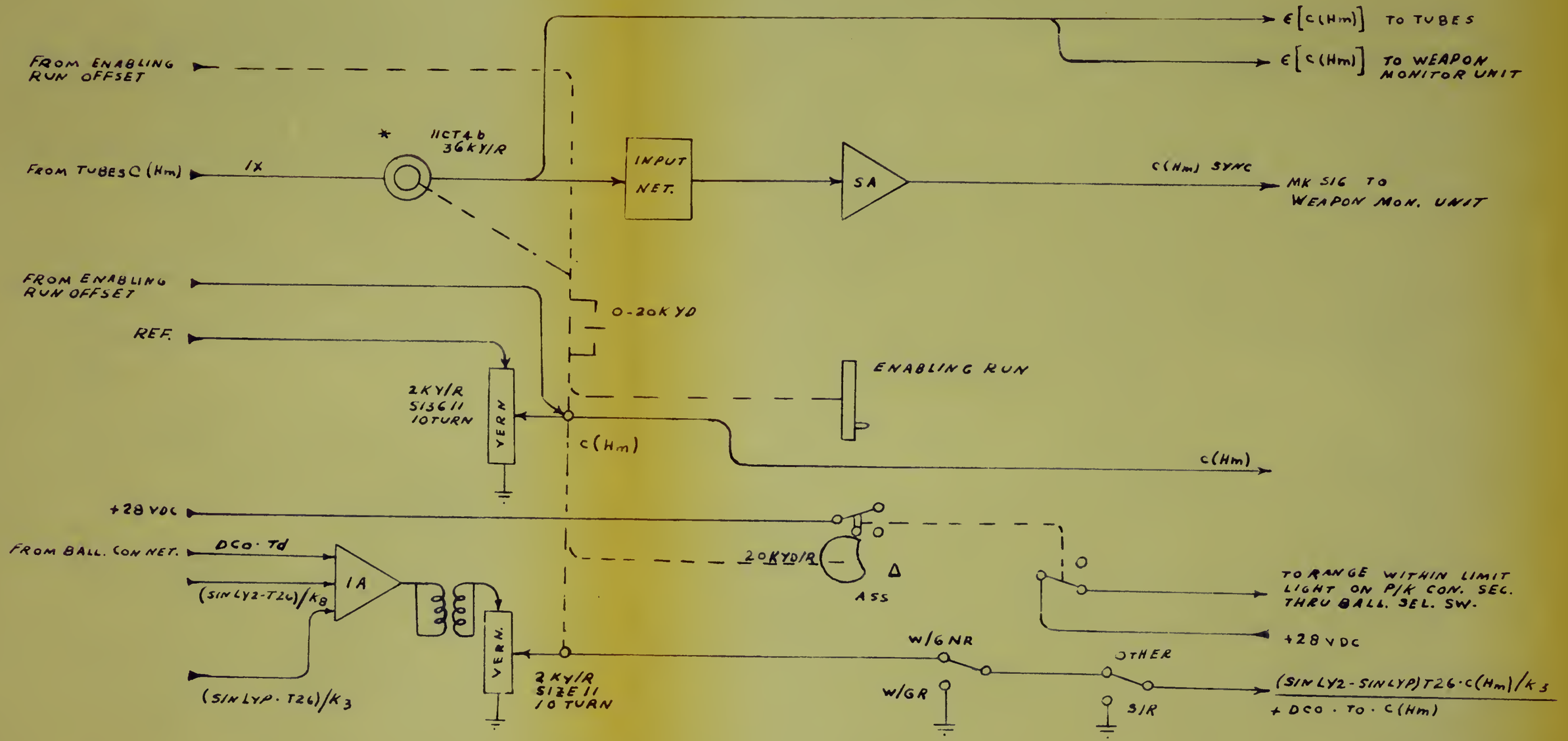

FIGURE 3

ENABLING RUN

difference between the sine of firing latitude and the sine of proofing latitude times half the product of the enabling run time and target turning rate, this minus the signal for gyro uncaging time, times own ship turning rate. These two quantities are multiplied by enabling run by the use of the vernistat.

$$\left[\frac{DC_m \cdot T_{26}}{2}(\sin L_{yp} - \sin L_{y2}) - DC_o \cdot T_d\right] c(Hm)$$

The output of this vernistat is sent as the perturbation to the lead angle servo loop, figure 4, previously discussed.

The analog voltage, c(Hm), from the Enabling Run Vernistat, is sent to the total run to burst module, figure 5, and to an isolation amplifier, which sums computed Enabling Run, c(Hm), and a torpedo path length correction, Hm_{corr}

$$Hm_{corr.} = - \left[Sg(Hm) \pm Hvmg_c\ (Hm) + Hvmg_c^2\ (Hm)\right]$$

(Note: The $Hvmg^2_{c(Hm)}$ term is used only with the Mk 37 Mod 0, high speed torpedoes.) The output of this amplifier is total torpedo run, (-) Hm27. This signal is sent to an impedance matching transformer in the input network of the isolation amplifier of the Weapon Time to Burst servo system. A vernistat on the Weapon Time to Burst module is the other input to the amplifier. This vernistat is referenced with torpedo or missile speed, Um', from an isolation amplifier having 3 ballistic constants f(Hmv), Um, j(Um) for inputs. The f(Hvm) signal, a function of depth, is a correction to the torpedo or missile speed, Um. This compensation is generated on the Run Depth module by a pot positioned proportionally to Run Depth, Hvm, and referenced from the ballistic constants network with a function f(Hvm). The voltage output of the T26 computing vernistat is proportional to torpedo speed Um' times weapon time to burst T26. When the product of

FIGURE 4

CEIL ANGLE (666)

LOCATION —— POSITION KEEPER DISPLAY UNIT IN THE ATTACK DIRECTOR

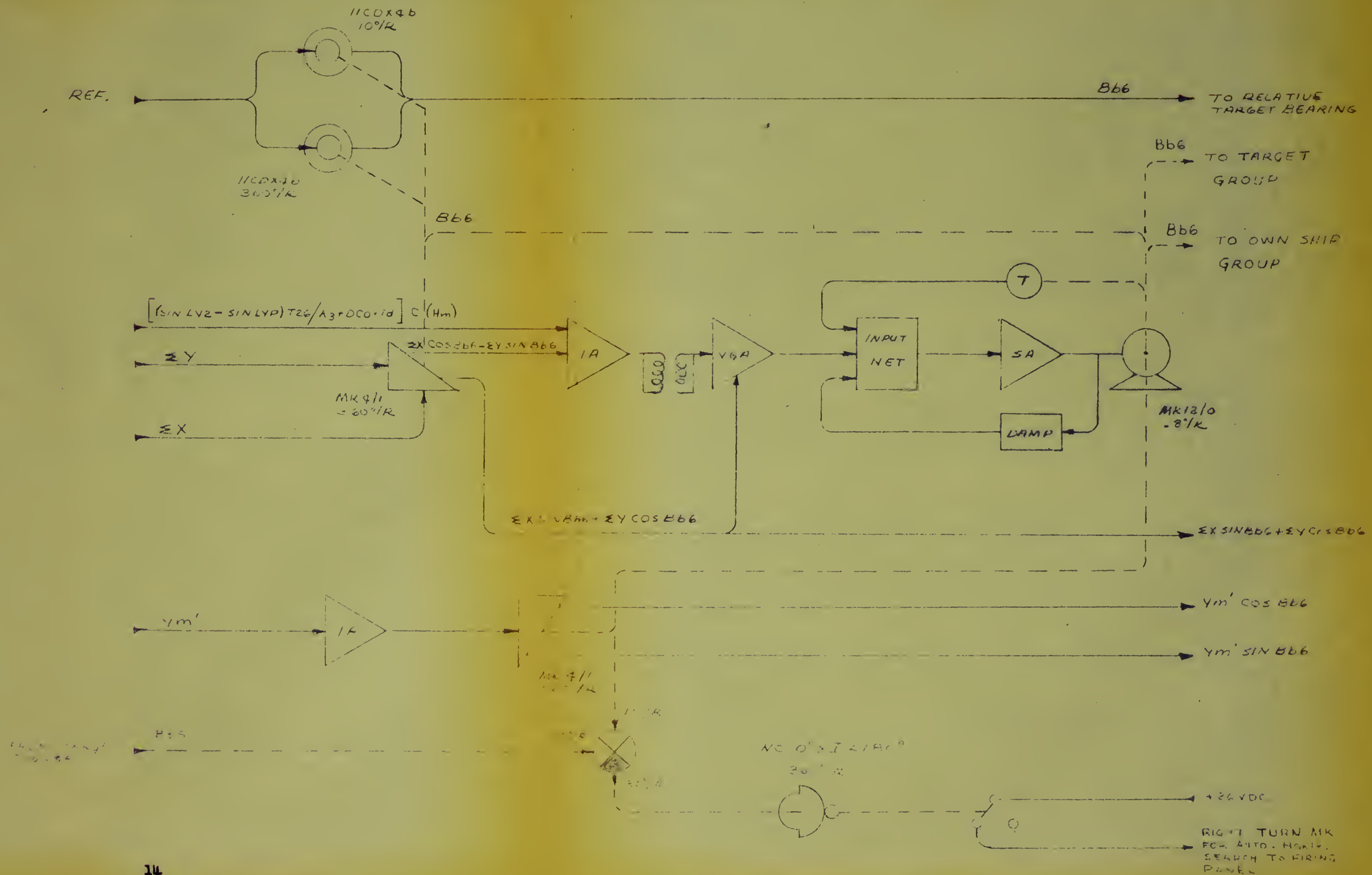

FIGURE 5

TOTAL RUN TO BURST

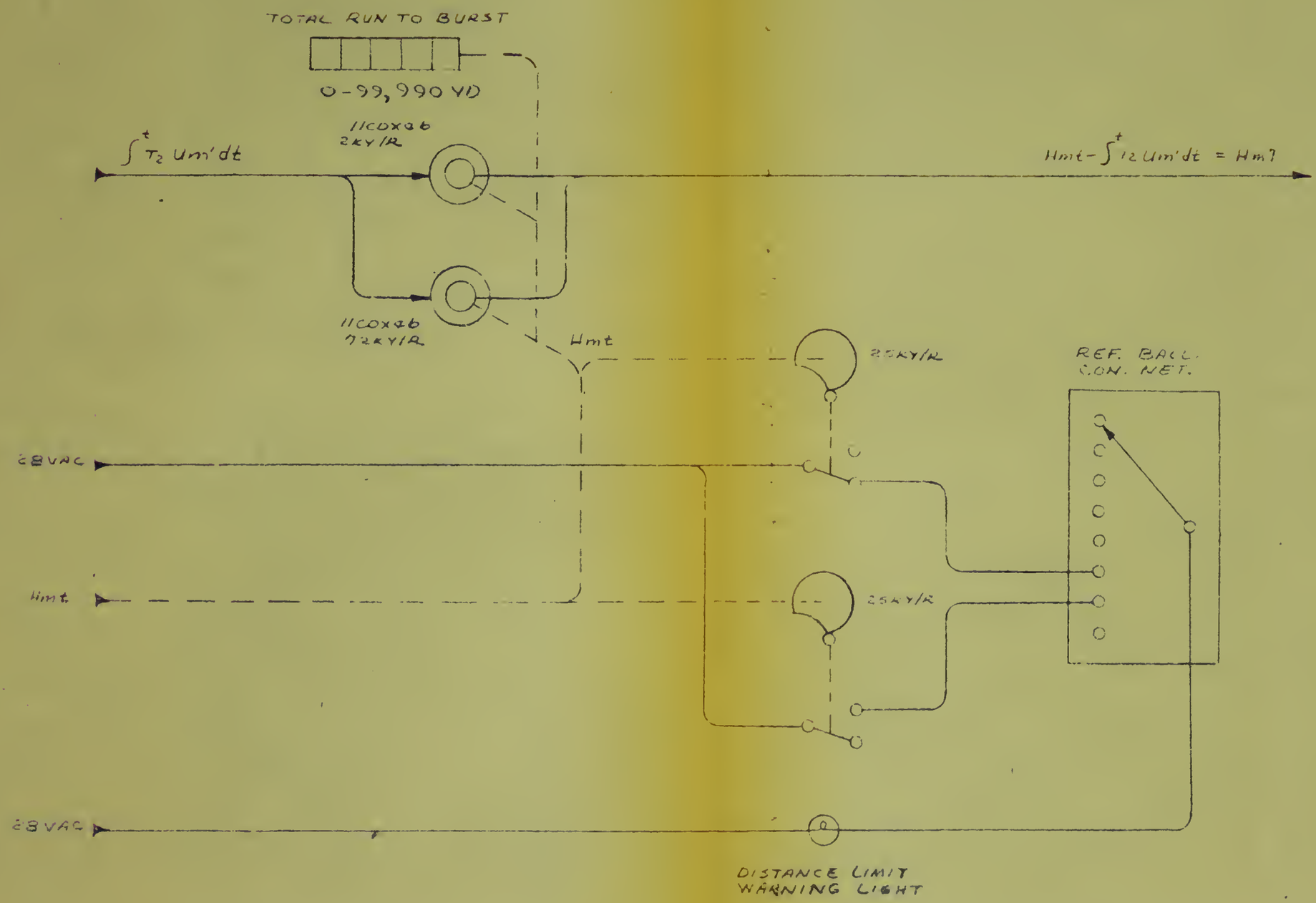

of speed and time (ecual to total run distance Hm_t), is compared with (-)H27 and passed through an isolation amplifier, it is an error signal, e(T26), used to position the Weapon Time to Burst, T26, servo system which displays T26. A vernistat referenced with the difference between the sine of proofing latitude and the sine of firing latitude times half the torpedo turning rate and positioned by the T26 servo system has an analog voltage output equal to the product of weapon time to burst and the compensation for firing latitude $\left[\frac{DCm}{2} \cdot T26 \ (\sin Lyp - \sin Lv2)\right]$. This signal is then summed at the input of an isolation amplifier with a contribution from the ballistic constant network. (-DCo . Td), where DCo is the Own Ship Turning Rate and Td is the Gyro Uncaging Time. The output of the isolation amplifier is used to reference the vernistat on the Enabling Run module previously discussed.

Another vernistat in the Weapon Time to Burst module sends a signal proportional to T26 to reference a vernistat on the Target Speed module.

This vernistat's output is a multiple of Target Speed, DMht; Weapon Time to Burst, T26 and K_1, to yield the distance the target travels from time of fire to time of impact. This signal is sent to an isolation amplifier, figure 2, that sums this distance and linear spread quantity H67, if present. The linear spread input is located in the firing panel. Linear spread is never used concurrently with Angular Spread quantities, sq(G), previously discussed. The output of this amplifier, the total distance travelled, is $\left[(Tf \cdot DMht \cdot K_1) + H67\right]$ or $\left[(T26 \cdot DMht \cdot K_1) + H67\right]$, and references a resolver in the Target Angle servo system. The output of this resolver is the sine and cosine of Target Angle, Bts, times the reference signal. These two signals become part of the inputs to the

two isolation amplifiers which yield ΣX and ΣY.

Generation of one of the other inputs to each of these amplifiers begins with the output of two isolation amplifiers. The input to these amplifiers is dependent upon the value of the Gyro Angle, G. Three conditions can be considered:

(1) For $170^\circ > G > 10^\circ$ and $350^\circ > G > 190^\circ$ the inputs into the turn-radius-isolation amplifier is just Ym' and the input into the reach-point-isolation amplifier is $Rh3 + Hvmg_{Rh3}$ where $Hvmg_{Rh3}$ is the correction to Rh3 for depth difference, (Hvo - Ph - Hvm). Under these conditions ΣX and ΣY are computed as:

$$\Sigma X = [Pdo \sin B - Pdn \cos B + (Rh3 + Hvmg_{Rh3}) \sin (B - B_g) - ym' \cos (B - B_g) + Ym' \cos Bb6 + (DMht \cdot T26 \cdot K_1 + H67) \sin Bts]$$

(2) For $350^\circ < G < 10^\circ$ the input to the gyro-turn-radius-isolation amplifier is zero; however, the reach-point-isolation amplifier is now $Rh3 + Hvmg_{Rh3} + (Ym' \cdot G \cdot \frac{\pi}{180^\circ})$. In addition to this change, additional circuitry removes (-Ym" sin Bb6) and (Ym' cos Bb6) from the ΣX and ΣY isolation amplifiers.

Hence ΣX and ΣY are computed as:

$$\Sigma X = Pdo \sin B - Pdn \cos B + (Rh3 + Ym' \cdot G \cdot \frac{\pi}{180^\circ})$$

$$\Sigma Y = Rh - Pdo \cos B + Pdn \sin B + (Rh3 + Hvmg_{Rh3} + Ym' G. \frac{\pi}{180^\circ}) \cos (B - B_g) + (DMht \cdot T26 \cdot K_1 + H67) \cos Bts$$

(3) For $170^\circ < G < 190^\circ$ the input to the gyro-turn-radius-isolation amplifier is 2 Ym' or twice the value used in case 1 above. The reach-point-isolation amplifier is the same as in case 1 and as

before, additional circuitry removes (Ym' sin Bb6) and Ym' cos Bb6) from the ΣX and ΣY isolation amplifiers.

Furthermore, it should be noted that the quantity Ym' used in (1) is actually Ym_l or Ym_r, depending on whether the condition $360 > G > 180$ exists or not.

In case (2) the same thing is true, however, its determination is due to the position of a pot positioned in the Gyro Angle module, figure 6.

In case (3) Ym' implies $2\dot{Y}m'_l$ or $2Ym'_r$, depending on how the Gyro Angle develops.

These signals described above for case one, two, and three, reference the stators on a resolver on the Relative Tube Bearing module. This module has two positions. One position is for the bearing of the port tube and other position is for the bearing of the starboard tube. The input signals come from the own ship section where these two bearings are stabilized. The distance to the Peach Point (point 3) and gyro-turn radius are measured along and associated with the tube bearing module references these quantities to own ship's centerline, (Own Ship's Course, Co.).

To these quantities are added the appropriate parallax components, Pdo, Pdn, of the ship by summing the applicable input in two isolation amplifiers. The output of these two amplifiers then reference a resolver on the Relative Target Bearing module. This resolver rotates the input quantities to distances along and across the bearing

FIGURE 6

GYRO ANGLE ORDER

NOTES:
1. * THERE ARE INDIVIDUAL PAIRS OF C.T.'s FOR EA. TUBE.
2. Δ THERE ARE INDIVIDUAL CAMS FOR EA. TYPE OF WEAPON.

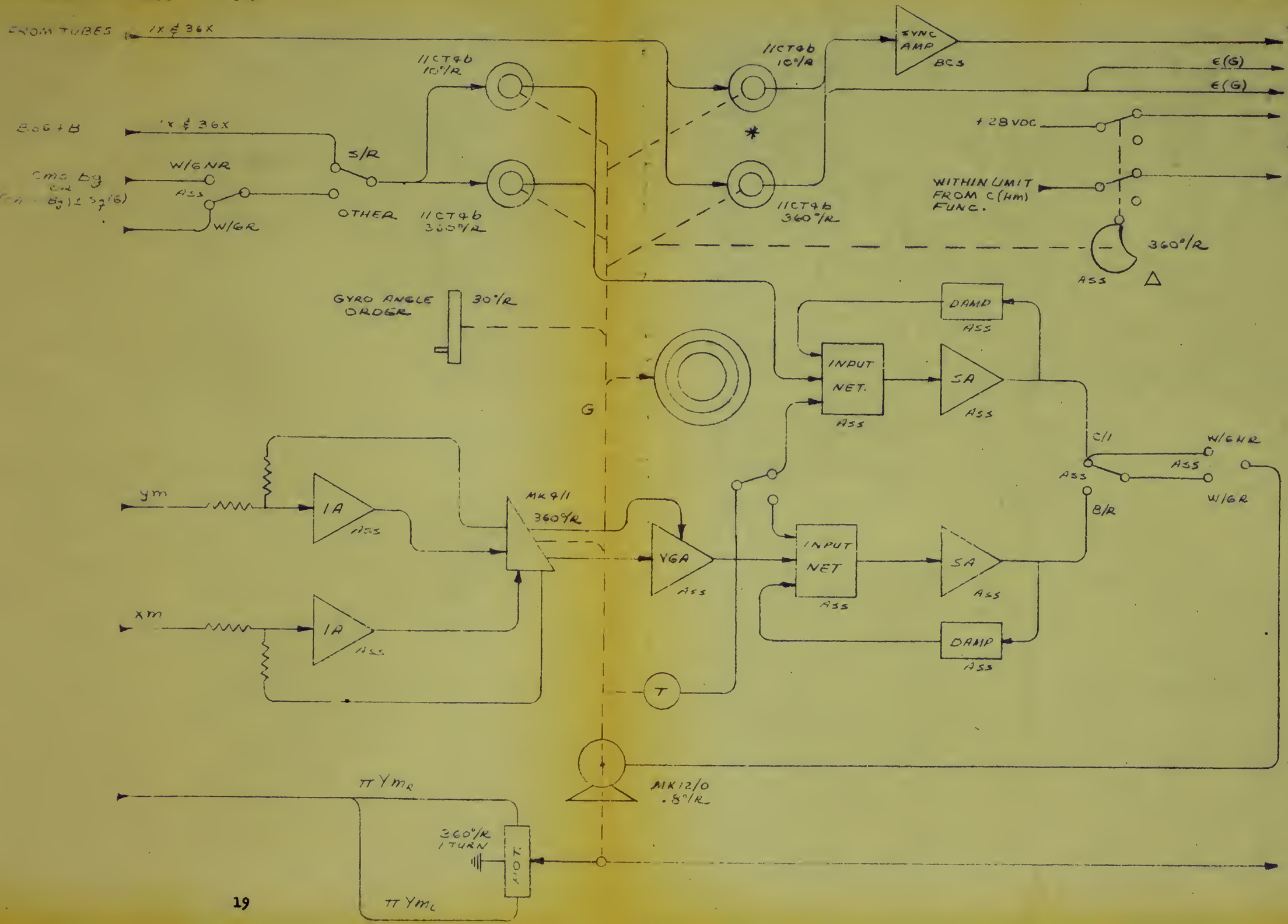

line (LOS). These quantities are then sent to the summing amplifiers mentioned before and yield ΣX and ΣY.

2.2 Objectives of Analysis

The analysis was undertaken to determine the response characteristics of the individual loops, the overall loop, check the system for stability, recommend potentiometer settings for optimum response and if found necessary recommend compensation networks.

2.3 Period of Time Allowed for Analysis

Work on this thesis was accomplished during eight weeks of the summer period between the second and third year of the Ordance Engineering Guided Missiles Curriculum ending in December of 1960.

III. Review or Introduction to Some Recent Developements in Servo Analysis Techniques

3.1 Determinantal Method of Analysis[1]

The theory of simple single loop control systems is well developed, and the block diagrams of such systems are not complicated. On the other hand, the block diagrams and theory of multi-loop, multi-input, multi-output, and multi-coupled control systems is not very well developed because of the complexity of the problem involved. The block diagrams of such systems are complicated and difficult to intepret. One approach to the solution of such a problem is to formulate and solve a set of simultanious equations for the system. This can best be accomplished by arranging such systems into a standard block diagram. Arranging the system in this manner greatly facilitates the writing of the equations.

Any system which has summing points in the main transmission path can be arranged in a block diagram by suitable block diagram manipulation as shown in figure 7. Writing the equations at the various nodes:

At node a

$$a = R_a - (G_{ab} \cdot G_{Aa})a - (G_{bc} \cdot G_{Ba})b - (G_{cd} \cdot G_{Ca})c$$

A more convenient notation is:

$$a = R_a - (G_{aa})a - (G_{ba})b - (G_{ca})c$$

At node b

$$b = R_b - (G_{bb})b + (G_{ab})a - (G_{cd})c$$

[1] CHU, Y., A Generalized Theory of Linear Multi-Loop Automatic Control Systems, Doctoral Dissertation, MIT, 1953

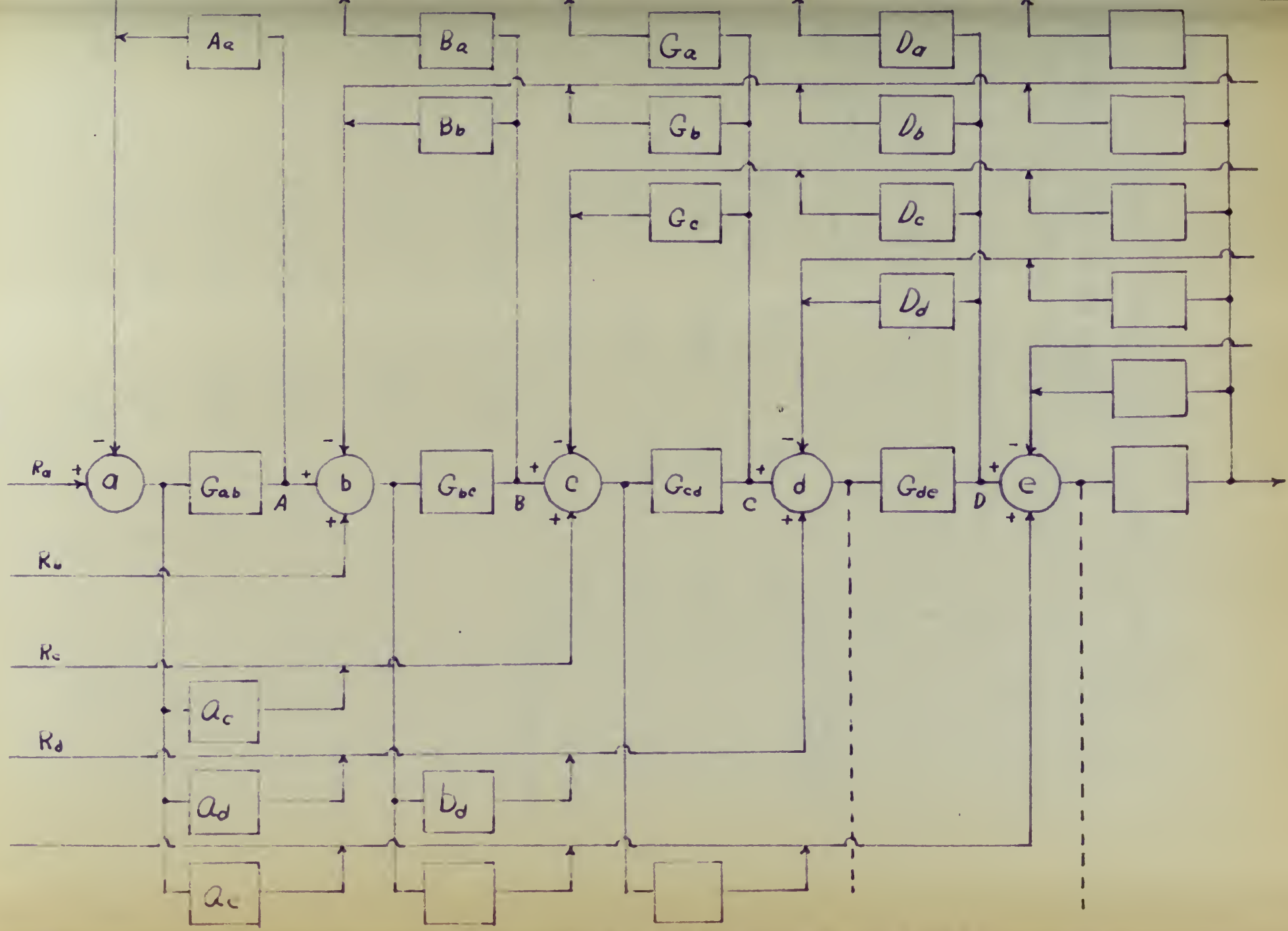

FIGURE 7 STANDARD BLOCK DIAGRAM

at node d

$$d = (-G_{dd})\,d + R_d + (G_{ad})\,a + (G_{bd})\,d + (G_{cd})\,c$$

Rearranging to bring out the symmetry

$$(1+G_{aa})\,a + (G_{ba})\,b + (G_{ca})\,c + (G_{da})\,d = R_a$$

$$(-G_{ab})\,a + (1+G_{bb})\,b + (G_{cb})\,c + (G_{db})\,d = R_b$$

$$(-G_{ac})\,a - (G_{bc})\,b + (1+G_{cc})\,c + (G_{dc})\,d = R_c$$

$$(-G_{ad})\,a - (G_{bd})\,d - (G_{cd})\,c + (1+G_{dd})\,d = R_d$$

Now, solving by Cramer's Rule

FEED BACK PATHES

$$\Delta = \begin{vmatrix} (1+G_{aa}) & G_{ba} & G_{ca} & G_{da} \\ -G_{ab} & (1+G_{bb}) & G_{cb} & G_{db} \\ -G_{ac} & -G_{bc} & (1+G_{cc}) & G_{dc} \\ -G_{ad} & -G_{bd} & -G_{cd} & (1+G_{dd}) \end{vmatrix}$$

MAIN DIAGONAL

FEEDFORWARD PATHS

For simplicity let us assume the inputs

$$R_a = \theta_i(t) \;;\; R_b = R_c = R_d = 0$$

Then the output will be $D = (G_{dc})\,d$

ROW ↓ COLUMN →

$$D = G_{dc}\,\frac{\begin{vmatrix} (1+G_{aa}) & G_{ba} & G_{ca} & R_a \\ -G_{ab} & (1+G_{aa}) & G_{cb} & 0 \\ -G_{ac} & -G_{bc} & (1+G_{cc}) & G_{dc} \\ -G_{ad} & -G_{bd} & -G_{cd} & (1+G_{dd}) \end{vmatrix}}{\Delta}$$

$$D = G_{dc} \frac{(-1)^{a+d} \Delta_{ad}}{\Delta} R_a$$

OR IF $R_a = 0$ AND $R_b \neq 0$

$$D = \frac{G_{dc} (-1)^{a+d} \Delta_{ad} R_b}{\Delta}$$

It is noted that Δ is equal to the characteristic equation of the system. For an example, take the four node system in figure 8.

$$D = \frac{G_4 (-1)^{(a+d)} \Delta_{ad}(1) R_a}{\Delta}$$

ROWS → ← COLUMNS

$$\Delta = \begin{vmatrix} a & b & c & d \\ a & (1+0) & 0 & 0 & G_4(1) \\ b & -K_1 & (1+0) & 0 & G_4 G_5 \\ c & 0 & -G_2 & (1+0) & 0 \\ d & 0 & 0 & -G_3 & (1+0) \end{vmatrix}$$

$$\Delta = (-1) \begin{vmatrix} 1 & 0 & G_4 G_5 \\ -G_2 & 1 & 0 \\ 0 & -G_3 & 1 \end{vmatrix} - G_4 \begin{vmatrix} -K_1 & 1 & 0 \\ 0 & -G_2 & 1 \\ 0 & 0 & -G_3 \end{vmatrix}$$

← Δ_{ad}

$\Delta = 1 + G_2 G_3 G_4 G_5 + G_4 (K_1 G_2 G_3)$ - characteristic equation of the system.

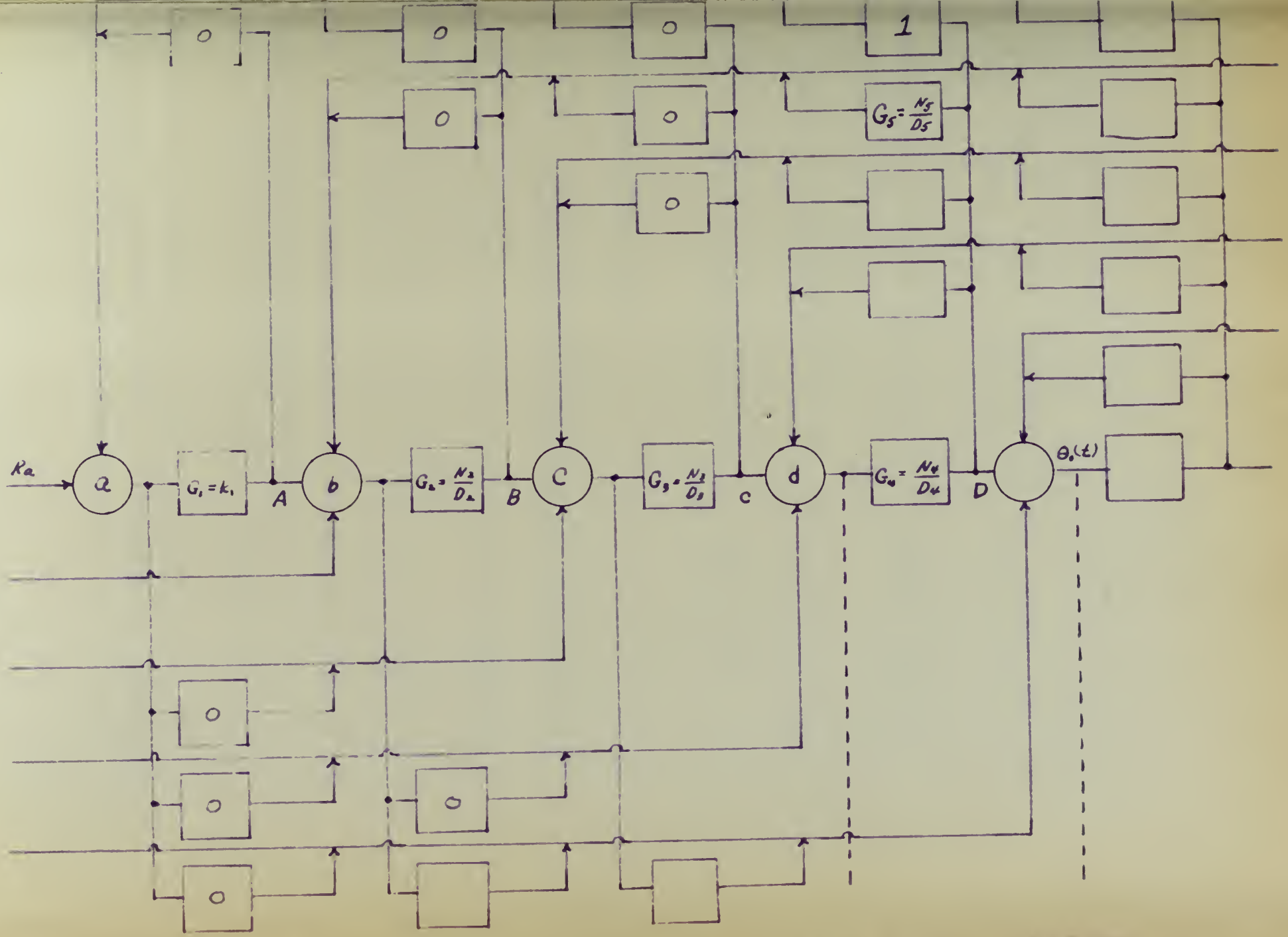

FIGURE 8 EXAMPLE OF USE OF STANDARD BLOCK DIAGRAM

$$D = \frac{G_4 R_a (k_1 G_2 G_3)}{1 + k_1 G_2 G_3 G_4 + G_2 G_3 G_4 G_5}$$

$$D = \theta_o(t)$$

$$\frac{\theta_o(t)}{\theta_i(t)} = F_c = \frac{k_1 G_2 G_3 G_4}{1 + k_1 G_2 G_3 G_4 + G_2 G_3 G_4 G_5}$$

Now putting the transfer functions in the form of numerator divided by denominator.

$$F_c = \frac{\frac{k_1 N_2 N_3 N_4}{D_2 D_3 D_4}}{1 + \frac{k_1 N_2 N_3 N_4 D_5}{D_2 D_3 D_4 D_5} + \frac{N_2 N_3 N_4 N_5}{D_2 D_3 D_4 D_5}}$$

Which when simplified becomes:

$$F_c = \frac{k_1 D_5 N_2 N_3 N_4}{D_2 D_3 D_4 D_5 + k_1 N_2 N_3 N_4 D_5 + N_2 N_3 N_4 N_5}$$

The roots of the transfer function are the zeros of the characteristic equation.

$$D_2 D_3 D_4 D_5 + k_1 N_2 N_3 N_4 D_5 + N_2 N_3 N_4 N_5 = 0$$

Now if we desire to determine the effect of the feedback path G5, we can rearrange the characteristic equation in the form

$$D_5 [D_2 D_3 D_4 + k_1 N_2 N_3 N_4] + N_2 N_3 N_4 N_5 = 0$$

The quantity in the brackets can be equated to zero and by root locus techniques the roots can be determined. The characteristic equation will then be $D_5 [(s + r_1)(s + r_2)(s + r_3)(s + r_4)] + N_2 N_3 N_4 N_5 = 0$

The final root locus equation will then be:

$$\frac{N_2 N_3 N_4 N_5}{D_5(S+r_1)(S+r_2)(S+r_3) S+r_4} = \frac{k_5 S^n (S+z_1) \; k_2 k_3 k_4}{(S+p_1)(S+r_1)(S+r_2)(S+r_3)(S+r_4)} = \epsilon^{j\pi}$$

The transfer function will then be:

$$F_c = \frac{k(S+z_1)(S+z_2)\cdots\cdots}{(S+P_1)(S+r_2)\cdots\cdots}$$

3.2 Determination of the Composite Open Loop Transfer Function and Velocity Constant for Multi-Loop Systems

$$F_c = \frac{F_o}{1+F_o} = \frac{N_c}{D_c}$$

$$F_c(1+F_o) = F_o$$

$$F_c + F_c F_o = F_o$$

$$F_o = \frac{F_c}{1+F_c}$$

In terms of numerator and denominator of the closed loop transfer function

$$F_o = \frac{N_c}{D_c - N_c}$$

Now applying the classical definition of the velocity constant

$$K_v = \lim_{S \to 0} S F_o$$

$$K_v = \lim_{S \to 0} S \frac{N_c}{D_c - N_c}$$

It is convenient to determine the open loop transfer function in this manner and then apply root locus techniques.

After the open loop function has been determined, it is quiet easy to determine the type and order of the system. It will have the form:

$$F_o = \frac{K(S+Z_1)(S+Z_2)(S+Z_3)\cdots}{S^n[(S+P_1)(S+P_2)(S+P_3)\cdots]}$$

The denominator of the open loop function is unfactored; the S^n can be factored out prior to performing the root locus or K versus real roots thus the type and number of the system can be determined. If the desired type is not obtained, this is a criteria for selection of suitable compensation. In any event it avoids the necessity of finding the roots of the system to determine the type number.

It is often necessary to perform a root locus or K versus real root plot to determine the poles of the open loop transfer function. As an example, consider the example of section 3.1. The closed loop transfer function is $F_c = \frac{K_1 D_5 N_2 N_3 N_4}{D_2 D_3 D_4 D_5 + N_2 N_3 N_4 N_5 + K_1 D_5 N_2 N_3 N_4}$

$$F_o = \frac{N_c}{D_c - N_c}$$

$$F_o = \frac{K_1 D_5 N_2 N_3 N_4}{D_2 D_3 D_4 D_5 + N_2 N_3 N_4 N_5}$$

The denominator then can be factored.

$$D_2 D_3 D_4 D_5 + N_2 N_3 N_4 N_5 = 0$$

$$\frac{N_2 N_3 N_4 N_5}{D_2 D_3 D_4 D_5} = \epsilon^{j\pi}$$

$$\frac{K_2 K_3 K_4 K_5 (S+Z_2)(S+Z_3)(S+Z_4)(S+Z_5)}{(S+P_2)(S+P_3)(S+P_4)(S+P_5)} = \epsilon^{j\pi}$$

The roots are then determined and the open loop transfer then becomes

$$F_o = \frac{K_1 \omega^5 N_2 N_3 N_4}{(S+R_1)(S+R_2)(S+R_3)(S+R_4)}$$

The closed loop roots are then determined in the usual manner.

3.3 Root Locus Gain versus Real Roots[2]

The usual method of determining the roots of a closed loop function is to apply the familiar root locus principals. A somewhat similiar technique which embodies some of the same principals is the method of plotting K (root locus gain) versus the real roots.

For illustration, let us consider this unity feedback loop shown below.

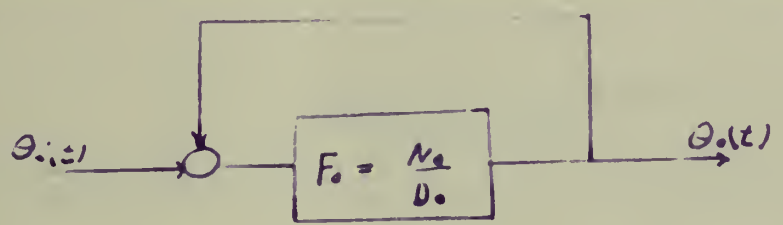

The closed loop transfer function is

$$F_c = \frac{F_o}{1+F_o} \qquad OR \qquad F_c = \frac{N_o}{D_o + N_o}$$

The roots of Fc are where $D_o + N_o = 0$ or $\frac{N_o}{D_o} = \epsilon^{j\pi}$

The open loop transfer function has this form:

$$\frac{N_o}{D_o} = \frac{k(S+Z_1)(S+Z_2)(S+Z_3)\cdots}{S^n(S+P_1)(S+P_2)(S+P_3)\cdots}$$

2. Wheeler, R. C. H., Unpublished Class Notes

Now plotting the poles and zeros on the S - plane:

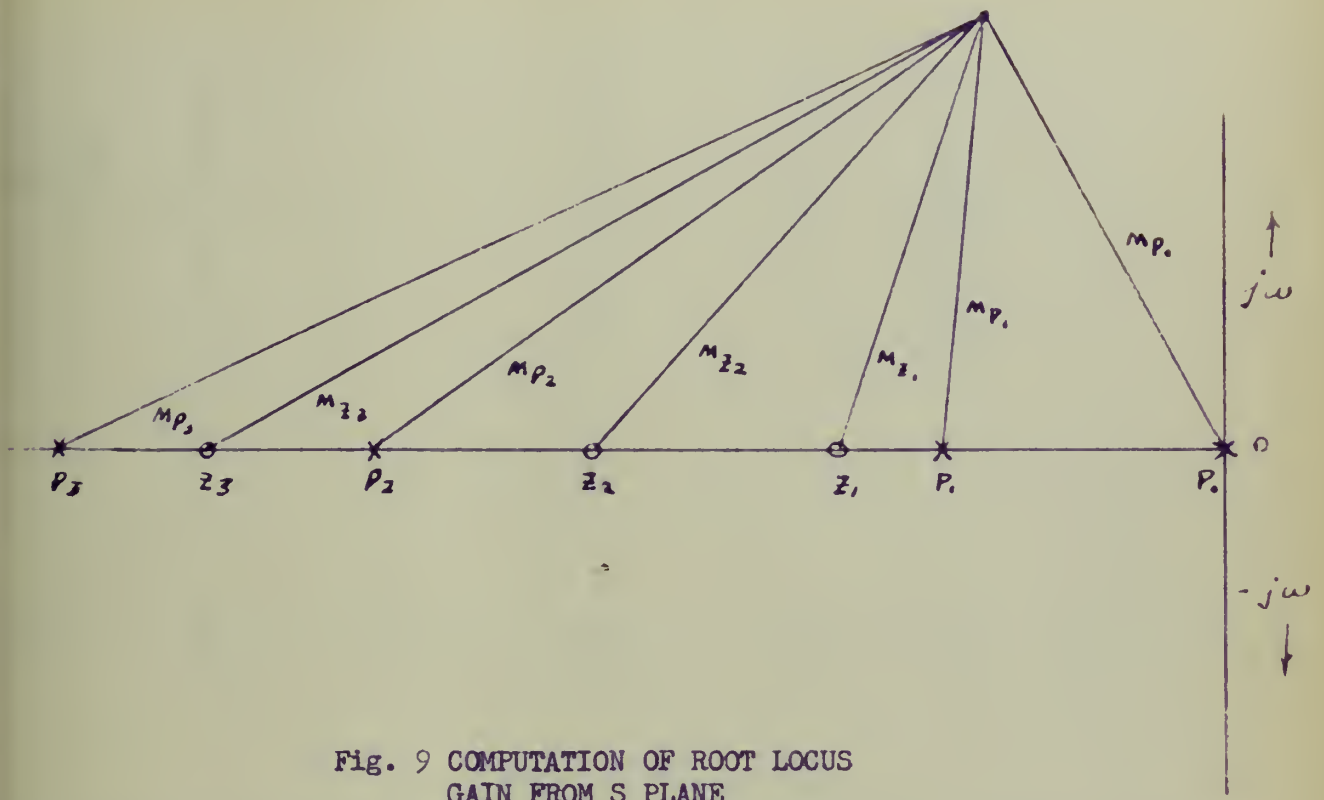

Fig. 9 COMPUTATION OF ROOT LOCUS
GAIN FROM S PLANE

By the Evan's method the closed loop roots are determined by summing angles to 180° and plotting the locus of the roots. Then knowing the gain associated with the system, a cut and try process is performed to locate the roots, by the relationship $K = \frac{M_{p_i}}{M_{z_i}}$. This process is necessary along the real axis where root locus exists. If these values along the axis are plotted the following curves will result. All the curves shown do not result from every open loop transfer function but are shown as an example of all possible configeration.

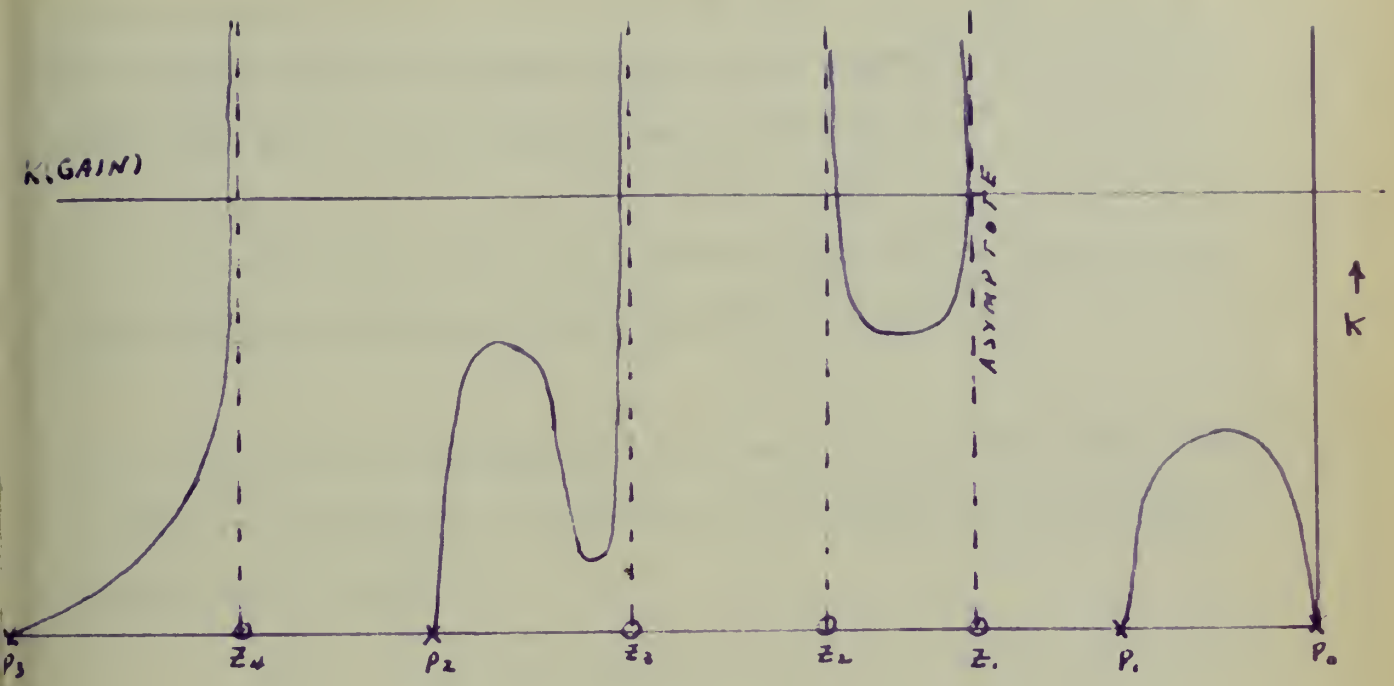

Fig. 10 PLOT OF ROOT LOCUS GAIN
VERSUS REAL ROOTS

It can be shown that the maximum between P_0 and P_1 is the "breakaway point" and the minimum between Z_1 and Z_2 is the entrance point in the Evan's Root Locus Method.

If the system gain is given or can be chosen, a horizontal line drawn which intersects these curves yields the real roots of the closed loop function. If it does not intersect as between P_0 and P_1, complex roots exist. Also between Z_3 and P_2, one real root and two complex roots exist with the gain chosen as shown.

This method works equally well with complex poles or zeros in the open loop function by using the same relationship for gain $K = \frac{M_{pi}}{M_{zi}}$, but one must remember that the distances to these complex quantities to the point at which the gain is being computed must be included.

From the foregoing discussion, it is seen that all the real roots of the closed loop can be determined without plotting the root locus.

It is a fact that the denominator of the closed loop function which is the characteristic equation of the system has the following form and possesses the below listed qualities:

$$A x^n + B x^{n-1} + C x^{n-2} - \cdots D = 0$$

A = 1

B = Sum of the roots of the closed loop function

C = Product of the roots of the closed loop function

Knowing the real roots from the plot of "K versus Real Roots" and using the relationship $r_1 + r_2 + r_3 - \cdots + (\alpha + j\omega_c) + (\alpha - j\omega_c) = B$

$$r_1 + r_2 + r_3 - \cdots + 2\alpha = B$$

we can now solve for the real part of the complex pair. Knowing this we can use the second relationship

$$r_1 r_2 r_3 (\alpha + j\omega_c)(\alpha - j\omega_c) = D$$

which becomes

$$r_1 r_2 r_3 (\alpha^2 + \omega_c^2) = D$$

Since r_1, r_2, r_3, AND D are known, we can solve for Wc thus all roots are known.

This method provides a criteria for selection of system gain since the effect of root location can be readily seen, and is faster than the rather laborious angle summation process necessary in the Evan's Method since in most cases only three points must be computed to determine a given curve.

IV. Derivation of Transfer Functions of Components and Minimum Velocity Constant Requirement

4.1 Servo Amplifier

The frequency response of the amplifier was measured and found to be flat to ± 1 db to 7,000 kc. Since this is beyond the system bandwidth the simplification of constant gain will be used throughout this thesis. It was found that this gain was approximately 150,000.

Because the input signal and the various feedbacks are not summed at a common node (see Fig. 11), the gain could not be considered in the conventional manner. Rather the gain seen by the various signals is different. It was found more convenient to consider the gain as a function of the variable resistors. This can best be seen by considering the equivalent circuit of Fig. 12.

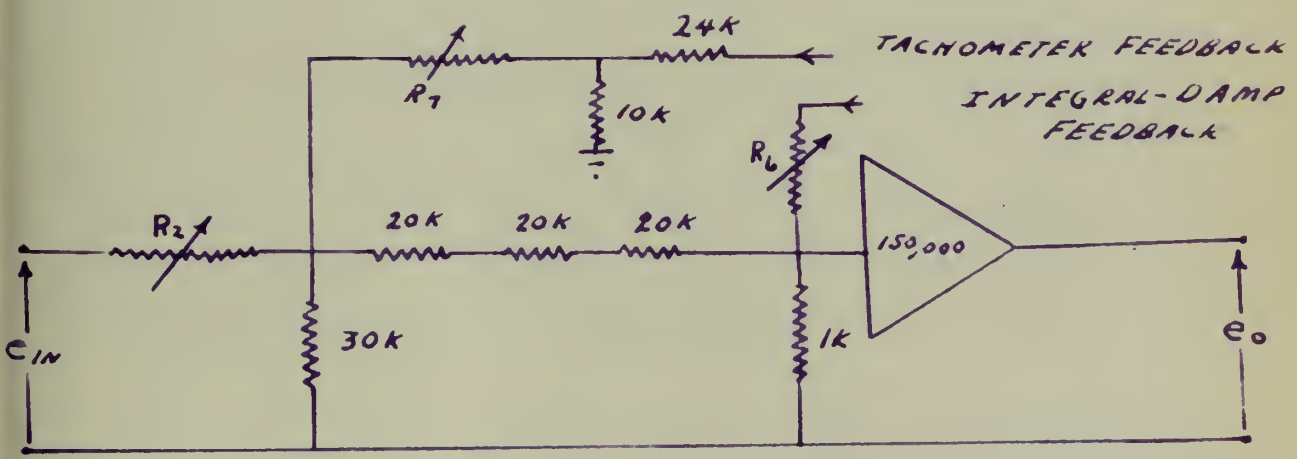

Fig. 12 EQUIVALENT CIRCUIT OF INPUT NETWORK TO SERVO AMPLIFIER

The gains as a function of the resistors R_2, R_6 and R_7 is shown in 5.1, Analysis of the Individual Loop. The entire closed loop equivalent circuit is shown in figure 18 and simplified block diagram equivalent is shown in figure 21.

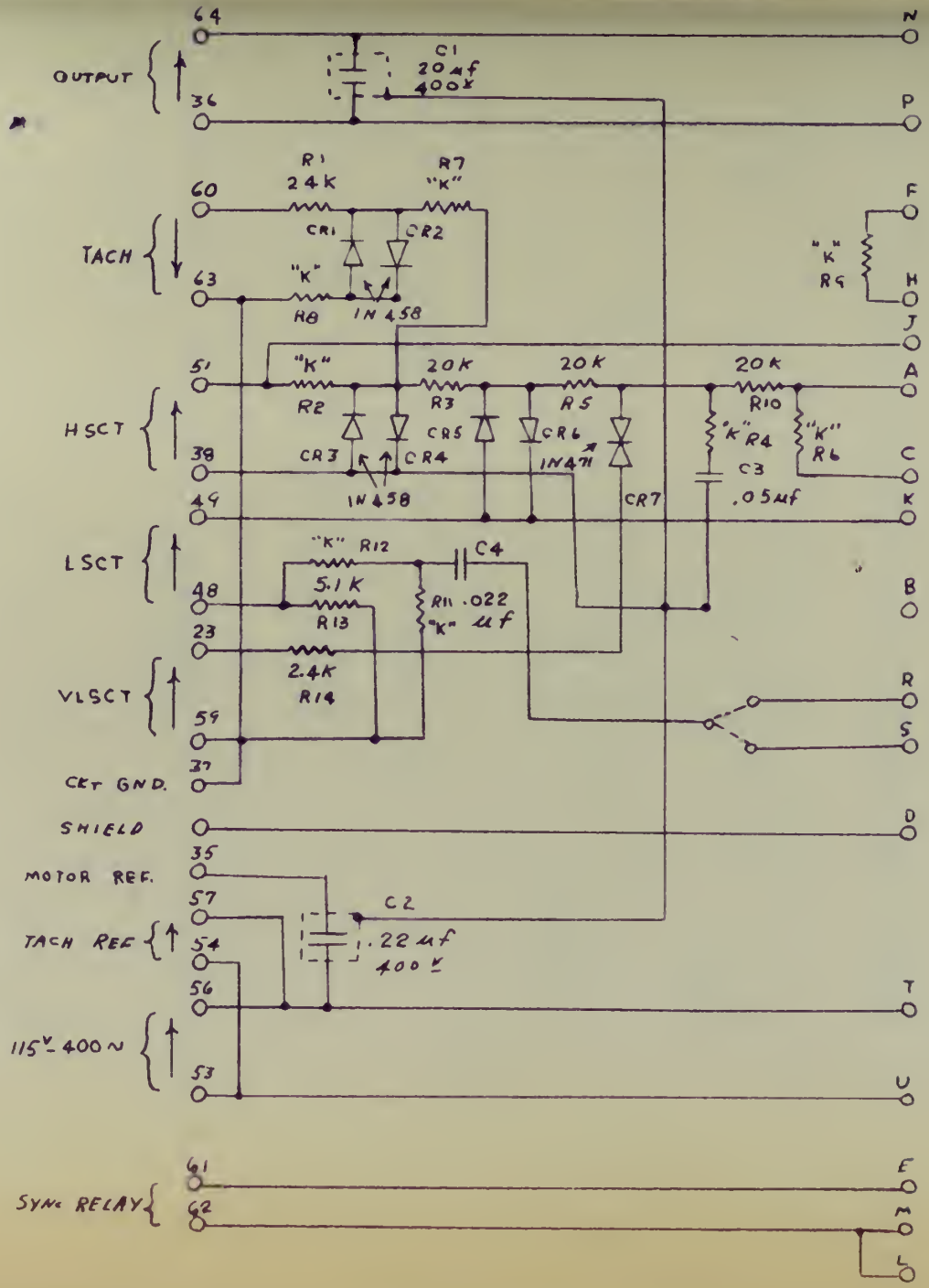

FIGURE 11

INPUT NETWORK

4.2 Integral Network

The integral-damping network is a means of compensating the amplifier and is shown schematically in Fig. 13. The equivalent circuit is shown in Fig. 14.

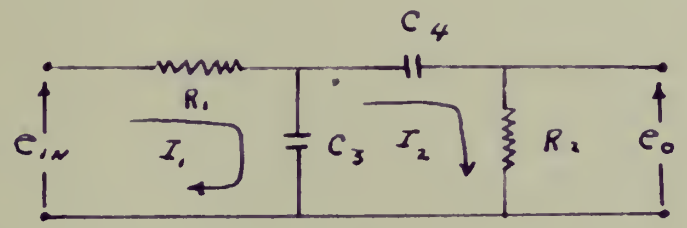

Fig. 14 EQUIVALENT CIRCUIT OF INTEGRAL-DAMP NETWORK

From Fig. 14 it can be shown that the transfer function is:

$$\frac{\theta_o}{\theta_i} = \frac{S\,(R_1C_1)}{(R_1C_1R_2C_2)S^2 + \dfrac{(R_1C_1 + R_2C_2 + R_1C_2)}{R_1C_1R_2C_2}S + \dfrac{1}{R_1C_1R_2C_2}}$$

Simplifying: $$\frac{\theta_o}{\theta_i} = \frac{\left(\frac{1}{R_2C_2}\right)S}{S^2 + \left(\frac{R_1C_1 + R_2C_2 + R_1C_2}{R_1C_1R_2C_2}\right)S + \frac{1}{R_1C_1R_2C_2}}$$

From Fig. 13 the various values of resistance and capacitance were obtained and substituted into the above transfer function which yeilds when simplified: $\frac{\theta_o}{\theta_i} = \frac{10S}{S^2 + 125S + 1110}$

Factoring: $\frac{\theta_o}{\theta_i} = \frac{10S}{(S+9.5)(S+115.5)}$

A frequency response analysis shown in Fig. 15 revealed that the actual transfer function was $\frac{\theta_o}{\theta_i} = \frac{26.68S}{(S+2)(S+200)}$. This transfer function was used in the analysis.

It was found later in the analysis that a value of $C_3 = C_4 = .25\,\mu f$ produced an improved response of the individual loop. Proceeding as above the resulting transfer function is $\frac{33.35}{(S+35)(S+112)}$. It is included in this section for convenience.

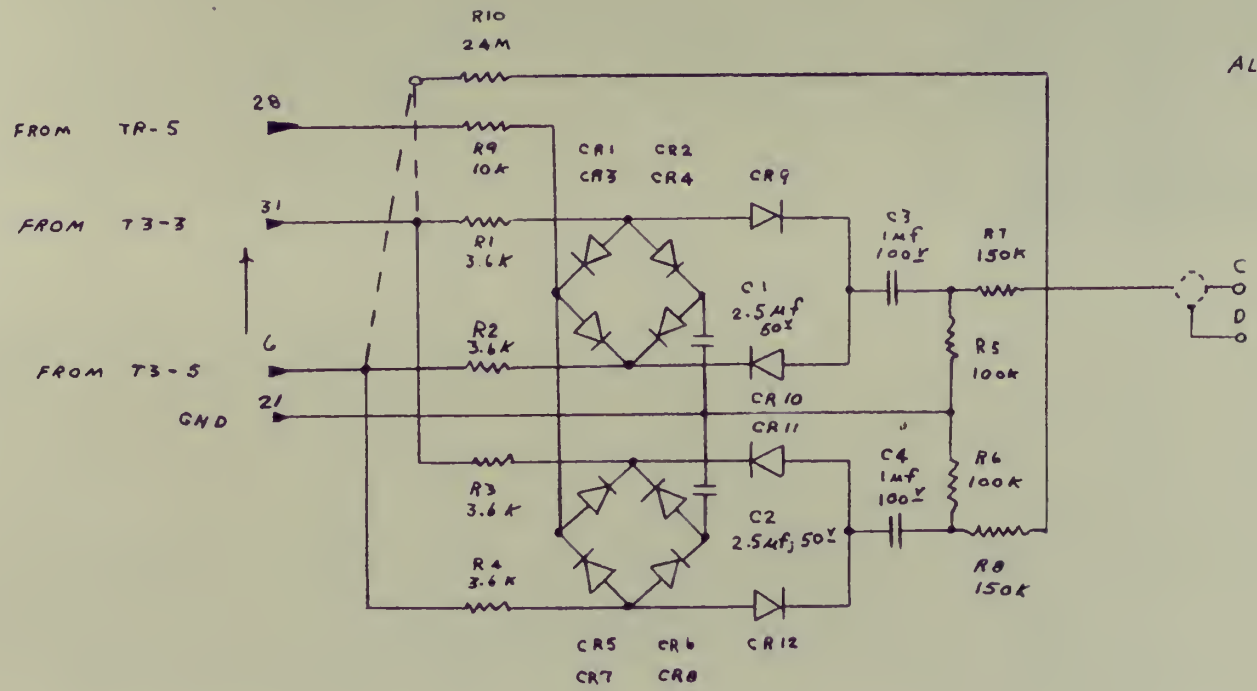

FIGURE 13

INTEGRAL-DAMPING NETWORK

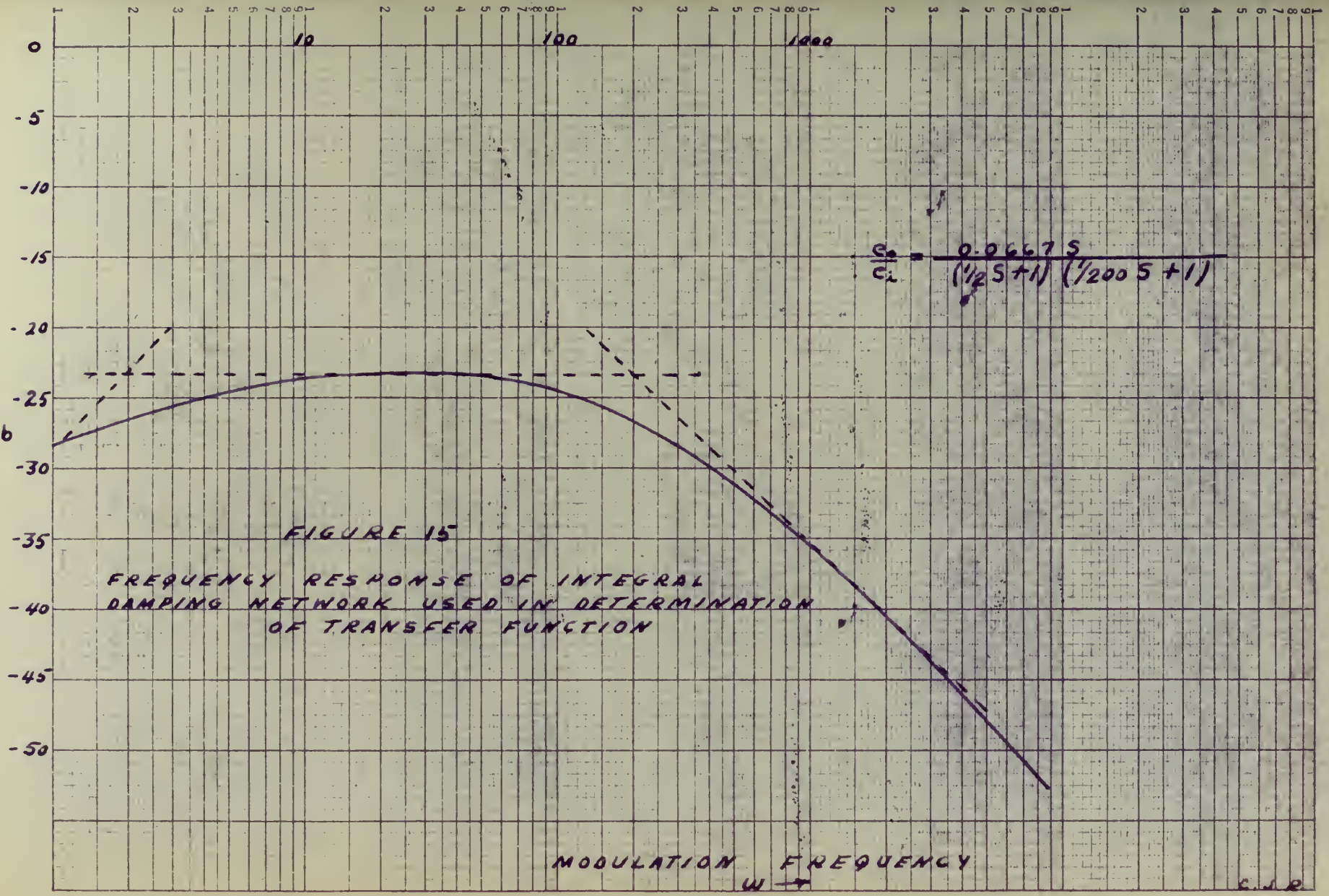

FIGURE 15

FREQUENCY RESPONSE OF INTEGRAL DAMPING NETWORK USED IN DETERMINATION OF TRANSFER FUNCTION

4.3 Servo Motor

The Servo motors Mk 12, Mod 0 used were manufactured by KEARFOTT COMPANY, INC., LITTLE FALLS, NEW JERSEY. To obtain the dynamic constants, it was recommended that the following relationships be used.

K_T (TORQUE CONSTANT) $= \frac{T}{E}$ DYNE-CM PER VOLT

K_v (VELOCITY CONSTANT) $= \frac{K_t}{F}$ $\frac{\text{RADIANS PER SEC}}{\text{VOLTS}}$

K_a (ACCELERATION COEFFICIENT) $= \frac{K_t}{J}$ $\frac{\text{RADIANS PER SEC}^2}{\text{VOLTS}}$

F (MOTOR FRICTION) $= \frac{T_s - T_v}{\dot{\theta}}$ $\frac{\text{DYNE - CM}}{\text{RADIANS PER SEC}}$

T_s = STALL TORQUE

T_v = DELIVERED TORQUE AT SHAFT VELOCITY $\dot{\theta}$

Using a plot of number of gear teeth versus inertia in $OZ\text{-}IN^2$ the total reflected inertia was found and added to the given inertia of the motor. The total inertia was found to be $J = 3.16 \times 10^{-2}$ $OZ\text{-}IN^2$ OR

$J = 5.78$ $Gm\text{-}Cm^2$.

$$F = \frac{1.0 - 3.0}{4700 - 2000} = \frac{1}{2700} \quad \frac{OZ\text{-}IN^2}{RPM}$$

By suitable change of units this becomes:

$$F = 250 \quad \frac{\text{DYNE - CM - SEC}}{\text{RAD}}$$

$$t_n \text{ (MECHANICAL TIME CONSTANT)} = \frac{J}{F} = \frac{5.78}{250} \frac{(Gr - Cm^2)}{(Cm - SEC.)}$$

$$t_n = .0231 \text{ SEC.}$$

$$K_t = \frac{T}{E} = \frac{1.45}{115} \frac{OZ - IN^2}{VOLTS} = .0126 \frac{OZ.-IN.}{VOLTS}$$

$$K_t = 890 \frac{DYNE - Cm}{VOLTS}$$

$$K_v = \frac{K_t}{F} = \frac{890}{250} \frac{\frac{DYNE - Cm}{VOLTS}}{\frac{DYNE - Cm - SEC}{RAD.}} = 3.56 \frac{RAD.}{VOLTS - SEC.}$$

$$\frac{\theta_o}{\theta_i} = \frac{3.56}{S(.0231 S + 1)}$$

$$\frac{\theta_o}{\theta_i} = \frac{154}{S(S + 43.3)}$$

When this transfer function was used in the computation to determine the closed loop response and checked against measured response, the results were found to be 35 per cent in error. Several different pole-zero configerations obtained by using various values of tachometer feedback were used and the 35 per cent error was found to be consistant. It became obvious that the motor time constant was in error. With this in view, an investigation to determine the response or a second order system was attempted by removing the tachometer and integral networks. Transient response curves were obtained at various amplifier gain settings and found to be almost identical for any setting of gain. The slight change was accredited to the pole of the amplifier at 6000. From these curves it can be seen that ts (settling time) = .355 using the relationship $t_s = \frac{5}{\alpha}$ it was found that $\alpha = 14.1$ or $2\alpha = 28.2$. This can be seen readily by looking at the root locus plot of the second order system shown in figure 16.

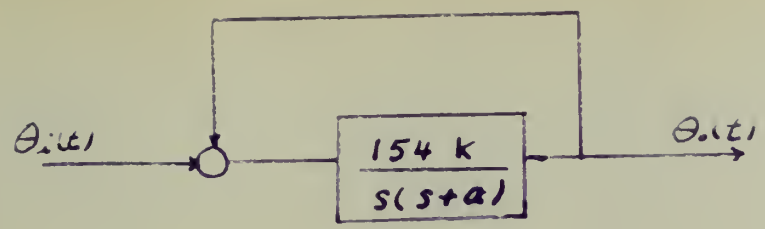

$$F_c = \frac{154k}{s(s+a)+154k}$$

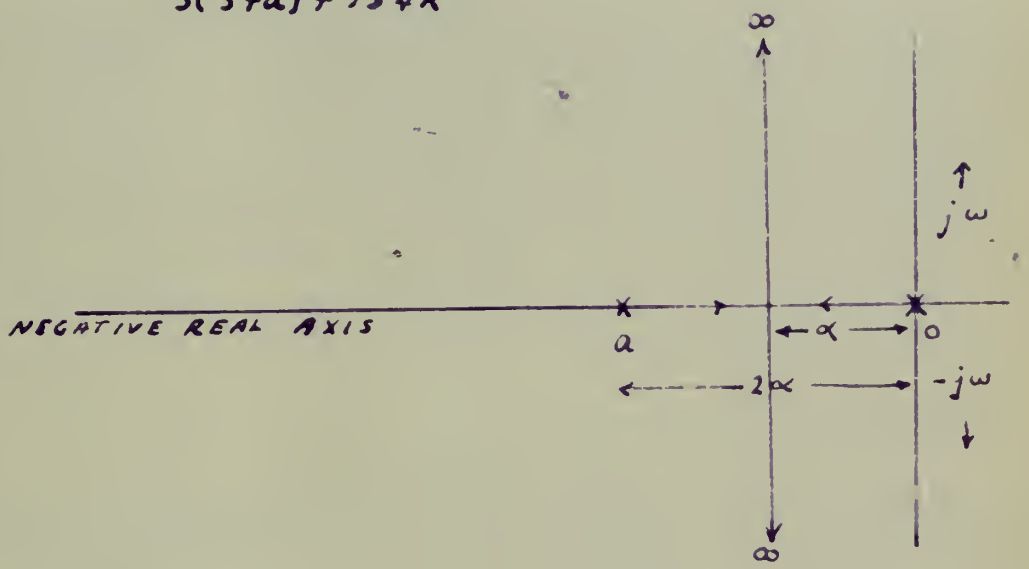

Fig. 16 ROOT LOCUS OF INDIVIDUAL LOOP AS A SECOND ORDER SYSTEM

From the response $\alpha = 14.1$

The motor transfer function then becomes:

$$F_M = \frac{100}{s(s+28.2)}$$

As a further check on the accuracy, a frequency response was performed. The plot of the magnitude M in decibels is shown in Fig. 17. It was originally intended to plot the results on a Nichols chart, transfer these results to a Bodie plot to find the break point or time constant. This was found too

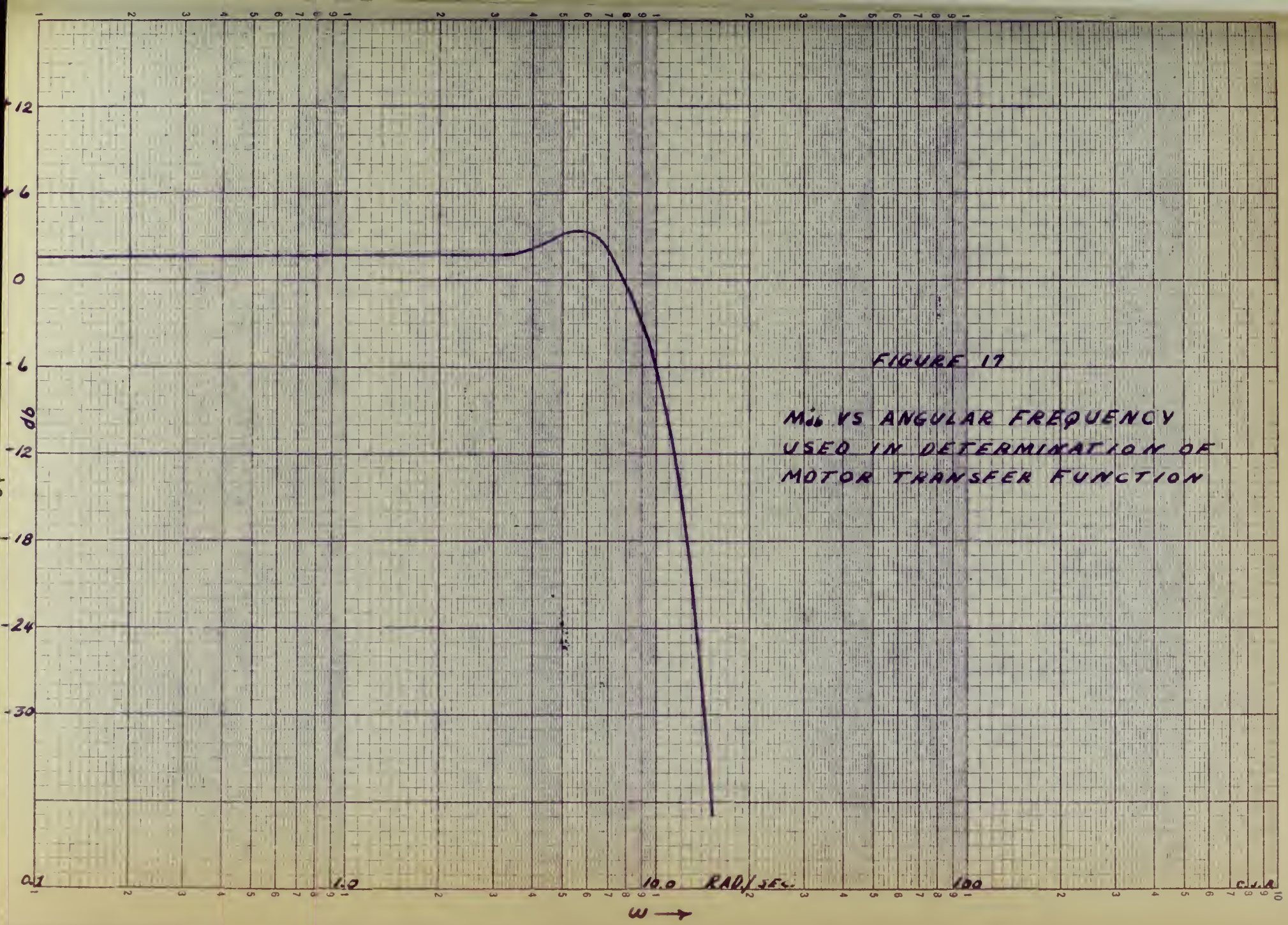

FIGURE 17

M_{db} VS ANGULAR FREQUENCY USED IN DETERMINATION OF MOTOR TRANSFER FUNCTION

impractical because there was enough backlash present to cause the phase angle to shift irrationally. Using the value of Mpw from Fig. 17, second order curves were utilized to determine δ the damping factor. Knowing δ and the natural frequency at which it occured, it was found that

$$\alpha = \delta \omega_n$$
$$\alpha = .37(37.6) = 13.9$$
$$2\alpha = 27.8$$

Averaging the results obtained from the transient and frequency response, it was found that the motor transfer function was:

$$F_M = \frac{74.6}{S(S+28)}$$

This transfer function was used in all the computations and was found to yeild excellant results.

4.3 Derivation of Theoretical Minimum Kv Requirement

The velocity constant requirement was not specified. Since the system under study is a computation mechanism it was imperitive that a realistic minimum value of accuracy required be determined and used as a goal in the analysis. Within reason it would, of course, be desireable to have Kv as large as possible in order to reduce steady state errors, but at the same time the system need not be designed to have greater accuracy than sensing devices within the fire control equipment.

In the submarine fire control problem, bearing rate in the early stages of the approach will generally range between 0-5° per minute (rarely

exceeding 2° per minute). As the submarine and target closes, the bearing rate will increase, depending upon the relative motion of the two and their range. At very close ranges (1000 yards or less) bearing rates may become as high as 60° per minute, although this is rare in typical problems encountered by present-day high speed submarines.

Consider the extreme case which could conceivably be encountered by two very-high speed submarines, each travelling 50 knots on opposite courses, and passing within 1000 yards of one another. Their relative speed is 100 knots (nautical miles per hour) and their range is 0.5 nautical miles.

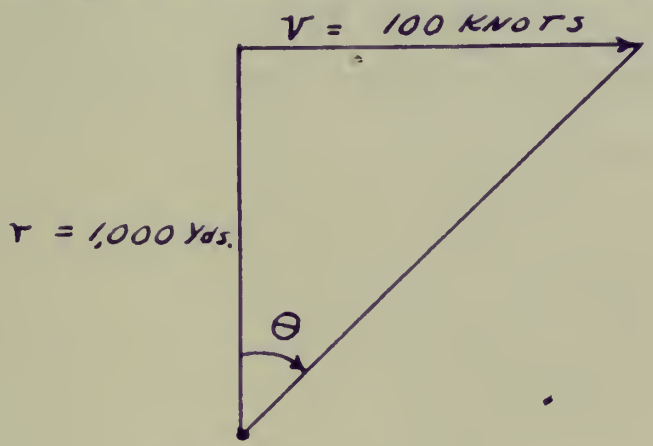

Then: $V = r\dot{\theta}$

V = Velocity

r = Radius

$\dot{\theta}$ = Rate of change of θ

$\dot{\theta} = \frac{V}{r} = \frac{100}{.5}$ = 200 Radians/hour

$$\dot{\theta} = \frac{200 \text{ RADIANS}}{\text{HOUR}} \quad \frac{1 \text{ HOUR}}{3600 \text{ SEC}} = \frac{1 \text{ RAD.}}{18 \text{ SEC.}} = \frac{57.3 \text{ DEG.}}{18 \text{ SEC.}}$$

$$\dot{\theta} = .0555 \text{ RAD/SEC.}$$

Individual components within the computer itself have accuracies generally of the order of 5 minutes or less. If a steady state error to a velocity input of the same magnitude is specified, then from the relationship:

$$\varepsilon_{ss} = \frac{\beta}{K_v}$$

$$K_v = \frac{\beta}{\varepsilon_{ss}} = \frac{3.18 \text{ DEG.}}{5' \text{ MIN.}} \doteq 38$$

This would represent nearly ideal tracking under the most severe conditions likely to be incountered in a submarine fire control problem within the next decade, and is a value toward which it would be desireable to work. Obviously, for the great majority of applications K_v would not have to be nearly as large to obtain 5 minutes or less tracking error.

V. Mathenatical Analysis of the System and Comparison with Observed Data

5.1 Analysis of Individual Loops

Since the four individual servo loops, Gyro Angle, Enabling Run, Weapon Time to Burst, are essentially identical, only one loop will be considered in detail. This is justified by measurements made on the other loops. For illustration let us consider the Gyro Angle Loop. As previously stated in section 4.1, the gain cannot be considered in the conventional manner. The closed loop equivalent circuit is shown in figure 18 below:

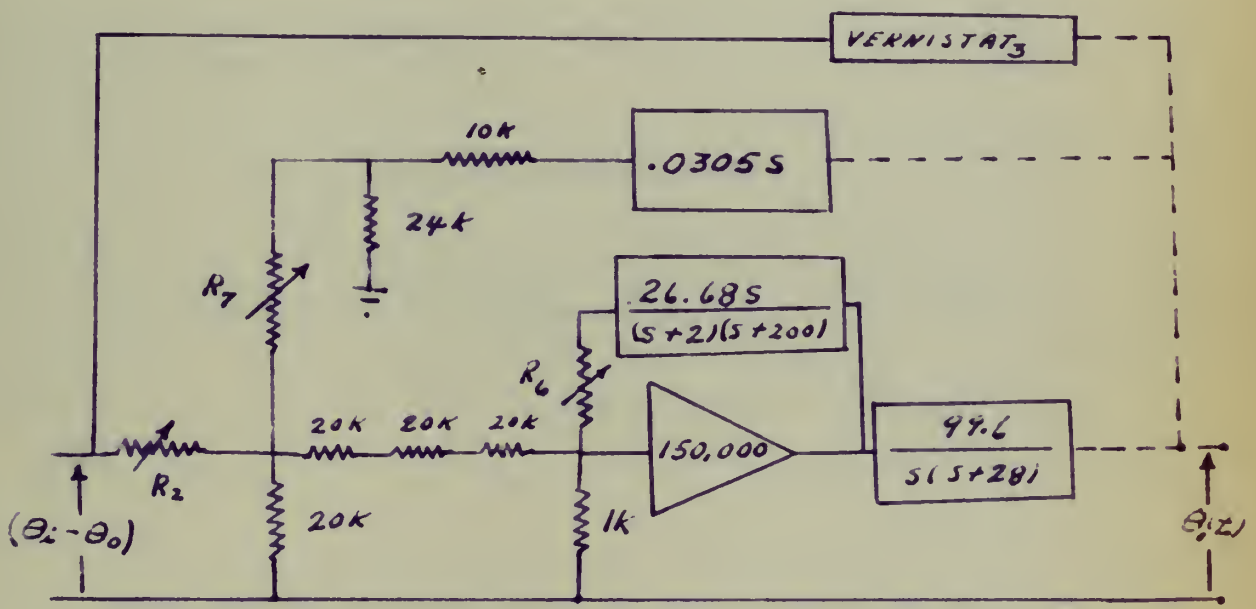

Fig. 18 CLOSED LOOP EQUIVALENT CIRCUIT OF INDIVIDUAL LOOP

It is noted that conventional summing resistors are not necessary. This can best be understood by considering the equivalent circuit of the input and feedback vernistat in figure 19.

[3] See Appendix I

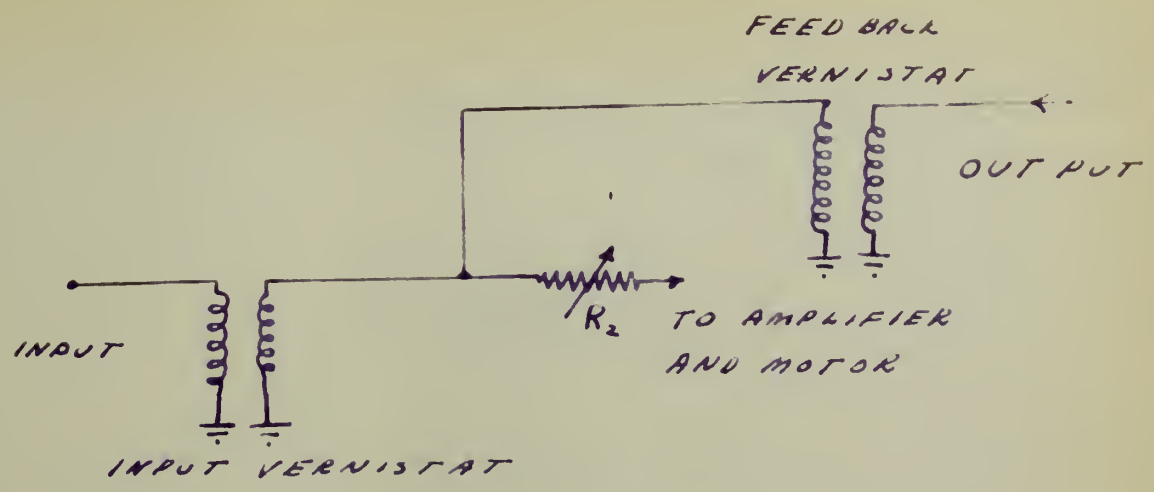

Fig. 19 EQUIVALENT CIRCUIT OF INPUT AND FEEDBACK VERNISTAT

Further simplifying:

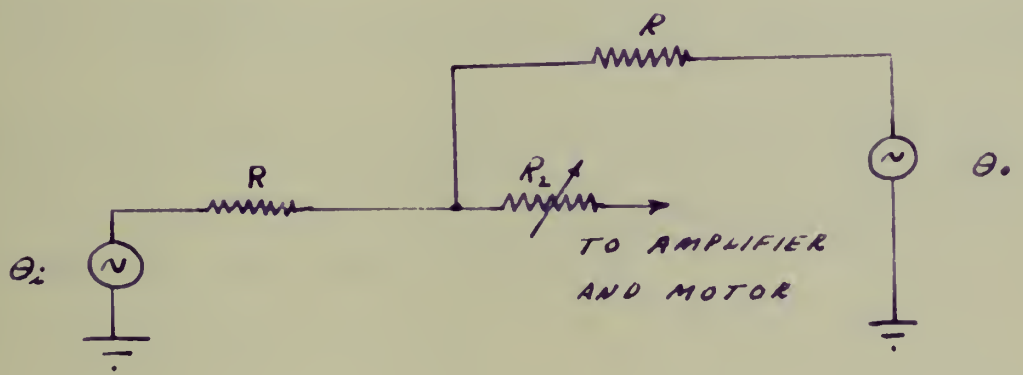

Since the reference voltage is variable and $R_2 >> R$ the circuit can be arranged in this manner.

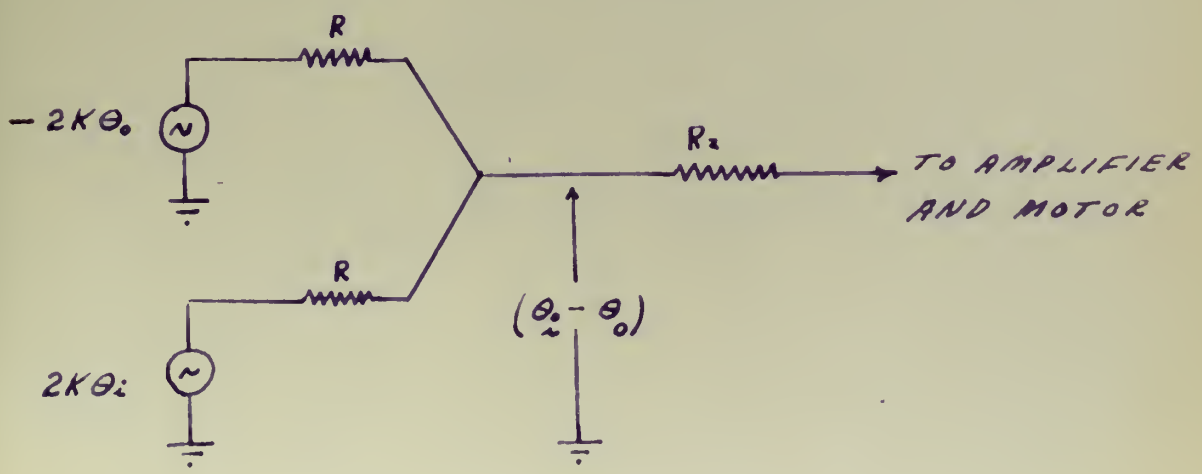

It is convenient to derive the transfer function of the circuit comprising the amplifier and integral damping network, figure 20, prior to proceeding with the analysis.

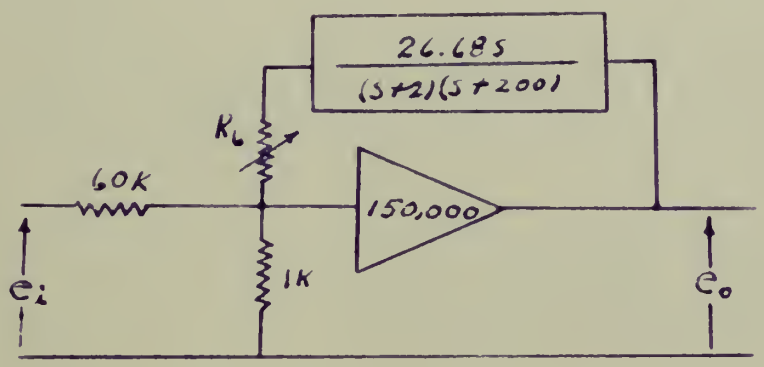

Fig. 20 EQUIVALENT CIRCUIT OF AMPLIFIER AND INTEGRAL DAMPING NETWORK

Breaking the circuit in this manner is justified since neglecting the shunting effect of 60K and R_6 = 3 megohms results in less error than incurred in assumed values of components.

The resulting block diagram is:

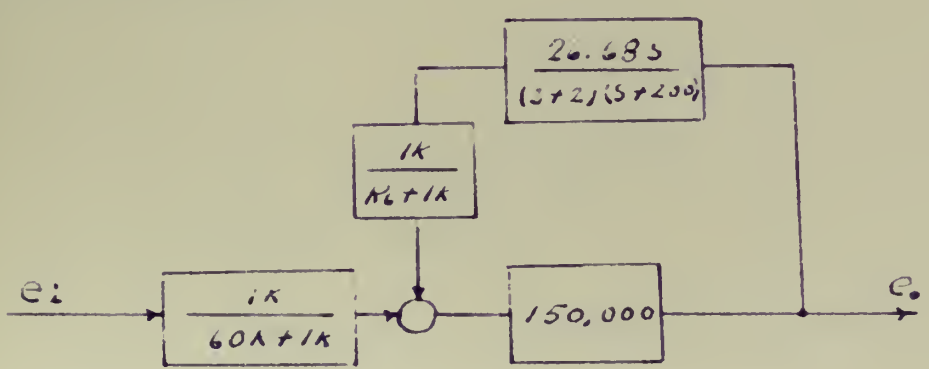

Simplifying:

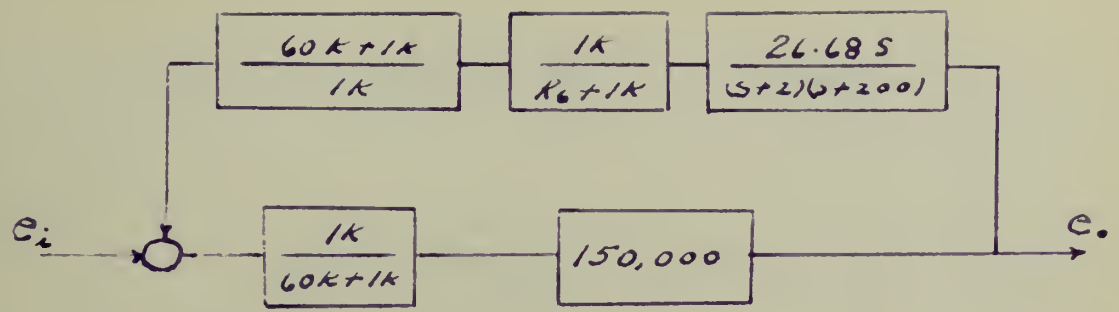

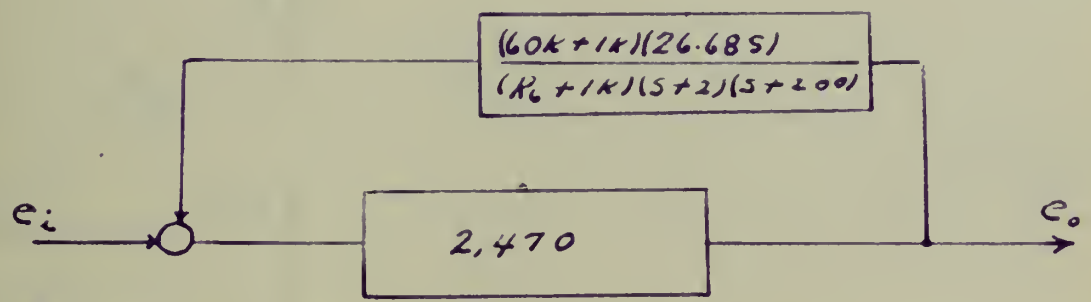

$Fc_A \triangleq$ closed loop transfer function of the Amplifier.

$$Fc_A = \frac{\frac{2,470}{\frac{150,000\,(26.68S)1K}{\frac{K_6+1K}{(S+2)(S+200)}}}}{1 + \frac{\frac{2,470}{\frac{150,000\,(26.68S)1K}{\frac{K_6+1K}{(S+2)(S+200)}}}}{1}}$$

$$Fc_A = \frac{2,470\,(S+2)(S+200)}{(S+2)(S+200) + \left[\frac{150,000(1K)}{K_6+1K}\right]\left[26.68S\right]} \qquad (5.1)$$

The Root Locus Equation is:

$$-1 = \frac{\left(\frac{150,000\,(26.68)1K}{K_6+1K}\right)}{(S+2)(S+200)} \qquad (5.2)$$

$$K_R = \left(\frac{150,000}{K_6+1K}\right) 26.68(1K) \triangleq \text{ROOT LOCUS GAIN}$$

The close loop transfer function of the amplifier network will ther have the form: $Fc_A = \frac{2,470(S+2)(S+200)}{(S+a)(S+b)}$

The equivalent circuit of the entire loop then becomes:

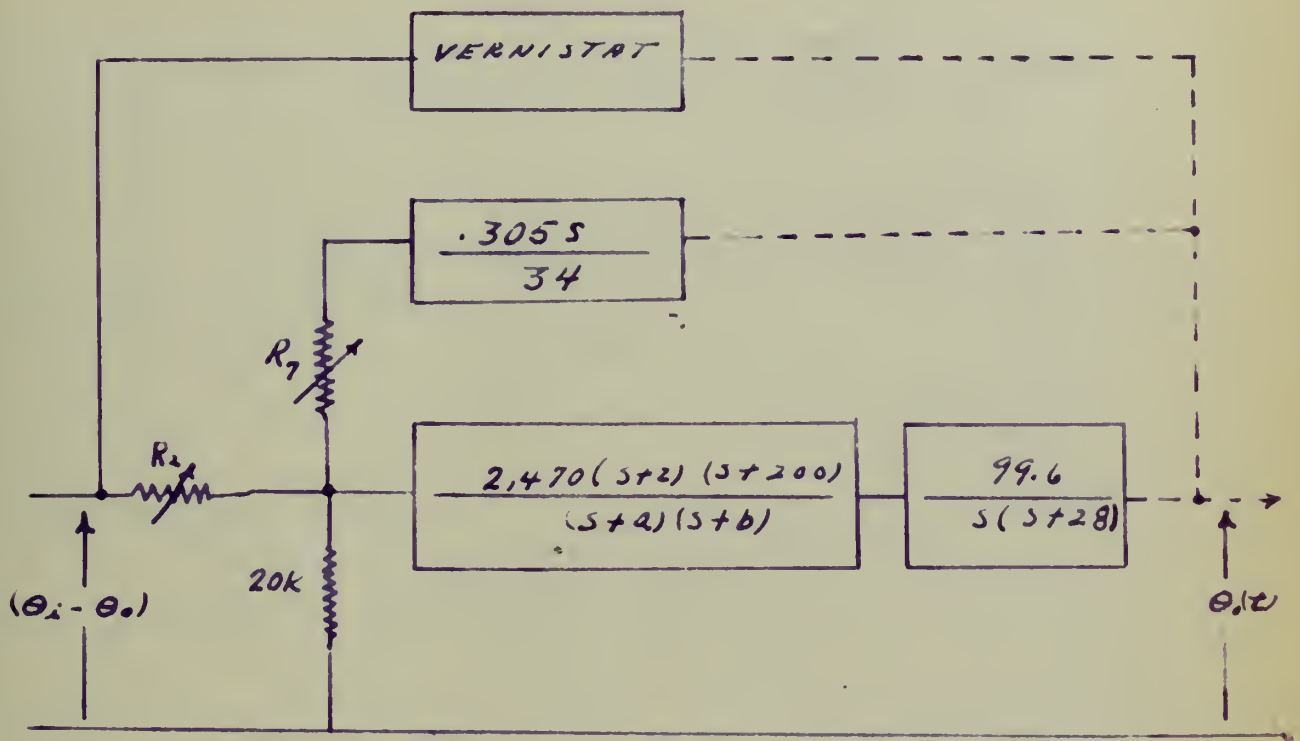

The block diagram representation is:

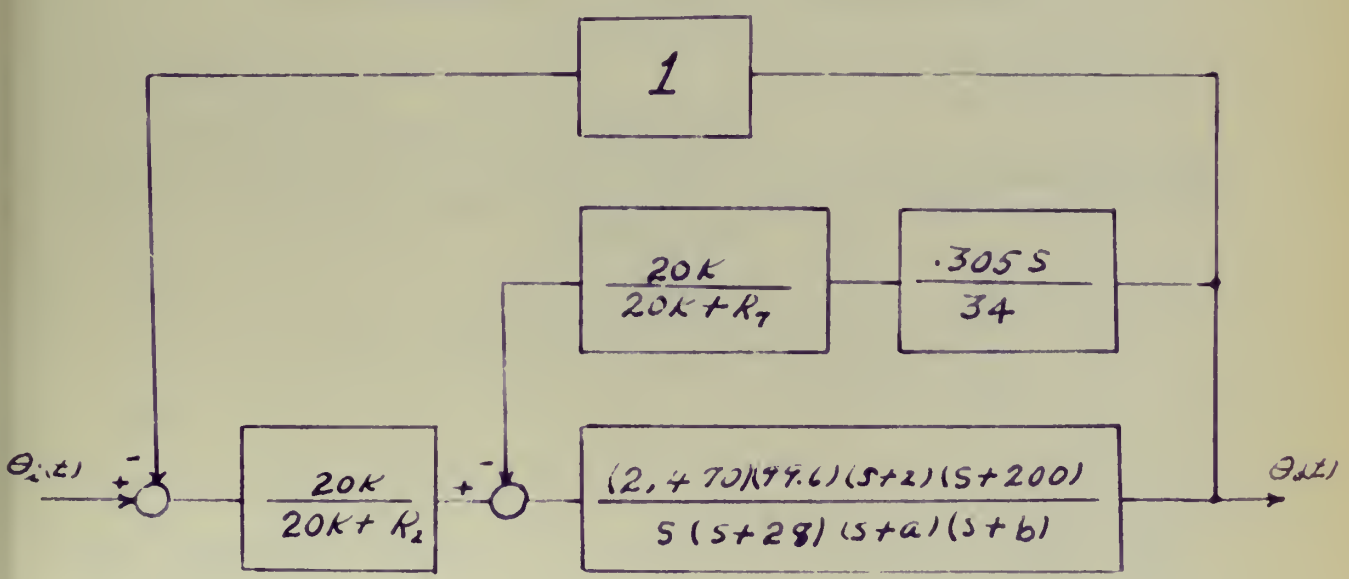

By block diagram manipulation:

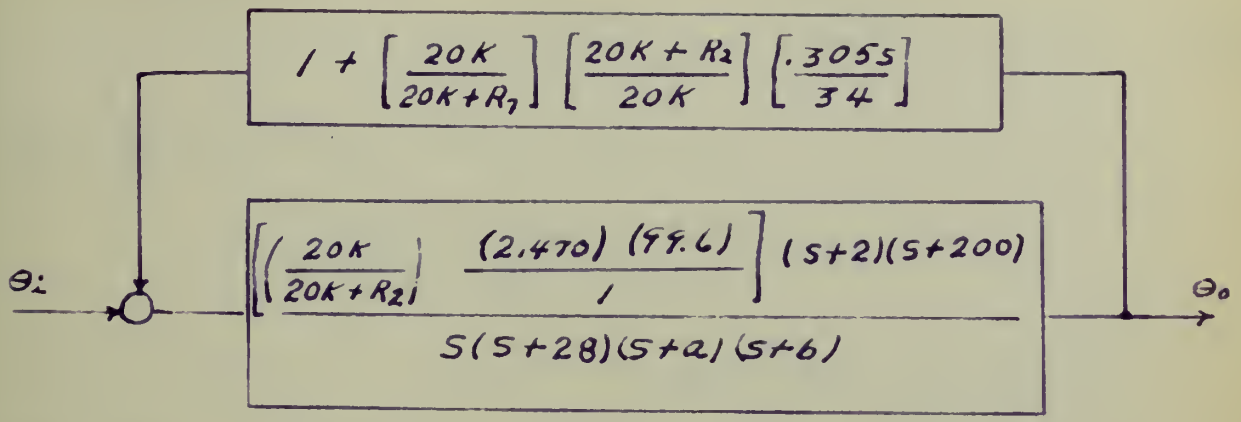

This simplifies to figure 21.

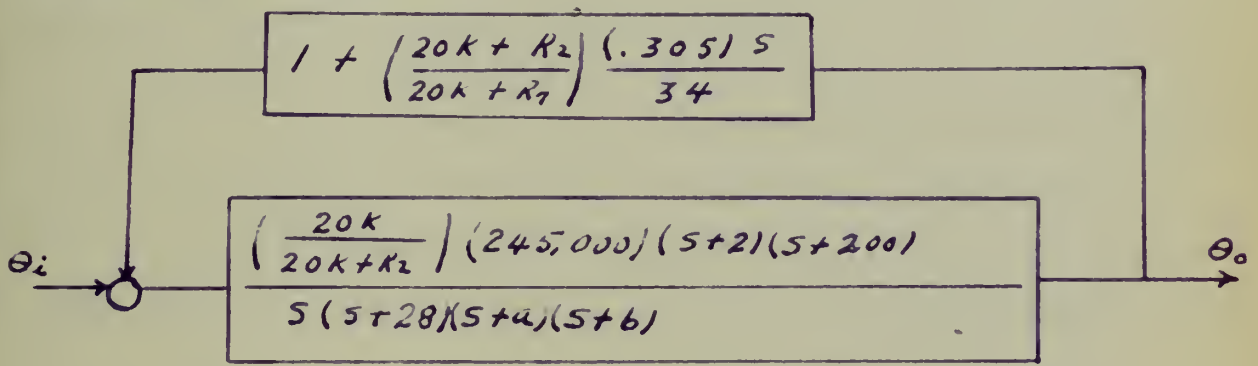

Fig. 21 REDUCED BLOCK DIAGRAM OF INDIVIDUAL LOOP

$$F_c = \frac{\left(\frac{20K}{20K+R_2}\right)(245,000)(S+2)(S+200)}{S(S+28)(S+a)(S+6)\left[\left(\frac{20K}{20K+R_2}\right)(245,000)(20K+R_2)(.305)\right]}$$

$$X \frac{1}{(S+2)(S+200)\,S + \frac{1}{.305(20K+R_2)}}$$

The root locus equation is:

$$\frac{(.305)(20K)(245K)}{34(20K)R_1}\left[(S+2)(S+200)\left(S + \frac{34(20K+R_1}{(20K+R_2)(.305}\right)\right] = -1$$
$$S(S+28)(S+a)(S+6)$$

Simplifying:

$$\frac{2200\left(\frac{20k}{20k+R_7}\right)(S+2)(S+200)(S+115.5)\left(\frac{20k+R_7}{20k+R_2}\right)}{S(S+28)(S+a)(S+b)} = -1 \qquad (5.4)$$

The closed loop function will have the form:

$$F_c = \frac{\frac{20k}{20k+R_2}(245k)(S+2)(S+200)}{(S+c)(S+d)(S+e)(S+f)}$$

It can be seen from the above equations that varying R_2 and R_7 varies the location of the zero due to the tachometer and simultaneously R_7 varies the root locus gain. It can be seen that within limits many settings of R_2 and R_7 will give identical results.

Since R_2 and R_7 enter into gain as well as zero location, the conventional method of considering a given pole-zero configeration and varying the gain to determine optimum response cannot be used. Further, if a composit open loop transfer function is obtained, it can be seen that these factors also enter into the computation of the Velocity Constant, K_v.

Using the relationship $F_o = \frac{N_c}{D_c - N_c}$ the open loop function is:

$$F_o = \frac{\left(\frac{20k}{20k+R_2}\right)(245k)(S+2)(S+200)}{\left\{\begin{array}{l}(S+28)\left[(S+2)(S+200) + 4\times10^4\left(\frac{1k}{R_c+1k}\right)S\right] \\ +\left(\frac{(.305)(20k)}{34(20k+R_7)}\right)(245k)(S+2)(S+200)\end{array}\right\}}$$

$$K_v = \lim_{S\to 0} S\,F_o$$

$$K_v = \frac{\left(\frac{20k}{20k+R_2}\right)(245k)(2)(200)}{28\left[(2)(200) + 0\right] + \left(\frac{.305(20k)}{34(20k+R_7)}\right)(245k)(2)(200)}$$

It is seen that three equations involving the two qualities, response and velocity constant, can be easily written.

$$K_K\,(\text{ROOT LOCUS GAIN}) = 2200\left(\frac{20k}{(20k+R_7)}\right)$$

$$R_7 = \frac{2200\,(20k)}{K_K} - 20k$$

$$Z_K\,(\text{ZERO DUE TO TALK}) = 111.5\left(\frac{20k+R_7}{20k+R_2}\right)$$

$$R_7 = \frac{20k+R_2}{111.5}\,Z_K - 20k$$

$$K_v = \frac{(245k)\,\dfrac{(20k+R_7)}{(20k+R_2)}}{\dfrac{28(20k+R_7)}{20k} + 2200}$$

$$R_7 = \frac{4900k^2 - K_v\left[44,560k + 2,228R_2\right]}{-245k + K_v\left[28 + \dfrac{28R_2}{20k}\right]}$$

Since the system cannot be optimumized by varying gain, a plot of these three equations will provide a criteria for choosing values of resistance for optimum response and maximum velocity constant.

From figures 22 and 23 it can be seen that a near optimum selection of resistance is $R_2 = 300k$ and $R_7 = 100k$. It is noted that these values give Kv in excess of the minimum derived in 4.3.

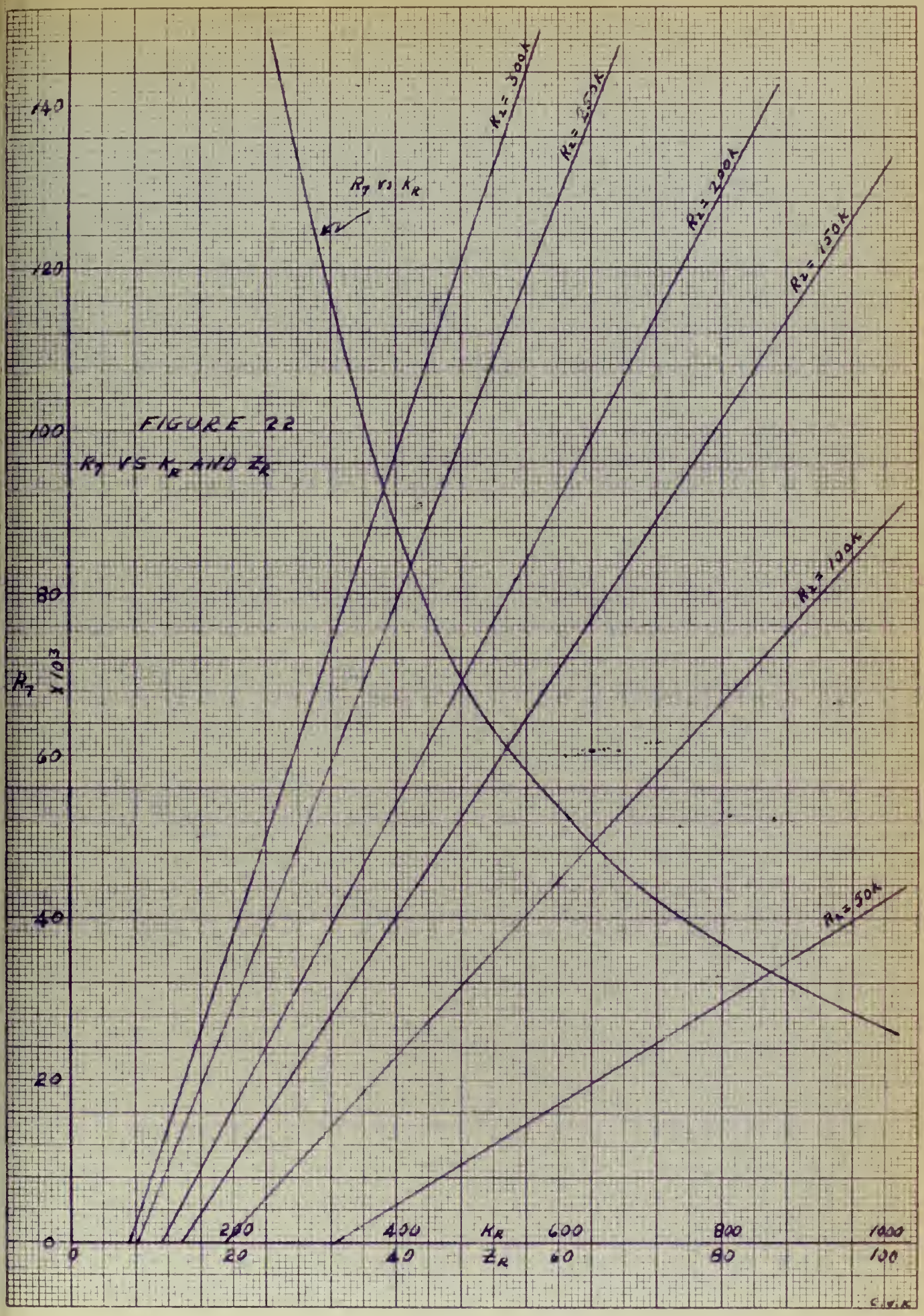

FIGURE 22

K_T VS K_R AND Z_R

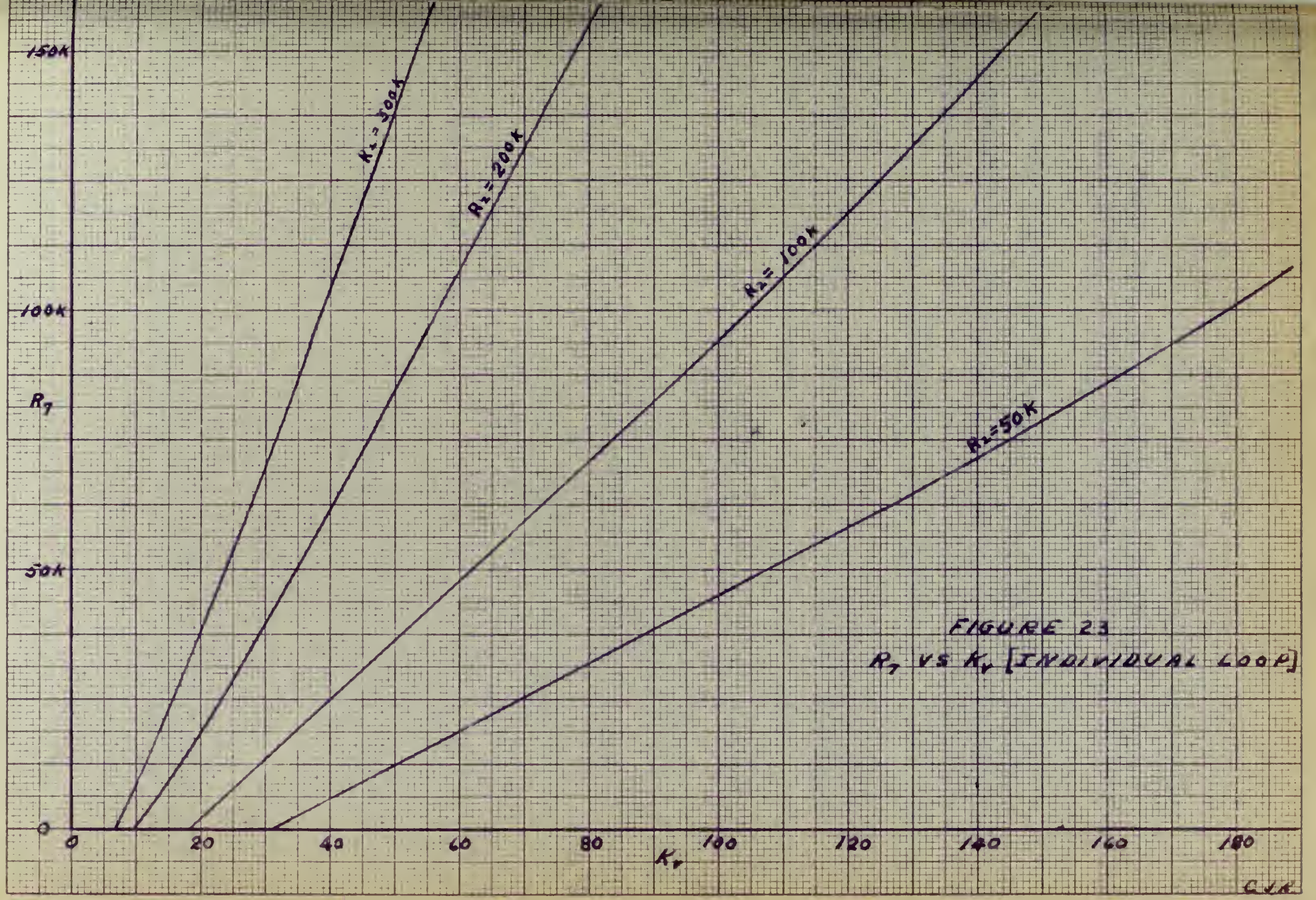

FIGURE 23
R_7 VS K_r [INDIVIDUAL LOOP]

With these values fixed, consider the loop in three configerations:

1. Single loop - Unity, tachometer, and integral-damp feedback
2. Single loop - Unity, and tachometer feedback
3. Single loop - Unity, and integral feedback

5.2 Single Loop - Unity, Tachometer, and Integral-damp Feedback

Substituting $R_2 = 300$ K , $R_7 = 100$ K , and $R_6 = 3$ Megohms equation (5.1) becomes:

$$F_{c_A} = \frac{150,000\,(S+2)(S+200)}{(S+2)(S+200) + 13345}$$

Equation (5.2), the root locus equation of the amplifier and Integral-damp feedback network becomes:

$$-1 = \frac{1334\,S}{(S+2)(S+200)}$$

$$F_{c_A} = \frac{2,470\,(S+2)(S+200)}{S^2 + 1536S + 400}$$

$$F_{c_A} = \frac{2,470\,(S+2)(S+200)}{(S+1536)(S+.26)}$$

The resulting block diagram is:

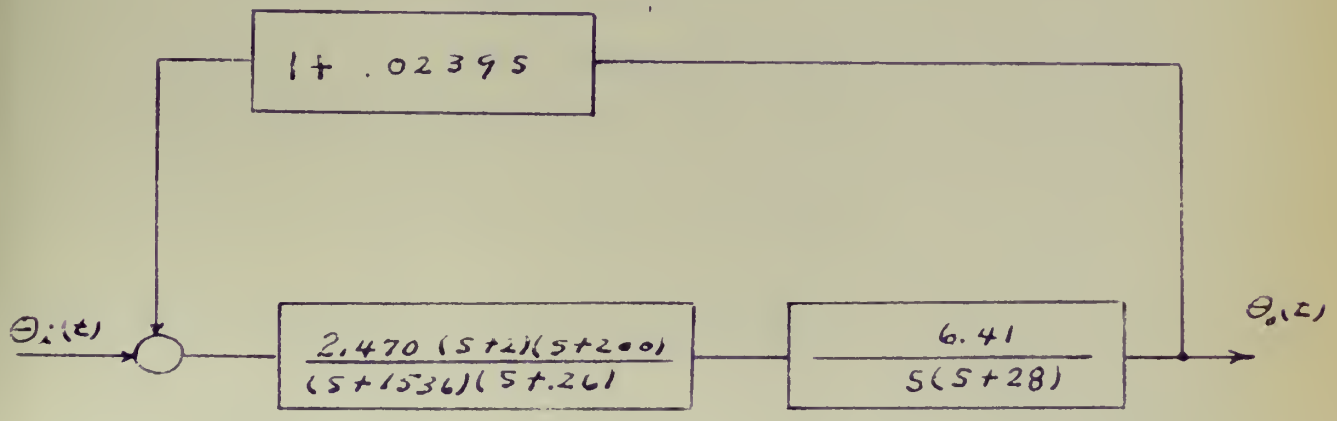

Equation (5.3) becomes:

$$F_c = \frac{(15,300)(S+2)(S+200)}{S[(S+28)(S+.26)(S+1536)+367(S+2)(S+200)]+15,300(S+2)(S+200)}$$

Simplifying:

$$F_c = \frac{15,300(S+2)(S+200)}{S^4+1931S^3+132,442S^2+3,248,600S+6,120,000} \qquad (5.4)$$

Equation (5.4), the final root locus or characteristic equation of the loop is:

$$-1 = \frac{367(S+2)(S+200)(S+41.9)}{S(S+28)(S+1536)(S+.26)}$$

The root locus plot is shown in figure 24. The roots are determined from K versus the real roots in figure 25.

The real roots were determined to be S = - 1862 and S = - 2.0332 . From the characteristic equation, denominator of equation (5.4), the coefficent of the second highest term is 1931 and the constant term is 6,120,000. Proceeding as outlined in section 3.3:

$$1862 + 2.0332 + (\alpha + j\omega_c) + (\alpha - j\omega_c) = 1931$$

$$2\alpha = 65.95$$

$$\alpha = 33.0$$

$$(1862)(2.0332)(33+j\omega_c)(33+j\omega_c) = 6,120,000$$

$$\omega_c = 22.65$$

The factored closed loop function then becomes:

$$F_c = \frac{15,300(S+2)(S+200)}{(S+2.0332)(S+1862)(S+33+j22.65)(S+33-j22.65)}$$

$$F_o = \frac{367\,(S+2)(S+200)(S+41.9)}{S(S+28)(S+1536)(S+.26)}$$

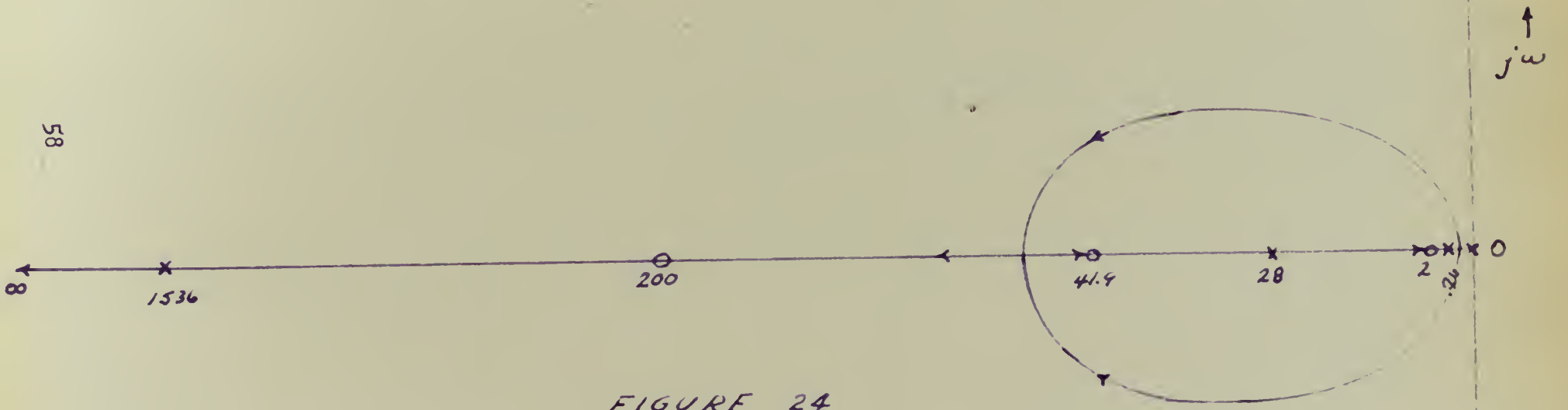

FIGURE 24

ROOT LOCUS PLOT FOR INDIVIDUAL LOOP WITH UNITY, INTEGRAL- DAMPING AND TACHOMETER FEEDBACK

NOT TO SCALE

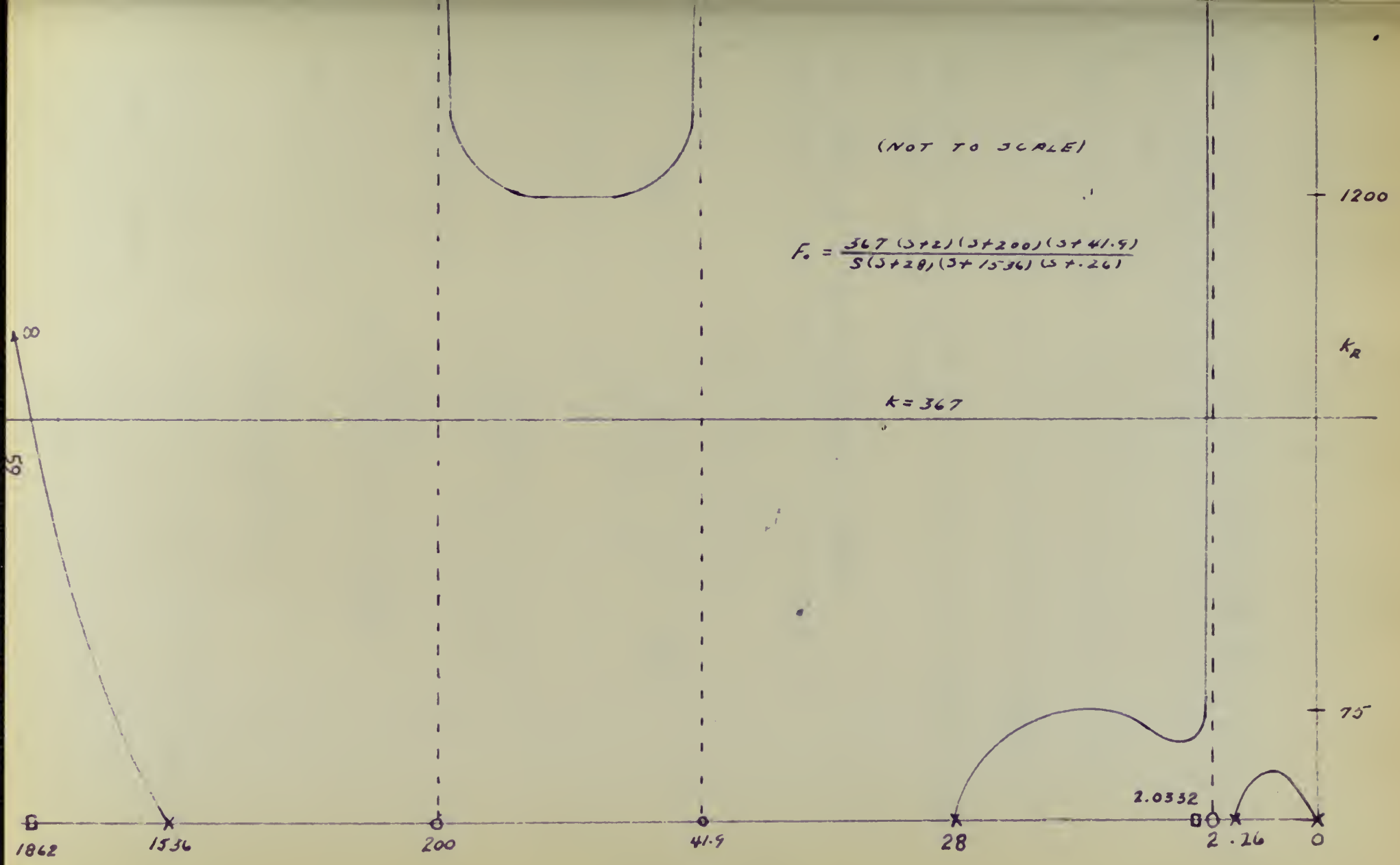

FIGURE 25

ROOT LOCUS GAIN VERSUS REAL ROOTS OF INDIVIDUAL LOOP WITH UNITY, INTEGRAL-DAMPING AND TACHOMETER FEEDBACK

The response to a unit step input is:

$$\overline{\theta_o(t)} = \frac{15,300\,(S+2)(S+200)}{(S+2.0332)(S+1862)(S+33+j\,22.65)(S+33-j\,22.65)}\left(\frac{1}{S}\right)$$

The inverse Laplace transform yeilds:

$$\theta_o(t) = 1 + .018\ \epsilon^{-2.0332t} + .005\ \epsilon^{-1862t} + 1.525\ \epsilon^{-33t}\ SIN(22.65t - 137.8°)$$

Figure 26 shows predicted θ_o as a function of time. Figure 27 shows the measured response obtained.

3.2 Single Loop - Unity and Tachometer Feedback

Removing the integral-damp network, the block diagram is:

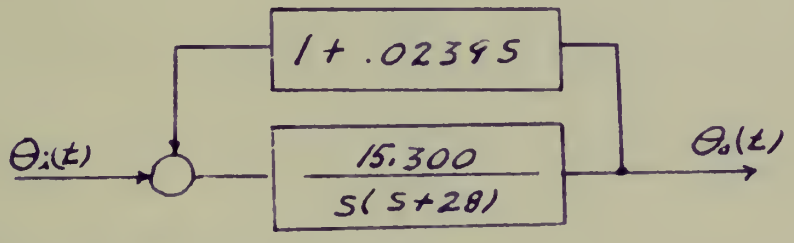

The closed loop transfer function is:

$$F_c = \frac{15,300}{S(S+28) + 367(S+41.9)}$$

Simplified becomes:

$$F_c = \frac{15,300}{S^2 + 395\,S + 15,300}$$

The root locus equation is:

$$-1 = \frac{367(S+41.9)}{S(S+28)}$$

The root locus is shown in figure 28. The Root Locus Gain versus Real is shown in figure 29.

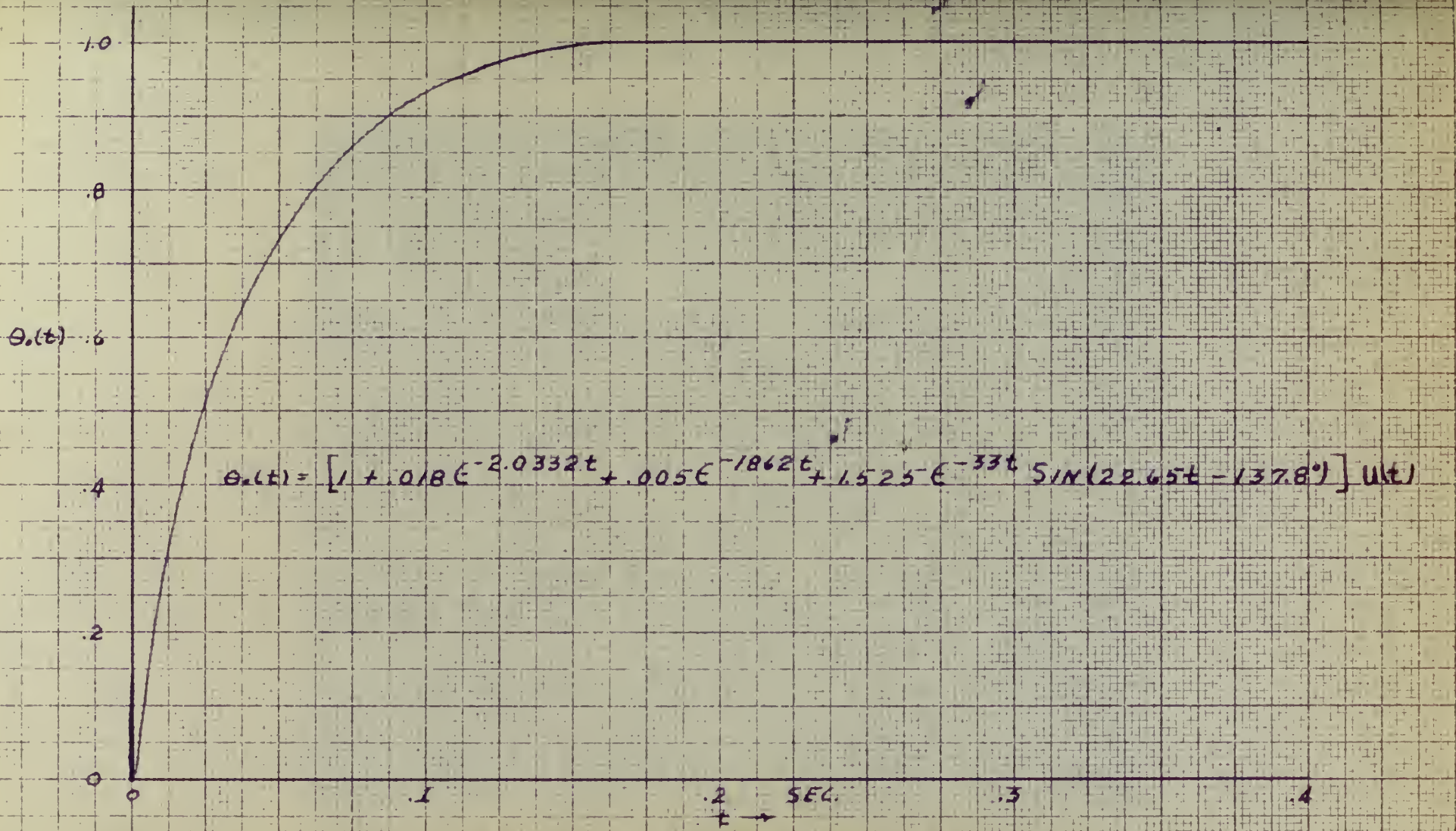

FIGURE 26

PREDICTED RESPONSE OF INDIVIDUAL LOOP, TO A STEP INPUT USING OPTIMUM VALUES OF INPUT RESISTANCE WITH UNITY, INTEGRAL-DAMPING, AND TACHOMETER FEEDBACK

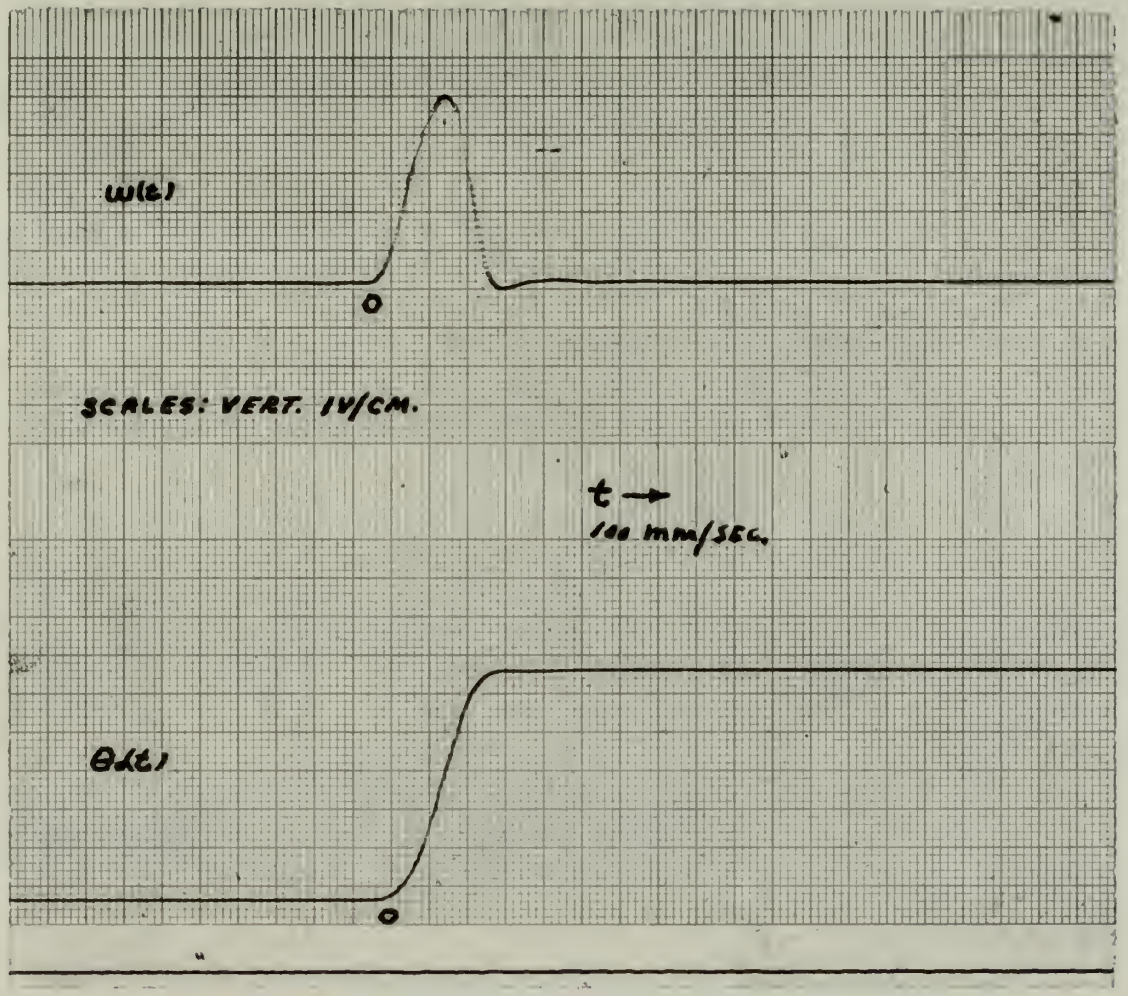

FIGURE 27

MEASURED RESPONSE OF INDIVIDUAL LOOPS, TO A STEP INPUT,
USING OPTIMUM VALUES OF INPUT RESISTANCE
WITH UNITY, INTEGRAL DAMPING AND TACHOMETER FEEDBACK

FIGURE 28

ROOT LOCUS PLOT FOR INDIVIDUAL LOOP
WITH UNITY AND TACHOMETER FEEDBACK

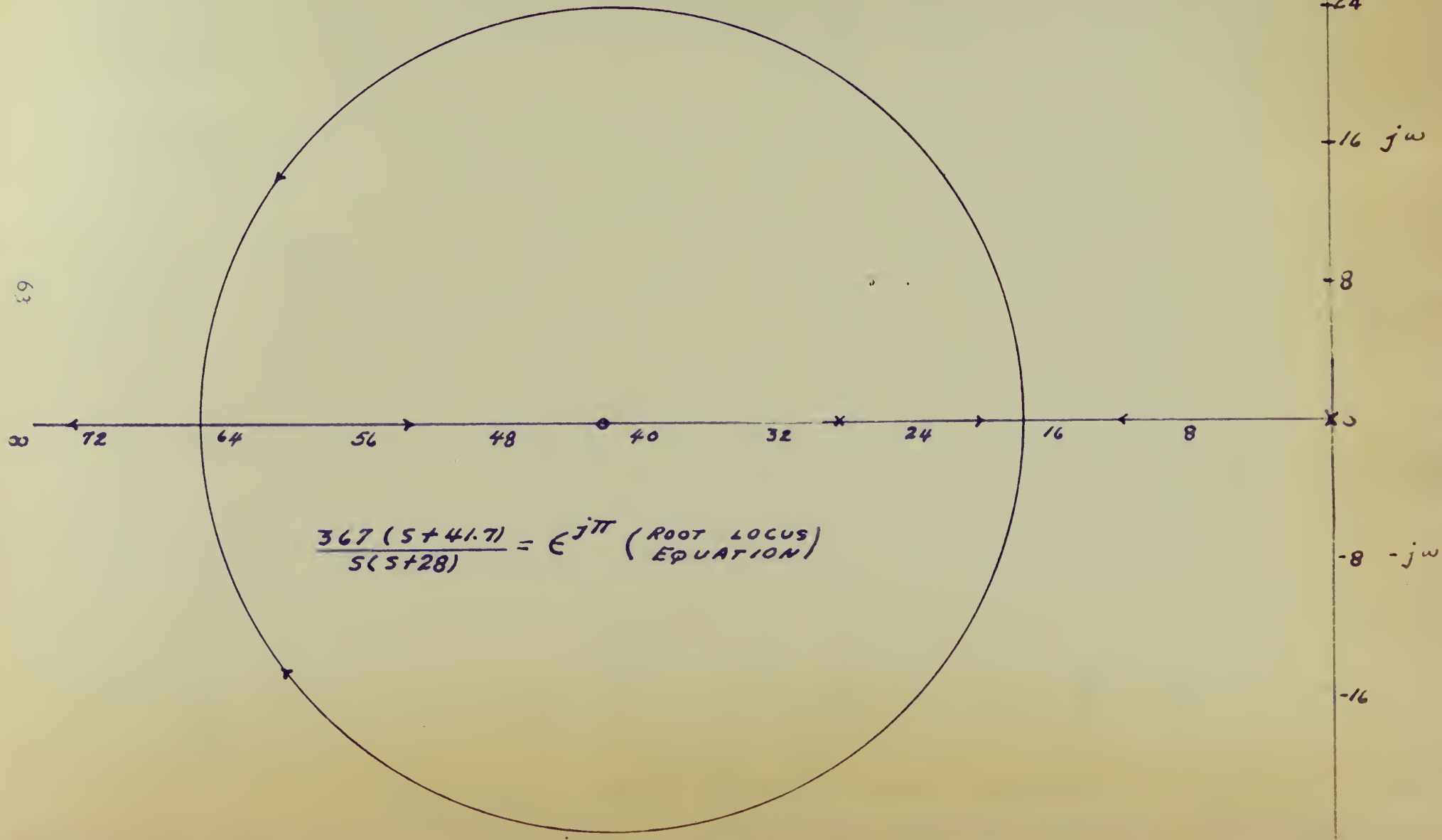

$$\frac{367(S+41.7)}{S(S+28)} = \epsilon^{j\pi} \quad \text{(ROOT LOCUS EQUATION)}$$

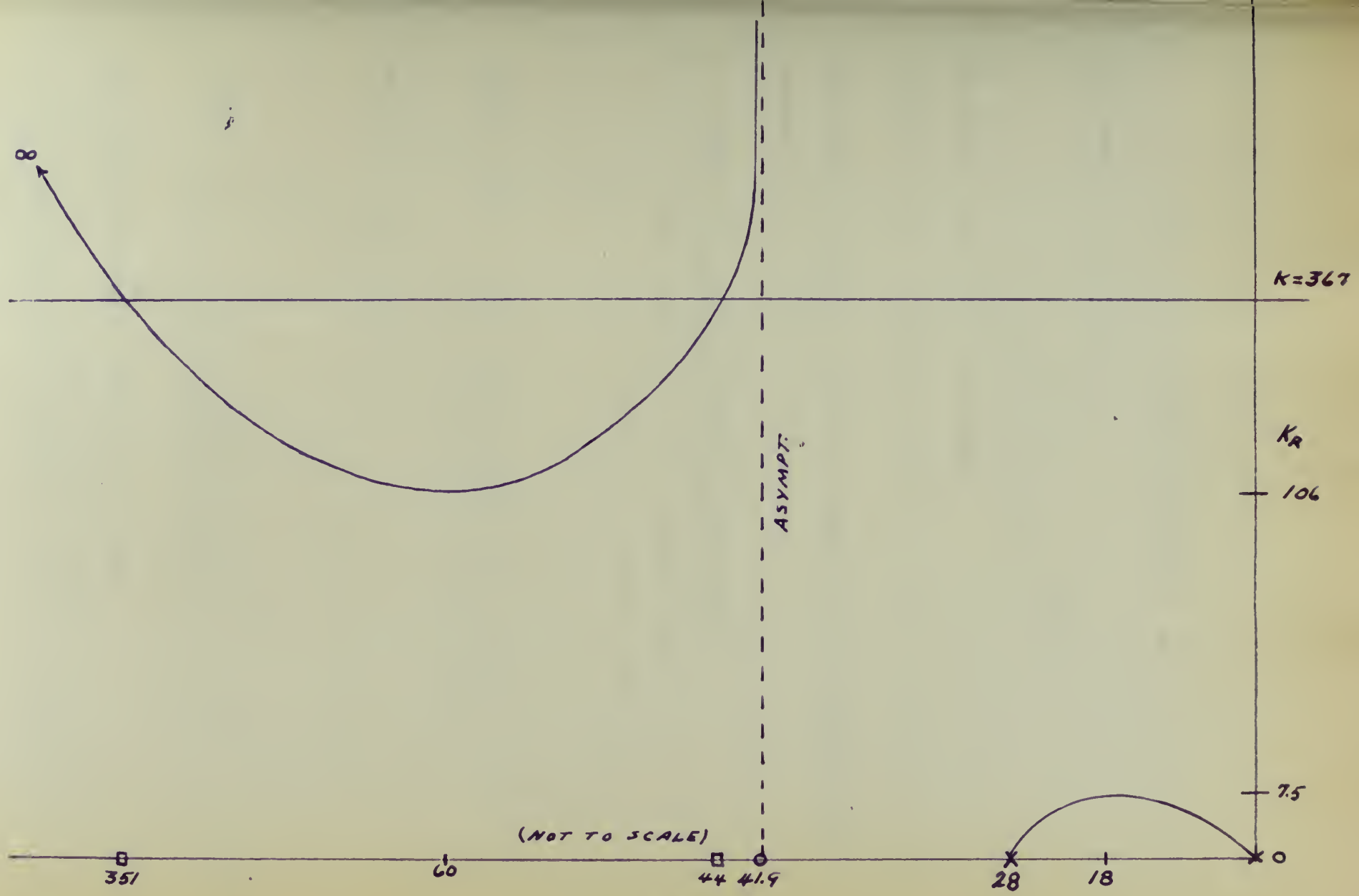

FIGURE 29

ROOT LOCUS GAIN VERSUS REAL ROOTS
OF INDIVIDUAL LOOP WITH UNITY AND TACHOMETER FEEDBACK

The factored closed loop transfer function is :

$$F_c = \frac{15,300}{(S+441)(S+351)}$$

The response to a unit step is:

$$\theta_o(S) = \frac{15,300}{(S+44)(S+351)}\left(\frac{1}{S}\right)$$

The inverse Laplace transform yields:

$$\theta_o(t) = \left[1 + 1.132\, \epsilon^{-44t} + .132\, \epsilon^{-351t}\right] u(t)$$

The predicted output as a function of time is shown in figure 30. The measured response is shown in figure 31.

3.3 Single Loop - Unity and Integral-damp Feedback

With no tachometer feedback, the block diagram becomes:

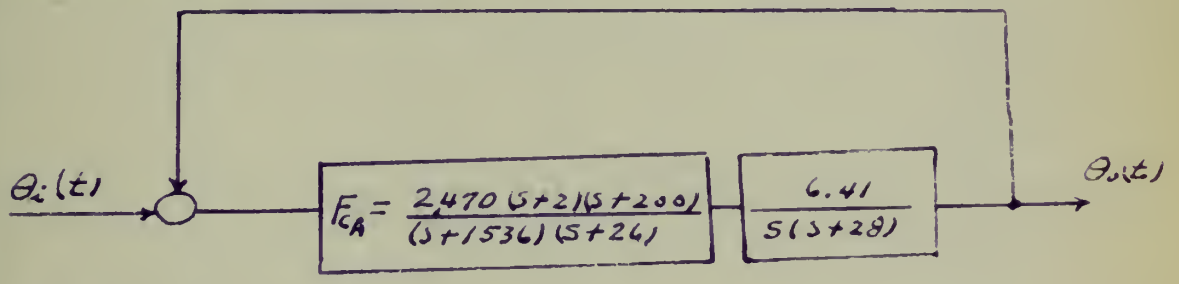

The block diagram simplifies to:

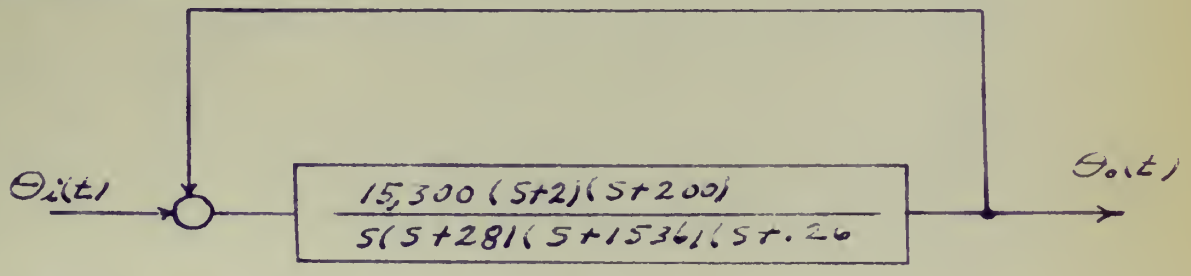

The closed loop transfer function then becomes:

$$F_c = \frac{15,300\,(S+2)(S+200)}{S(S+28)(S+.26)(S+1536) + 15,300(S+2)(S+200)}$$

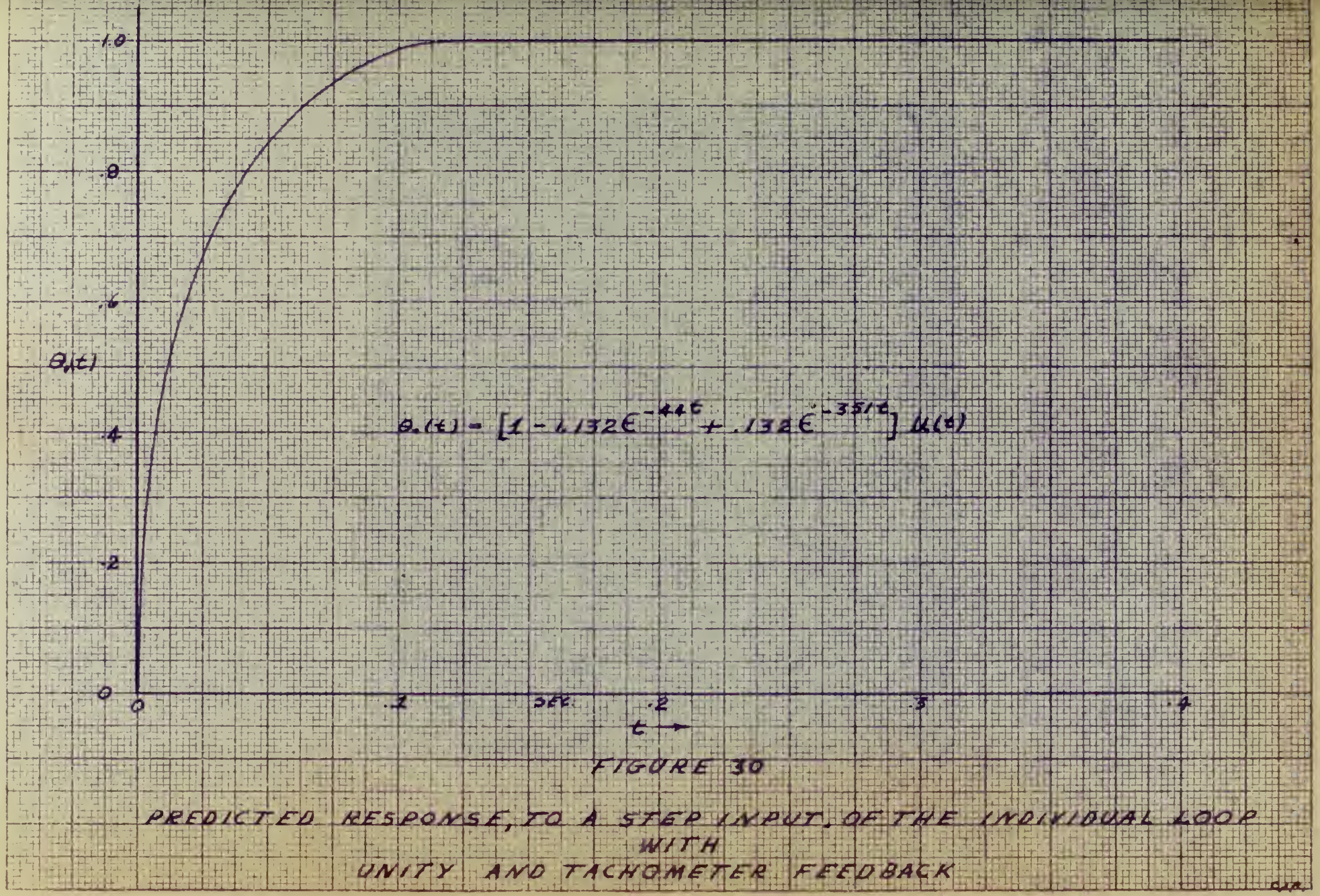

FIGURE 30

PREDICTED RESPONSE, TO A STEP INPUT, OF THE INDIVIDUAL LOOP WITH UNITY AND TACHOMETER FEEDBACK

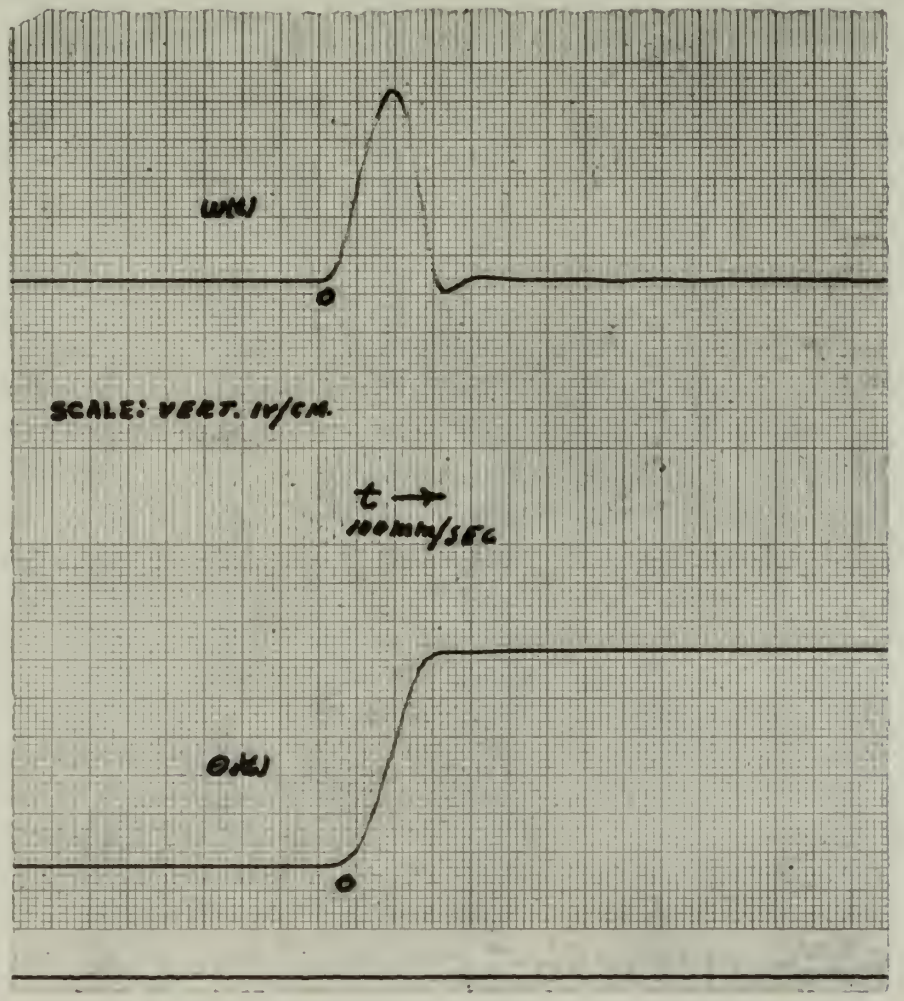

FIGURE 31

MEASURED RESPONSE, TO A STEP INPUT, OF THE INDIVIDUAL LOOP WITH UNITY AND TACHOMETER FEEDBACK

Simplified:

$$F_c = \frac{15,300\ (S+2)(S+200)}{S^4 + 156\,4S^3 + 58,308\,S^2 + 3,101,800S + 6,120,000}$$

The root locus equation is:

$$\frac{15,300\ (S+2)(S+200)}{S(S+28)(S+1536)(S+.26)} = -1$$

The root locus plot is shown in figure 32. The plot of K versus Real Roots is shown in figure 33. The factored closed loop transfer function is:

$$F_c = \frac{15,300\ (S+2)(S+200)}{(S+2.044)(S+1524)(S+16.44+j\,41.8)(S+16.44-j\,41.8)}$$

The response to a unit step is given by:

$$\theta_o(S) = \frac{15,300\ (S+2)(S+200)}{(S+2.044)(S+1524)(S+16.44+j\,41.8)(S+16.44-j\,41.8)}$$

The inverse Laplace transform yields:

$$\theta_o(t) = \left[\begin{array}{l} 1 + .01645\ \epsilon^{-2.044t} + .00578\ \epsilon^{-1524t} \\ + 1.02\ \epsilon^{-16.44t}\ SIN(44.8t - 98.7°) \end{array}\right] u(t)$$

The predicted output as a function of time is shown in figure 34. The measured response is shown in figure 35.

5.2 Qualitative Stability and Performance Analysis of Overall System

Section 3.1 outlines the Determinantal Method of analysis used in reducing the functional diagram, figure 36, to the configeration shown in figure 37.

It is noted that the Torpedo Lead angle Loop is inherently non-linear because of the resolver which is used for a function generator and a

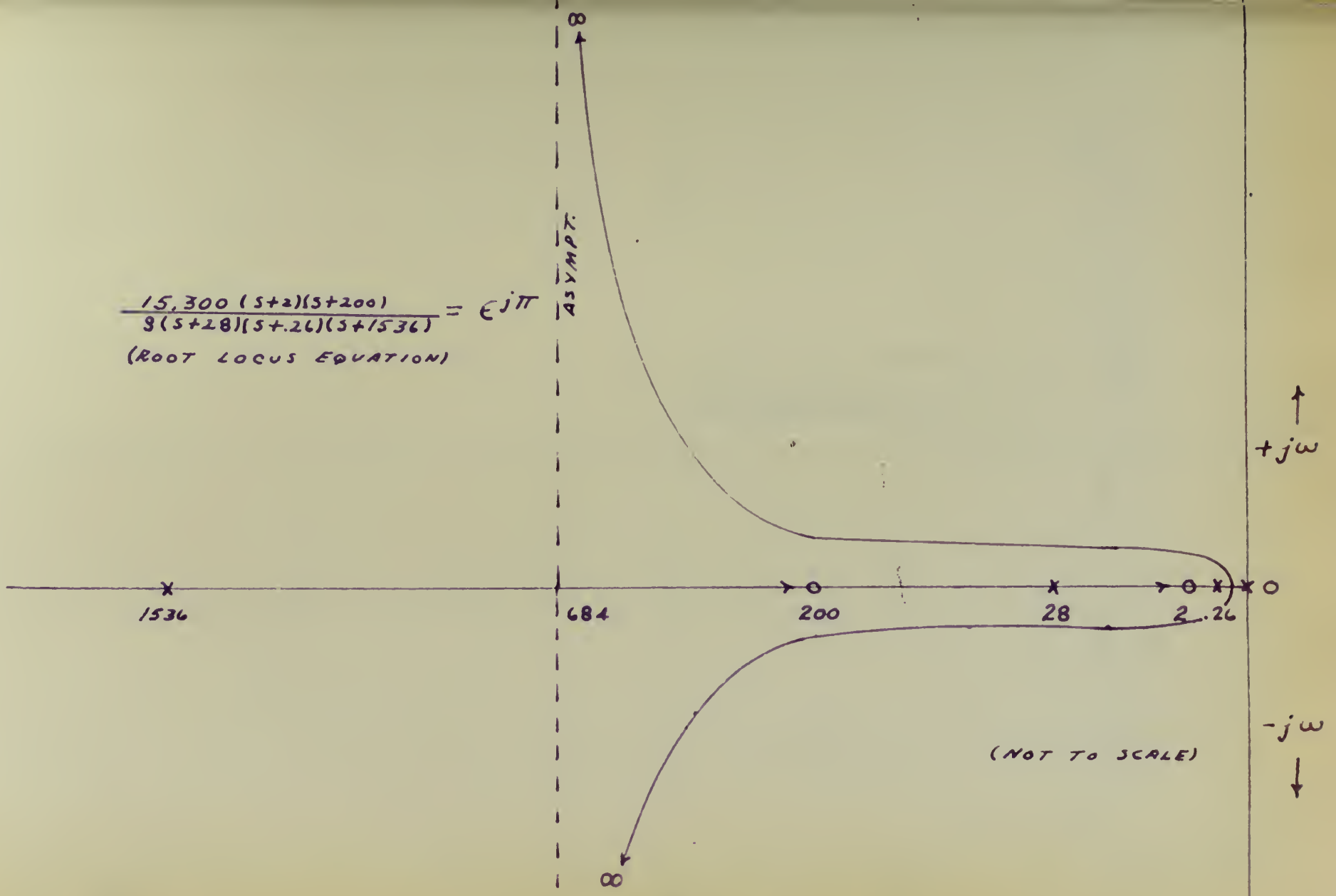

FIGURE 32

ROOT LOCUS PLOT OF INDIVIDUAL LOOP
WITH UNITY AND INTEGRAL-DAMPING FEEDBACK

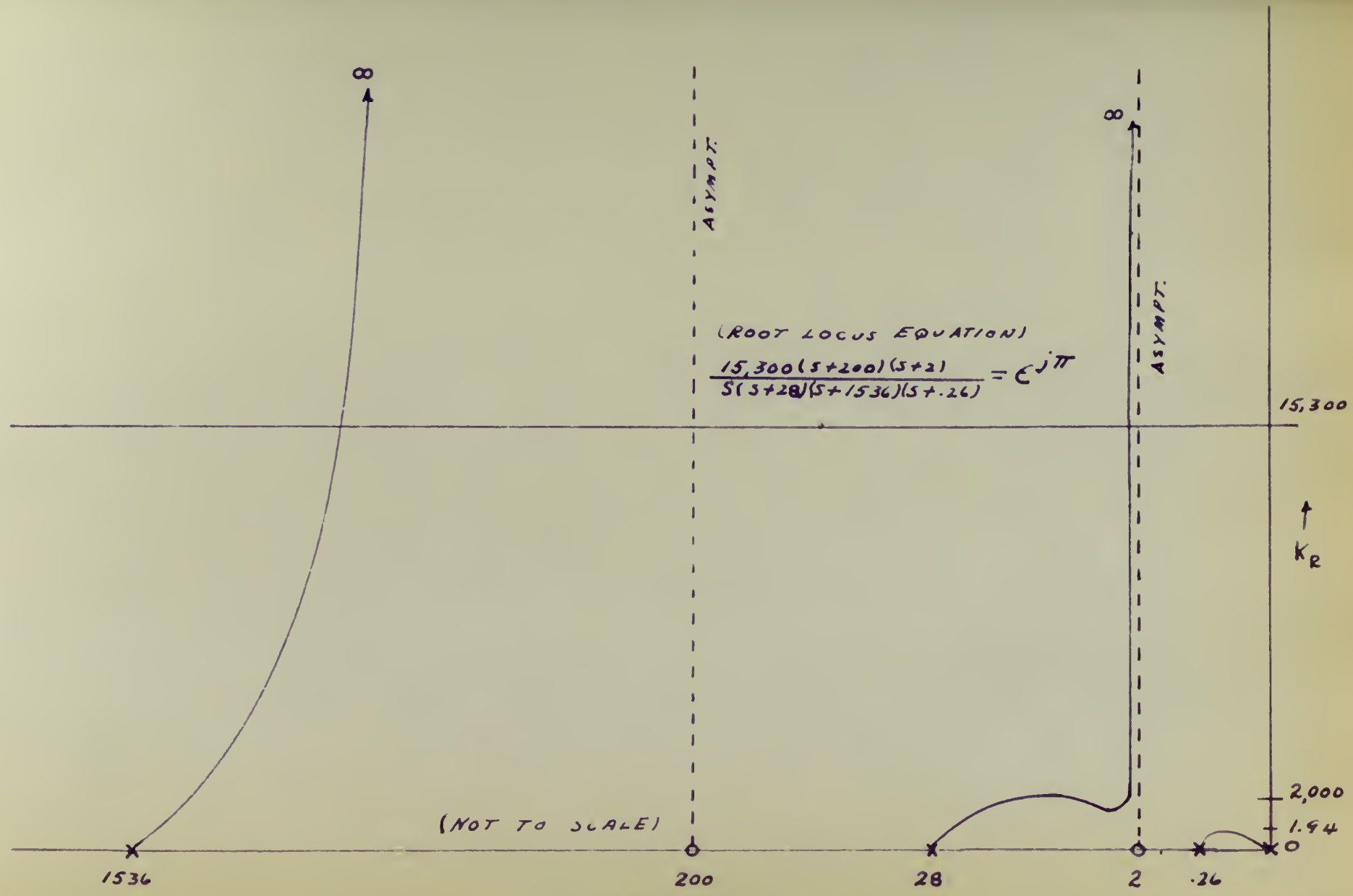

FIGURE 33

ROOT LOCUS GAIN VERSUS REAL ROOTS

OF INDIVIDUAL LOOP WITH UNITY AND INTEGRAL-DAMPING FEEDBACK

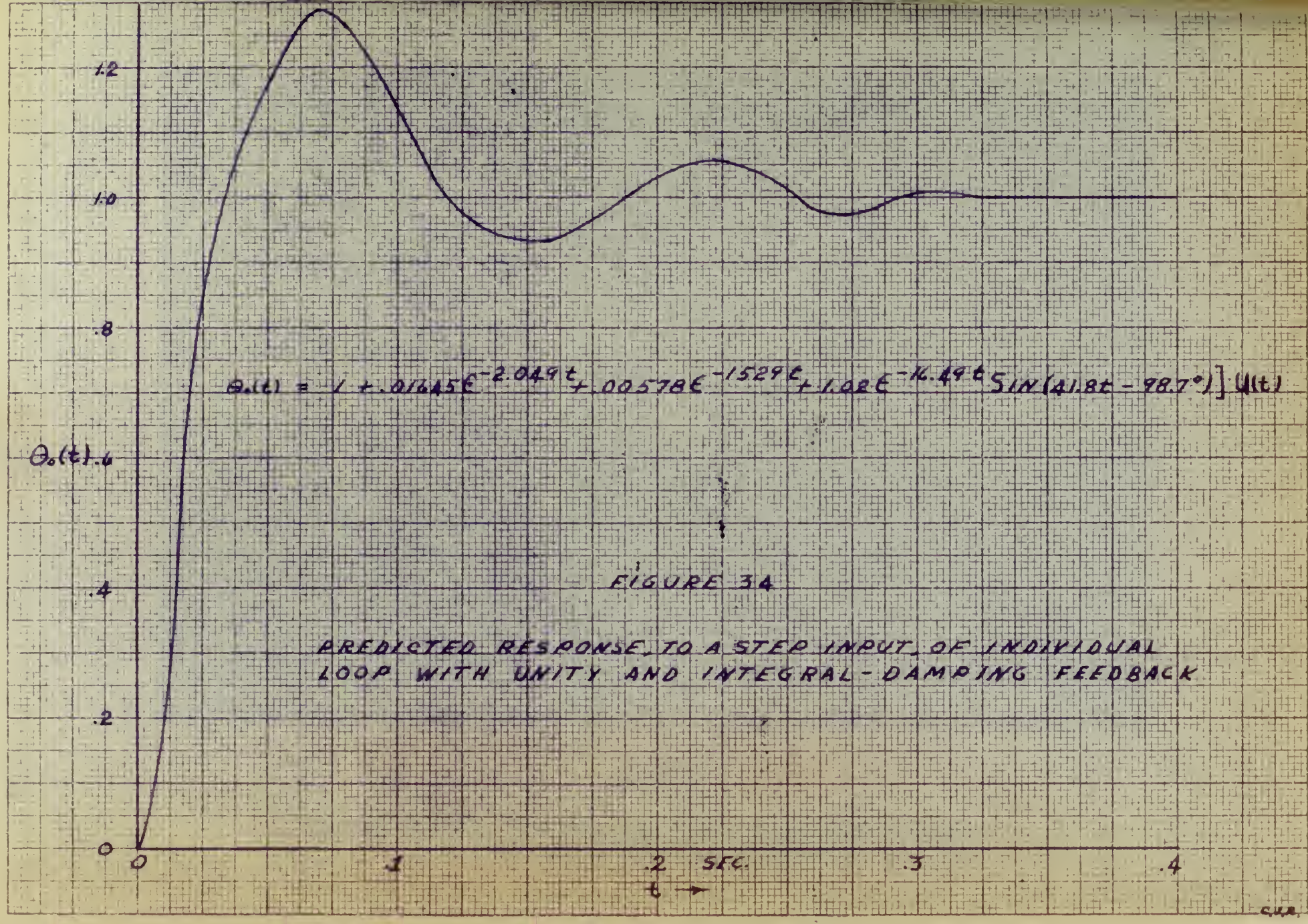

FIGURE 34

PREDICTED RESPONSE TO A STEP INPUT OF INDIVIDUAL LOOP WITH UNITY AND INTEGRAL-DAMPING FEEDBACK

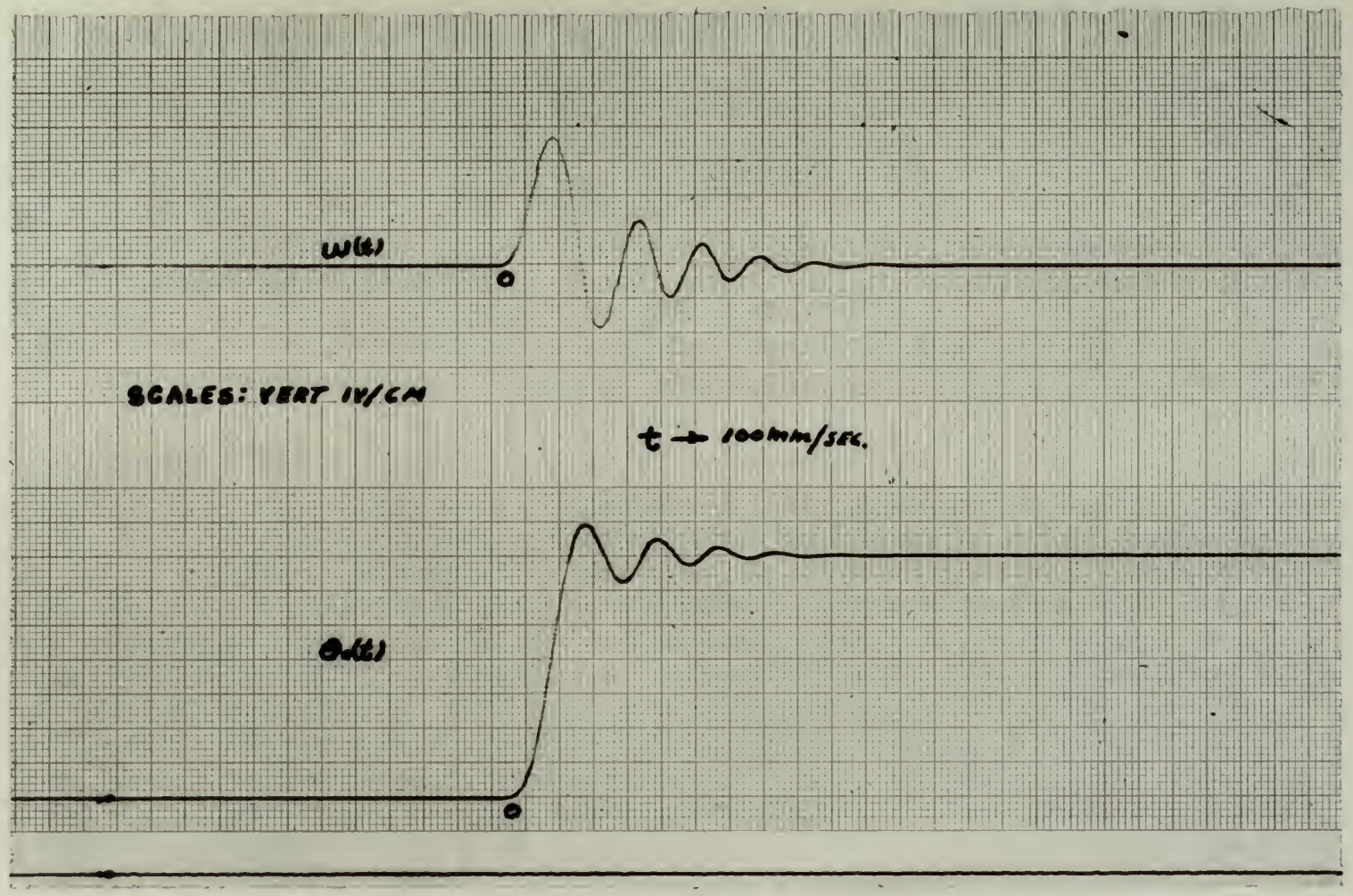

FIGURE 35

MEASURED RESPONSE, TO A UNIT STEP INPUT, OF THE INDIVIDUAL LOOP WITH UNITY AND INTEGRAL-DAMPING FEEDBACK

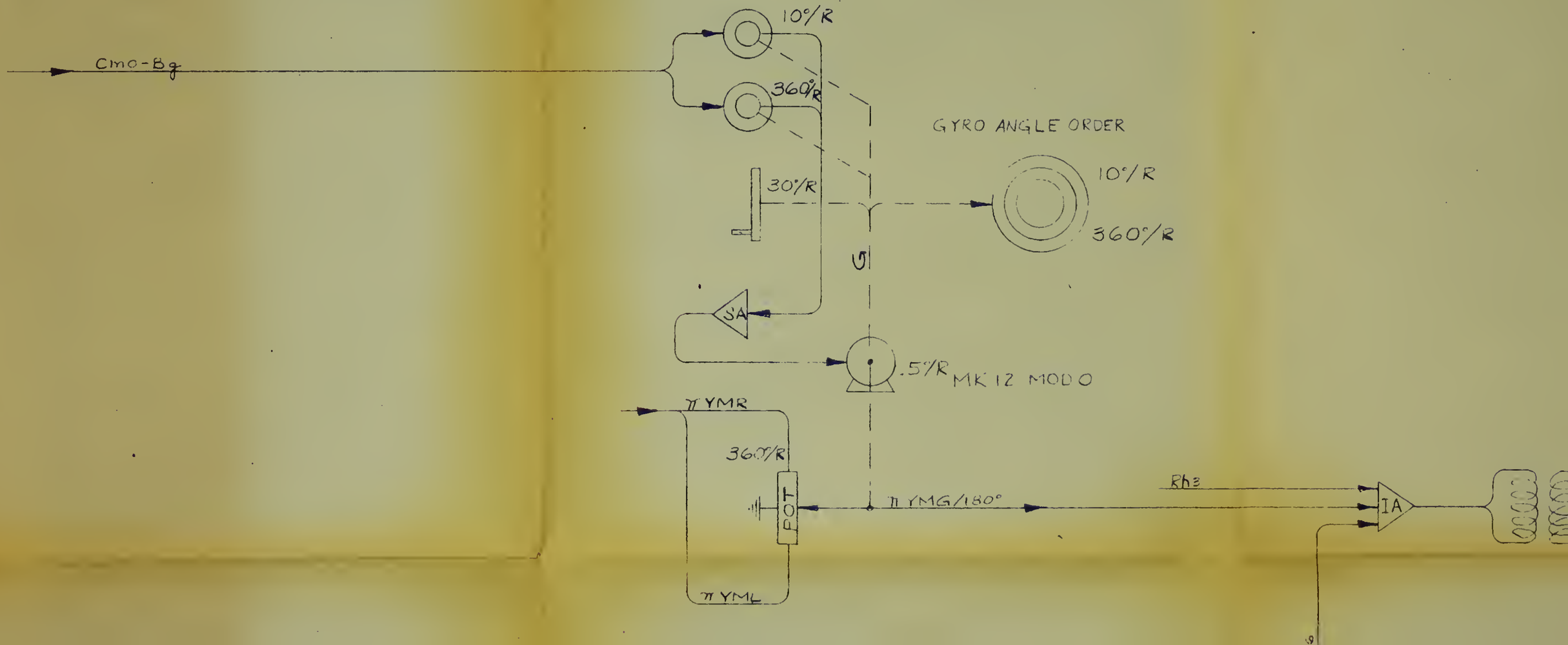
Cmo-Bg
10°/R
360°/R
30°/R
GYRO ANGLE ORDER
10°/R
360°/R
SA
.5°/R MK 12 MOD 0
π YMR
360°/R
POT
π YMG/180°
Rh3
IA
π YML

30°/R

TARGET ANGLE

Bts

360°/R

IA

K. T26 DMhτ

VERN

10KT/R

DMhτ

TARGET SPEED

10KT/R

REF

VERN

4MIN/R

T26

TORPEDO SPEED Vm'

VERN

4MIN/R

T26

.02MIN/R

SA

VGA

IA

WEAPON TIME TO BURST

2000 Y/R

VERN

ENABLING RUN

IA

SA

10Y/R

C(Hmτ)

100Y/R

100Y/R

REF

C(Hm)

VERN

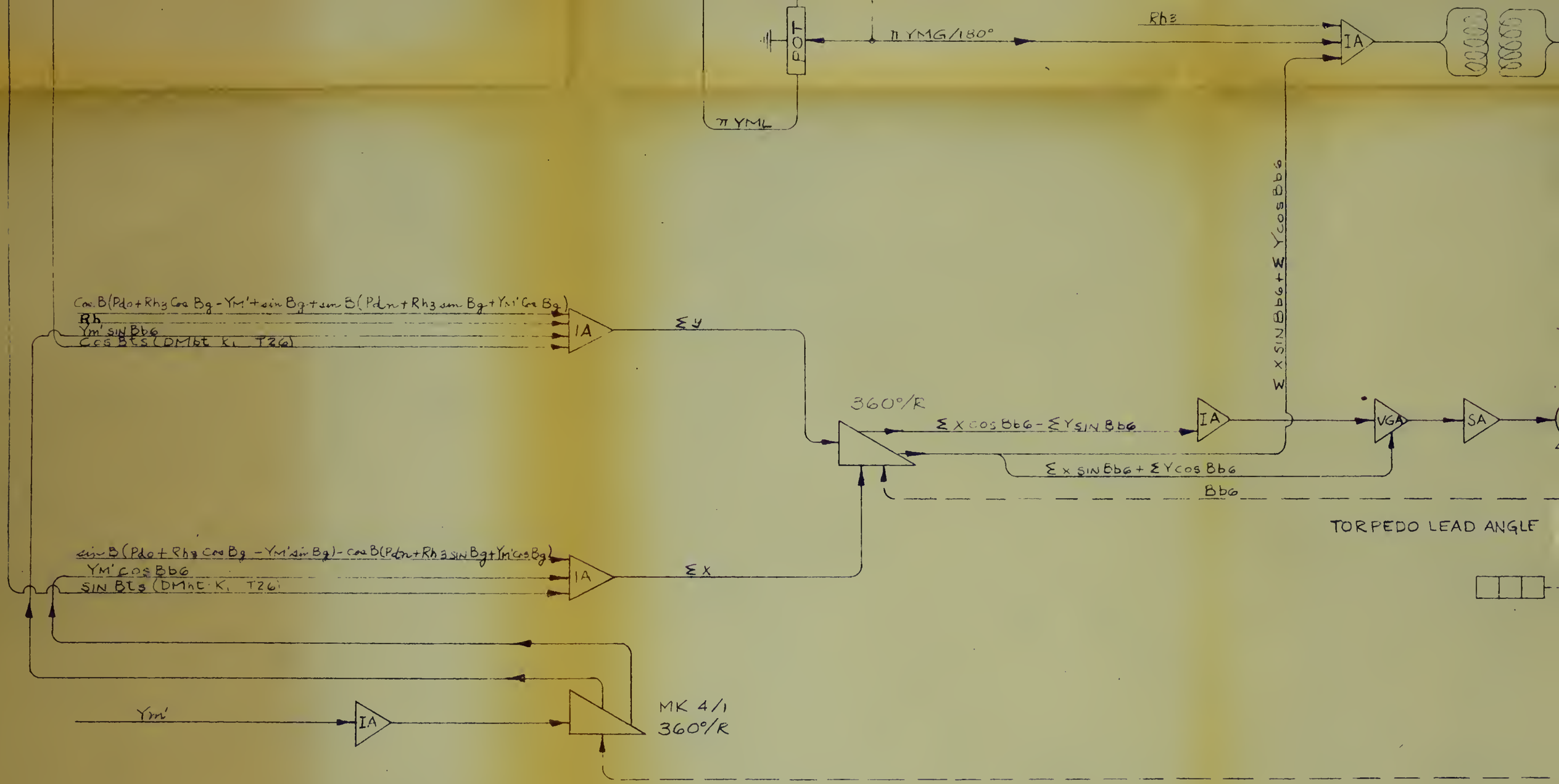

POT
π YML
π YMG/180°
Rh3
IA
Σ X SIN Bb6 + Σ Y cos Bb6
Cos B(Pdo + Rh3 Cos Bg - YM' + sin Bg + sin B(Pdn + Rh3 sin Bg + YM' Cos Bg)
Rh
Ym' sin Bb6
Cos Bts (DMbt K1 T26)
IA
Σ y
360°/R
Σ X cos Bb6 - Σ Y sin Bb6
IA
VGA
SA
Σ x sin Bb6 + Σ Y cos Bb6
Bb6
TORPEDO LEAD ANGLE
sin B(Pdo + Rh3 Cos Bg - YM' sin Bg) - cos B(Pdn + Rh3 sin Bg + YM' cos Bg)
YM' cos Bb6
SIN Bts (DMht K1 T26)
IA
Σ X
Ym'
IA
MK 4/1
360°/R

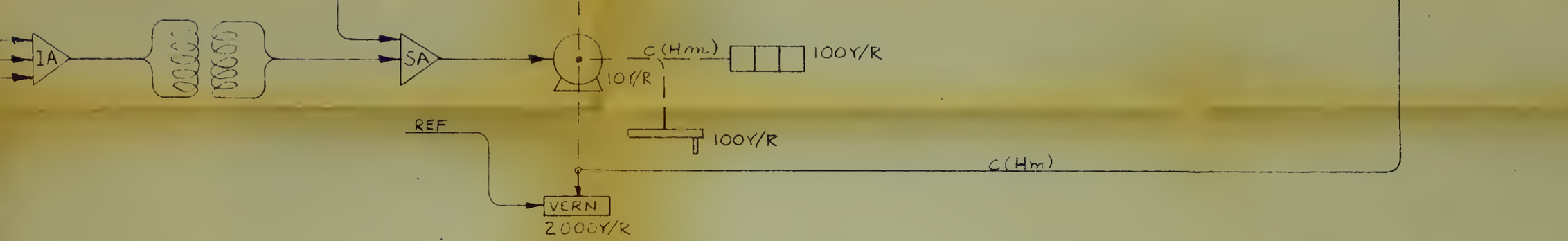

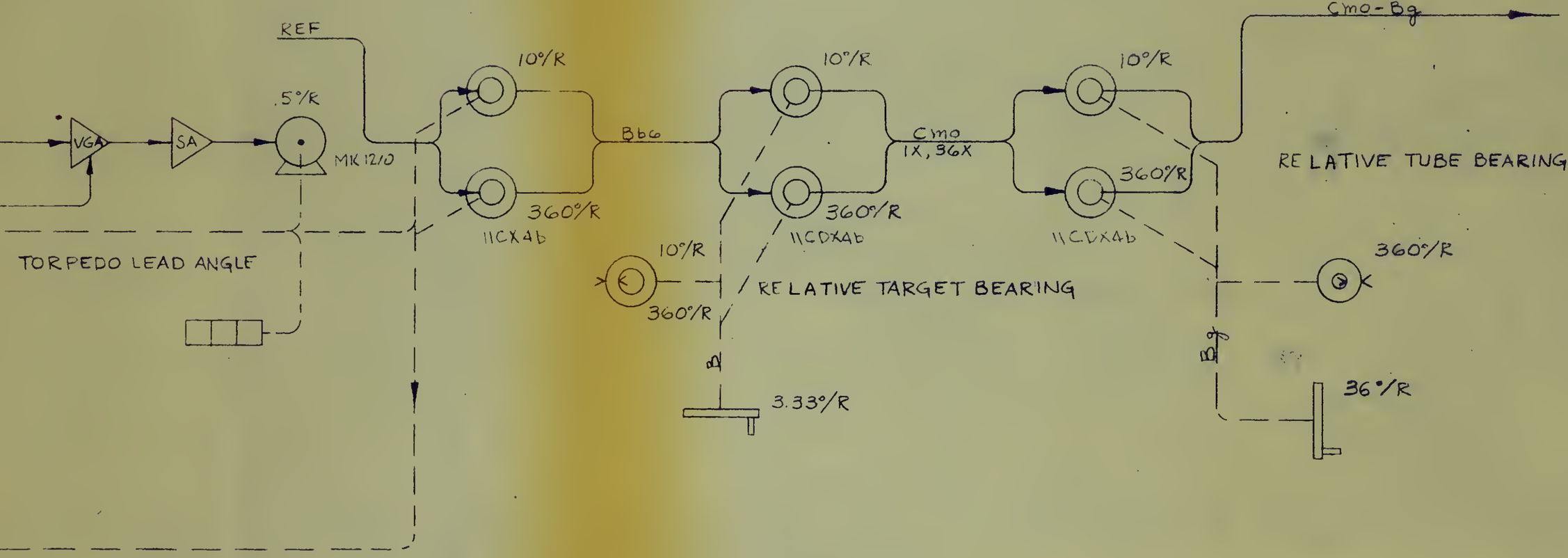

FIGURE 36

SYSTEM FUNCTIONAL DIAGRAM

nulling point. The output from the resolver is $\Sigma X \cos Bb6 - \Sigma Y \sin Bb6$ which tends to zero when Bb6 is computed correctly.

Because of this non-linearity, it was assumed that the inputs $\Sigma X \cos Bb6$ and $\Sigma Y \sin Bb6$ were constant inputs and not a function of time. The resolver was represented as a summer. Several of the actual constants were combined with the scale factors of the loop for convenience and simplicity. This is justified since it does not effect the accuracy of the stability analysis and it is highly unlikely that quantitative response can be predicted with the assumptions made concerning the resolver unless a prohibitive number of small perturbations are considered.

The assumption is also made and justified in section 6.1 that for signals which do not saturate the amplifier or motor that the Enabling Run, Weapon Time to Burst, and Gyro Lead Angle transfer functions are essentially identical. For large signals this assumption is especially invalid in the Weapon Time to Burst Loop because of the 40 to 1 gear ratio which permits the motor to saturate.

With these assumptions in mind, the "Standard Block Diagram" becomes that shown in figure 37. Where:

$$F_1 = F_2 = F_3 = F_4 = \frac{15{,}300\,(S+2)(S+200)}{(S+2.0332)(S+1862)(S+33+j22.65)(S+33-j22.65)}$$

$$G_1 = K_1 F_1 \triangleq \frac{N_1}{D_1} \; ; \qquad G_4 = -\frac{K_5 K_6}{1} \triangleq \frac{N_4}{D_4}$$

$$G_2 = K_2 F_2 F_3 \triangleq \frac{N_2}{D_2} \; ; \qquad G_5 = \frac{F_4}{1} \triangleq \frac{N_5}{D_5}$$

$$G_3 = \frac{K_3}{1} \triangleq \frac{N_3}{D_3} \; ; \qquad G_6 = \frac{K_6}{1} \triangleq \frac{N_6}{D_6}$$

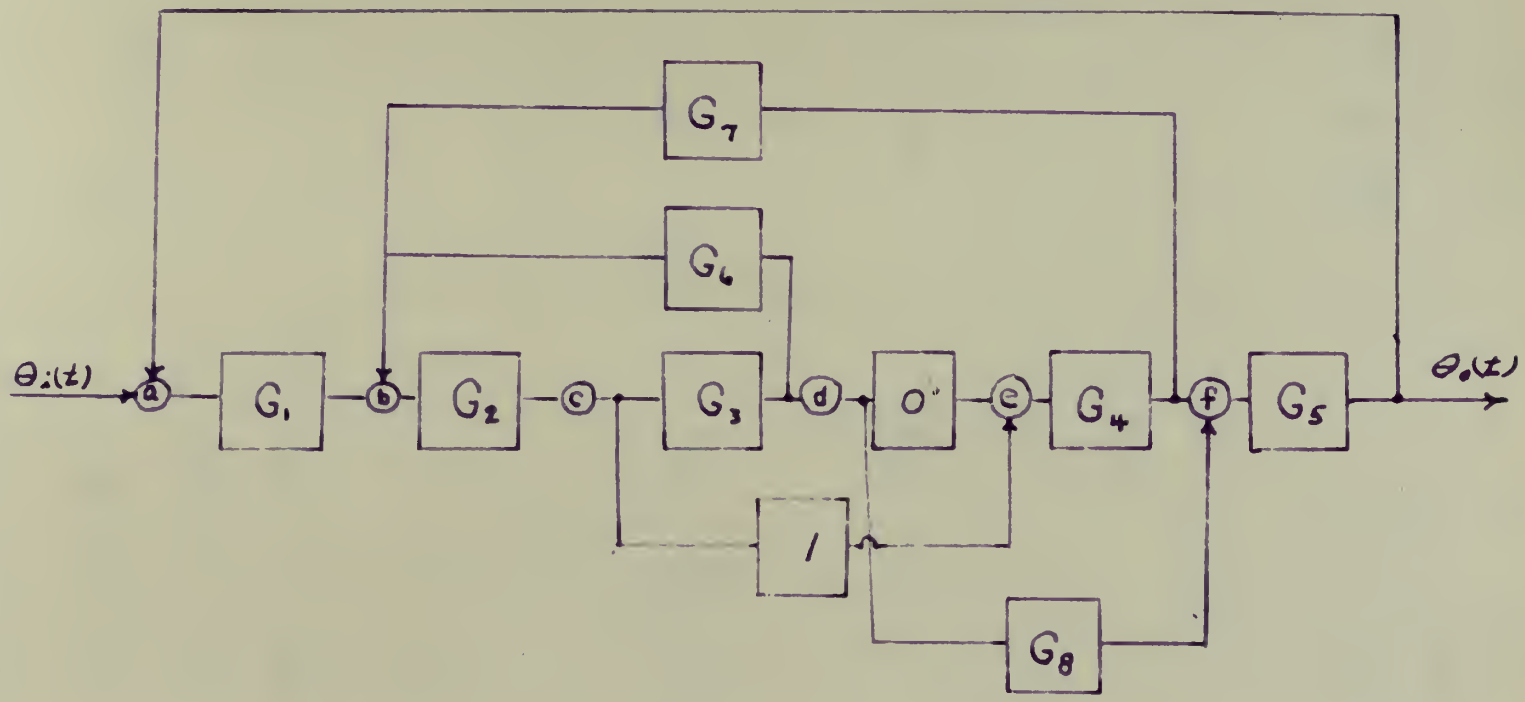

Fig. 37 STANDARD BLOCK DIAGRAM OF THE OVERALL SYSTEM

$$G_7 = \frac{\frac{K_4}{K_6}}{1} \triangleq \frac{N_7}{D_8} \qquad K_1 = Y'_m$$

$$K_3 = \sin B\pounds s$$

$$G_8 = \frac{K}{1} \triangleq \frac{N_8}{D_8} \qquad K_5 = \cos B\pounds s$$

K_2 = TARGET SPEED

$K_4 = \cos BB6$

$K_6 = \sin BB6$

Looking at the output: $\frac{\theta_o(t)}{\theta_i(t)} = F_c = \frac{BB6}{\theta_i(t)}$

$$\theta_o(t) = G_5 f$$

$$F_c = \frac{\theta_o(t)}{\theta_i(t)} = \frac{G_5 \Delta_{af} (-1)^{a+f}}{\Delta}$$

The delta of the system is:

$$\Delta = \begin{array}{c|cccccc} & a & b & c & d & e & f \\ a & (1+o1) & 0 & 0 & 0 & 0 & G_5 \\ b & -G_1 & (1+o1) & G_3G_6 & 0 & G_4G_7 & 0 \\ c & 0 & -G_2 & (1+o1) & 0 & 0 & 0 \\ d & 0 & 0 & -G_3 & (1+o1) & 0 & 0 \\ e & 0 & 0 & -1 & 0 & (1+o1) & 0 \\ f & 0 & 0 & 0 & -G_8 & -G_4 & (1+o1) \end{array}$$

It is convenient to expand the delta so that the Δ_{af} can be obtained since it will be used in the numerator of the closed loop function.

$$\Delta = (1)\begin{vmatrix} 1 & G_3G_6 & 0 & G_4G_7 & 0 \\ -G_2 & 1 & 0 & 0 & 0 \\ 0 & G_3 & 1 & 0 & 0 \\ 0 & -1 & 0 & 1 & 0 \\ 0 & 0 & -G_8 & -G_4 & 1 \end{vmatrix} - G_5 \begin{vmatrix} -G_1 & 1 & G_3G_6 & 0 & G_4G_7 \\ 0 & -G_2 & 1 & 0 & 0 \\ 0 & 0 & -G_3 & 1 & 0 \\ 0 & 0 & -1 & 0 & 1 \\ 0 & 0 & 0 & G_8 & G_4 \end{vmatrix}$$

Simplified

$$\Delta = 1 + G_2G_4G_7 + G_2G_3G_6 + G_1G_2G_3G_5G_8 + G_1G_2G_4G_5$$

$$\Delta_{af} = G_1G_2G_3G_8 + G_1G_2G_4$$

The closed loop function becomes

$$F_c = \frac{G_5[G_1G_2G_3G_8 + G_1G_2G_4]}{1 + G_2G_4G_7 + G_2G_3G_4 + G_5[G_1G_2G_3G_8 + G_1G_2G_4]}$$

Using the relationship $F_o = \frac{N_c}{D_c - N_c}$ the open loop function is

$$F_o = \frac{G_5[G_1G_2G_3G_8 + G_1G_2G_4]}{1 + G_2G_4G_7 + G_2G_3G_6}$$

Since each function G_1G_2 etc. has the form of a numerator divided by a denominator, let us define $G_{i\ i=1-8} = \frac{N_i}{D_i}$. Substituting and simplifying:

$$F_o = \frac{N_1N_2N_3N_5N_8 + N_1N_2N_4N_5D_3D_6D_7D_8}{D_1D_2D_3D_4D_5D_6D_7D_8 + N_2N_4N_7D_1D_3D_5D_6D_8 + N_2N_3N_6D_1D_4D_5D_7D_8}$$

In terms of numerators and denominators of the various functions, the closed loop function becomes:

$$F_c = \frac{N_1N_2N_3N_5N_8D_4D_6D_7 + N_1N_2N_4N_5D_3D_6D_7D_8}{D_1D_2D_3D_4D_5D_6D_7D_8 + N_2N_4N_7D_1D_3D_5D_6D_8 + N_2N_3N_6D_1D_4D_5D_7D_8 + N_1N_2N_3N_5N_8D_4D_6D_7 + N_1N_2N_4N_5D_3D_6D_7D_8}$$

Substituting the various values for the numerator and denominator of the functions, the open and closed loop transfer functions become:

$$F_o = \frac{(15{,}300)^4 K K_2 [K_3 K_4 - K_5 K_6] (S+2)^4 (S+200)^4}{\left[\begin{array}{l}(S+1862)^2 (S+2.0332)^2 (S+33+j\,22.65)^2 \\ (S+33-j\,22.65)^2\end{array}\right]} \qquad (5.5)$$

$$\left[\begin{array}{l}(S+1862)^2 (S+2.0332)^2 (S+33+j\,22.65)^2 \\ +\,(15{,}300)^2 (S+2)^2 (S+200)^2 K_2 (K_4 K_5 + K_3 K_4)\end{array}\right]$$

$$F_c = \frac{(15{,}300)^4 K_1 K_2 [K_3 K_4 - K_5 K_6] (S+2)^4 (S+200)^4}{[(S+1862)^2 (S+2.0332)^2 (S+33+j\,22.65)^2]}$$

$$\left[\begin{array}{l}(S+1862)^2 (S+2.0332)^2 (S+33+j\,22.65)^2 \\ +\,(15{,}300)^2 (S+2)^2 (S+200)^2 K_2 (K_4 K_5 + K_3 K_6) \\ +\,(15{,}300) K_1 K_3 [K_3 K_4 - K_5 K_6] (S+2)^4 (S+200)^4\end{array}\right]$$

Observing equation 5.5 the open loop transfer function is of the form $F_o = \frac{K(S+Z_1)(S+Z_2)}{S^n(S+P_1)(S+P_2)}$ where n = 0. This indicates, of course, that the system is type zero.

$$K_v = \lim_{S \to 0} S F_o$$

$$K_v = \lim_{S \to 0} S \left[\frac{K (S+Z_1)(S+Z_2) \cdots}{(S+P_1)(S+P_2) \cdots}\right] = 0$$

The steady state error to a ramp is:

$$\varepsilon_{ss} = \frac{\beta}{K_v} \qquad \beta \triangleq \text{SLOPE OF RAMP}$$

$$\varepsilon_{ss} = \frac{\beta}{0} = \infty$$

This indicates that the steady state error would be infinite and the system must be compensated in such a way to make it a type one if ramp inputs of large magnitude or long duration are expected to be incountered.

Since, of necessity, certain linerizations were made; therefore, no conclusions can sensibly be made concerning stability except that the necessary condition that all the coefficients of the characteristic equation are positive is met. This being the circumstance, a frequency response analysis was made. The results were plotted on a Nichol's chart. It was found that there was a gain margin of 26 db and a phase margin of 72°. This, of course, shows that the overall system is highly stable. The results obtained from the Nichol's chart were then plotted on a Bodie diagram, figure 38, to determine the dominant time constant of the system and to acertain experimentally that the system was actually type zero. These results are discussed in section 5.3-b.

5.3 Discussion of Analysis and Observed Data

5.3a Individual Loop

The individual loop was analyzed in three possible configerations,unity, tachometer, and integral-damp feedback; unity and tachometer feedback; and unity and integral-damp feedback.

By using figure 22 and 23 it was found that near optimum values of resistance were R_2 = 300 K and R_7 = 100 K. It was found that the value of R_6 used had little effect on the response of the system; however, considerations of noise in the system dictated a value of approximately three megohms. Using these values of resistance, computations were made to predict the response of the loop. The predicted and measured response is shown in figure 26 and 27 respectively.

Prior to the determination of the values of resistances, the best response obtained was a critically damped case with a settling time in excess of

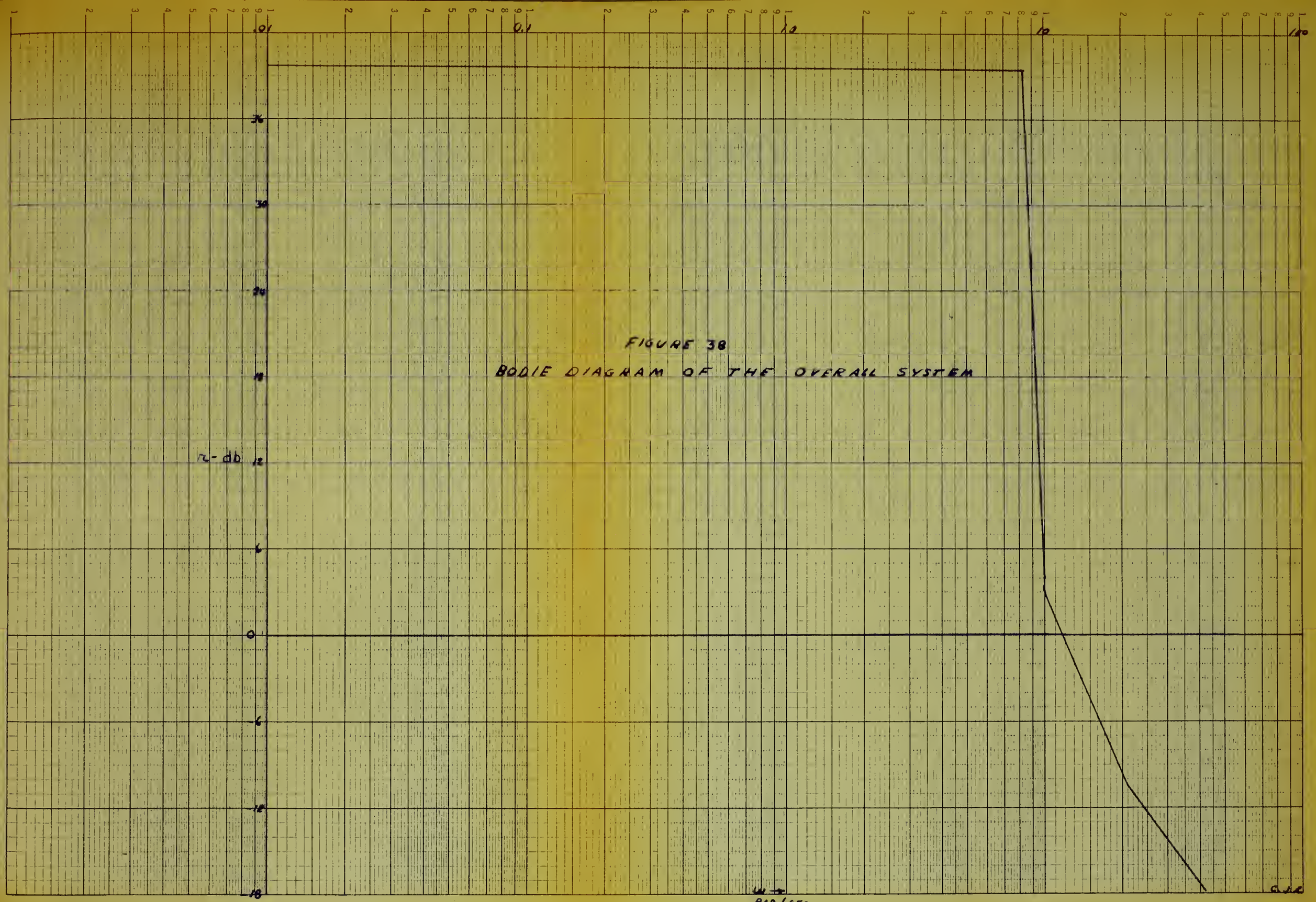

FIGURE 38
BODIE DIAGRAM OF THE OVERALL SYSTEM

.24 seconds. It can be seen that the predicted response and measured response agree exactly and a settling time of .15 seconds was obtained. This shows an improvement in response of 37.5 per cent.

The analysis of the loop without the integral-damp network was performed in section 3.2. The measured response is shown in figure 31. Comparing this with the predicted response in figure 30, it is again seen that the measured and predicted values agree. It is also noted that an improvement in response was obtained with a settling time of .11 seconds. This,of course, is desireable; however, at steady state there was audible noise caused by gear chatter. This noise did not show up in the output but would cause excessive wear in the gear train near the motor; therefore, the integral-damp network is considered desirable. It was found analytically that by changing capacitors C_3 and C_4 (See figures 13 or 14) to .25 μf a predicted and measured response with a settling time of .12 seconds was obtained without any associated noise problems. The theoretical pole location is calculated in section 4.2.

The last configeration considered involved unity and integral-damp feedback. From figures 34 and 35 it can be seen that the predicted and measured response are again in agreement except the peak overshoot is somewhat greater in the actual system. Settling time is .3 seconds. It is noted that substantial tachometer feedback must be used since for smooth computation each loop must be critically damped.

5.3b Overall System

As discussed in section 5.2, the overall system is highly stable with a phase margin of 72° and a gain margin of 24 db. The data from the Nichol's plot is used to construct figure 38. From this it is noted that the

first asymptote has a zero db slope; therefore, type zero system. The time constant agrees reasonably with the actual obtained from the measured response shown in figure 39. The theoretical settling time is .6 seconds and the measured is .7 seconds (See figure 39). The response to a ramp input is shown in figure 40.

Since the theoretical computations and frequency response indicated that the system was type zero with a finite error to a step input and an infinite error to a ramp input, it was considered advantageous to measure these errors. The inputs and resulting errors are shown in figures 41 and 42.

The results are therefore conclusive that the system is in fact type zero. While the multi-loop system is unmodified (i.e., a type 0 servomechanism), there will be a constant error to a step and a corresponding, increasing error to a ramp input. The measurements in figures 41 and 42 show the magnitude of the errors involved. The first is a measurement of the error versus time for the step and the second is the measurement of the error versus time corresponding to the ramp. From the first the error ratio to the step input can be calculated to be:

$$\frac{40\,mV}{7.5\,VOLTS} = .00534$$

In a typical submarine problem, the total bearing change from initial contact to the firing point is approximately 150 degrees. This means that, under these circumstances, the error at firing point will be:

$$(.00534)(150°) = .8°$$

One degree = 17.6 yards/1000 yards. Therefore, the following errors

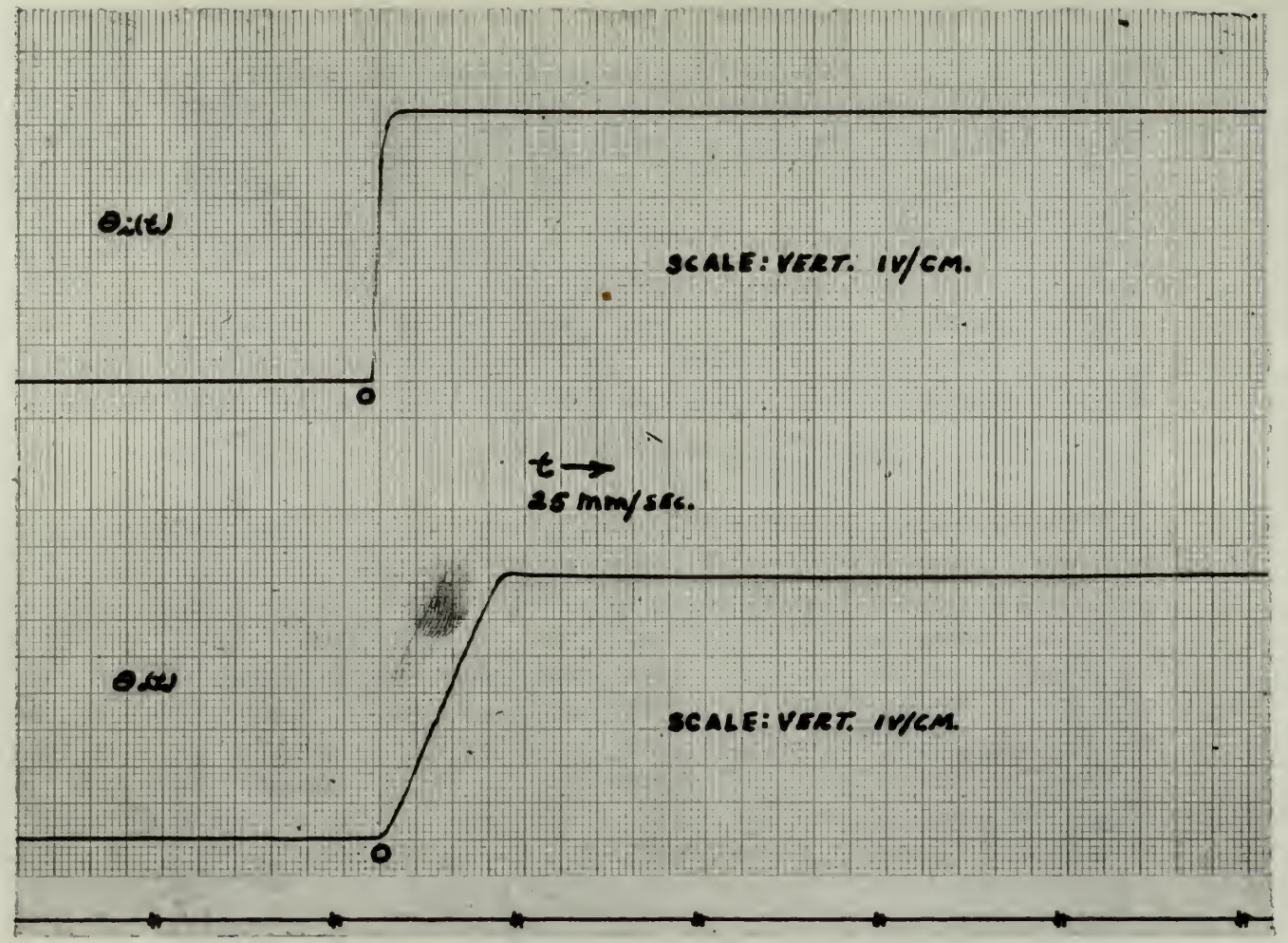

FIGURE 39

MEASURED RESPONSE OF THE OVERALL SYSTEM TO A STEP INPUT

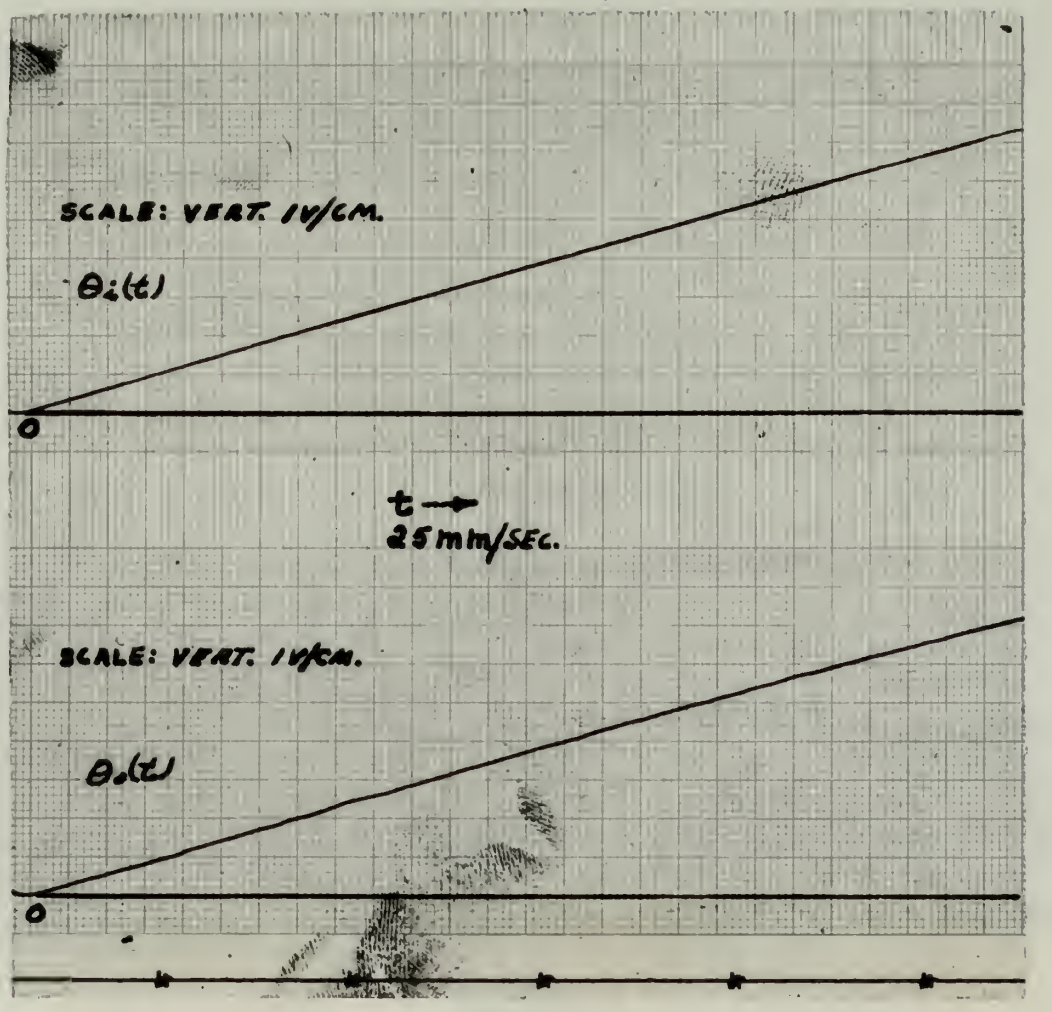

FIGURE 40

MEASURED RESPONSE OF THE OVERALL SYSTEM TO A RAMP INPUT

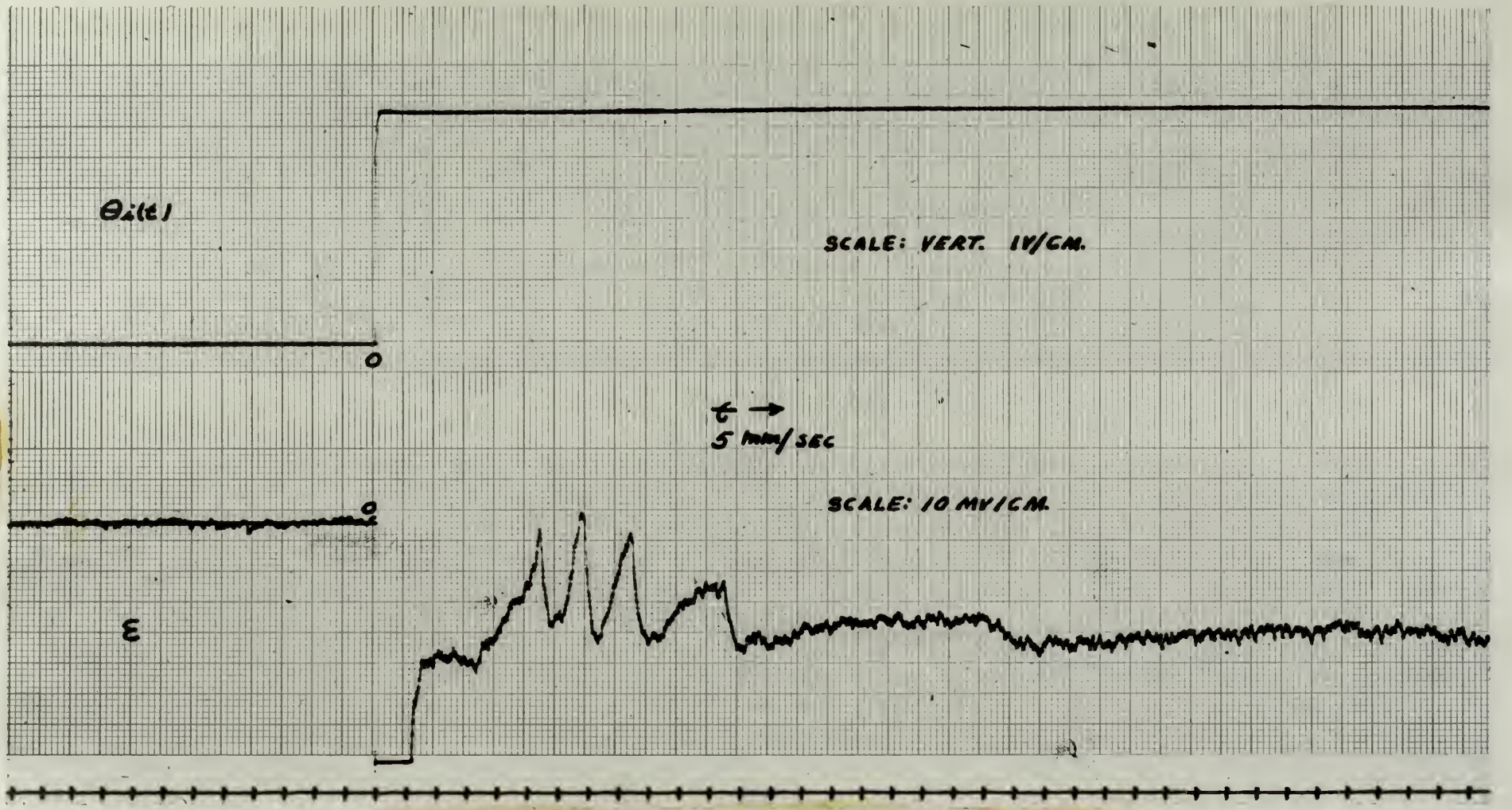

FIGURE 41

MEASURED ERROR OF THE OVERALL SYSTEM TO A STEP INPUT

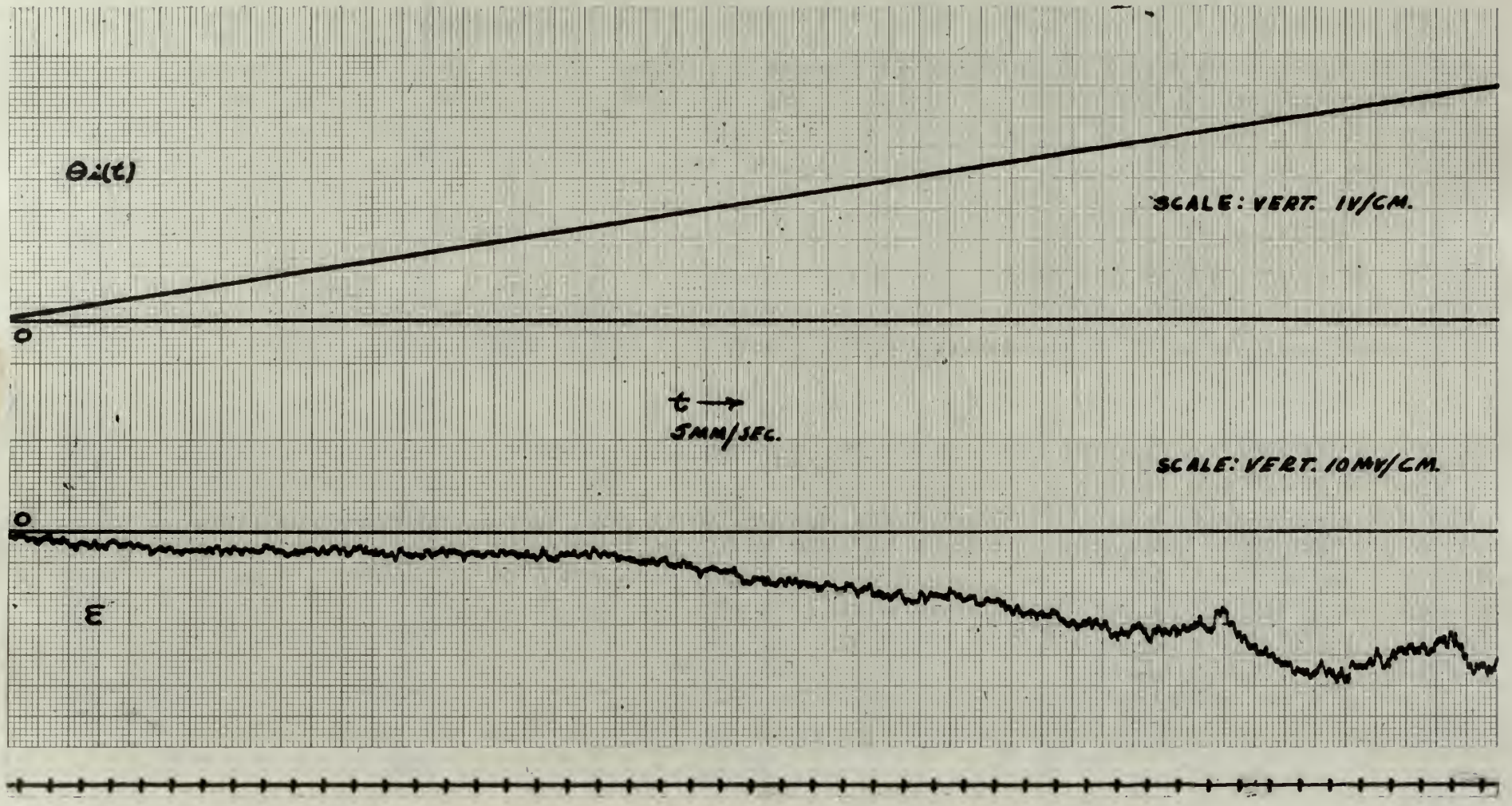

FIGURE 42

MEASURED ERROR OF THE OVERALL SYSTEM TO A RAMP INPUT

would result with a computed error in the Gyro Lead Angle Computation Loop of 0.8°:

at: 1,000 yds. : 14.05 yds.
2,000 yds. : 28.10 yds.
3,000 yds. : 42.15 yds.
4,000 yds. : 56.20 yds.

These errors are, of course, in addition to any other errors generated in other parts of the computer. It can be readily seen that if fire control problems of short range with the resultant large ramp or long ranges where tracking is done for long periods of time, a significant error may develope.

Looking at equation (5.5), the open loop transfer function of the system, it is seen that an integration is required or an "S" is needed in the denominator to have a type one system. It appears that a feed forward loop added to the block diagram, figure 37, would accomplish the desired results. The resultant standard block diagram is shown in figure 43.

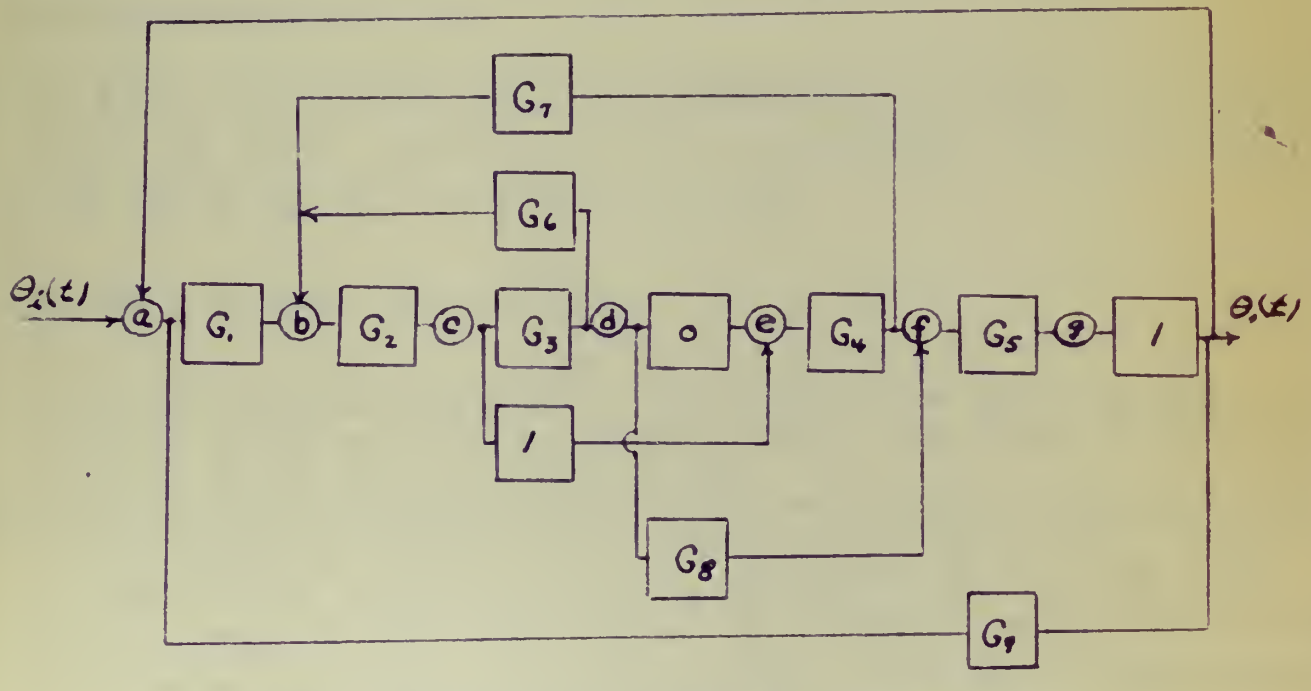

Fig. 43 STANDARD BLOCK DIAGRAM WITH COMPENSATION NECESSARY TO PRODUCE A TYPE ONE SYSTEM

The determinant for delta becomes

$$\Delta = \begin{array}{c|ccccccc} & a & b & c & d & e & f & g \\ a & 1 & 0 & 0 & 0 & 0 & 0 & 1 \\ b & -G_1 & 1 & G_3G_6 & 0 & G_4G_7 & 0 & 0 \\ c & 0 & -G_2 & 1 & 0 & 0 & 0 & 0 \\ d & 0 & 0 & -G_3 & 1 & 0 & 0 & 0 \\ e & 0 & 0 & -1 & 0 & 1 & 0 & 0 \\ f & 0 & 0 & 0 & -G_8 & -G_4 & 1 & 0 \\ g & G_9 & 0 & 0 & 0 & 0 & -G_5 & 1 \end{array}$$

The determinant reduces to

$$\Delta = 1 + G_2G_4G_7 + G_2G_3G_6 + G_9 + G_2G_4G_7G_9 + G_2G_3G_6G_9 + G_1G_2G_4G_5 + G_1G_2G_3G_5G_8$$

$$\Delta_{a_f} = G_9 + G_2G_4G_7G_9 + G_2G_3G_6G_9 + G_1G_2G_4G_5 + G_1G_2G_3G_5G_8$$

The closed loop function is

$$F_c = \frac{[G_9 + G_2G_3G_6G_9 + G_2G_4G_7G_9 + G_1G_2G_4G_5 + G_1G_2G_3G_5G_8]}{\left[\begin{array}{l} 1 + G_2G_4G_7 + G_2G_3G_6 + G_9 + G_2G_4G_7G_9 + G_2G_3G_6G_9 \\ + G_1G_2G_4G_5 + G_1G_2G_3G_5G_8 \end{array}\right]}$$

In terms of numerator and denominators

$$F_c = \frac{\begin{array}{l} N_9D_1D_2D_3D_4D_5D_6D_7D_8 + N_2N_4N_7N_9D_1D_3D_5D_6D_8 \\ + N_2N_3N_6N_9D_1D_4D_5D_7D_8 + N_1N_2N_4N_5D_3D_6D_7D_8D_9 \\ + N_1N_2N_3N_5N_8D_4D_6D_7D_9 \end{array}}{\begin{array}{l} D_1D_2D_3D_4D_5D_6D_7D_8D_9 + N_2N_4N_7D_1D_3D_5D_6D_7D_8D_9 \\ + N_2N_3N_6D_1D_4D_5D_7D_8D_9 + N_9D_1D_2D_3D_4D_5D_6D_7D_8 \\ + N_2N_4N_7N_9D_1D_3D_5D_6D_8 + N_2N_3N_6N_9D_1D_4D_5D_7D_8 \\ + N_1N_2N_4N_5D_3D_6D_7D_8D_9 + N_1N_2N_3N_5N_8D_4D_6D_7D_9 \end{array}}$$

The open loop function is

$$F_o = \frac{\begin{array}{l} N_9 D_1 D_2 D_3 D_4 D_5 D_6 D_7 D_8 + N_2 N_4 N_7 N_9 D_1 D_3 D_5 D_6 D_8 \\ + N_2 N_3 N_6 N_9 D_1 D_4 D_5 D_7 D_8 + N_1 N_2 N_4 N_5 D_3 D_6 D_7 D_8 D_9 \\ + N_1 N_2 N_3 N_5 N_8 D_4 D_6 D_7 D_9 \end{array}}{\begin{array}{l} D_1 D_2 D_3 D_4 D_5 D_6 D_7 D_8 D_9 + N_2 N_4 N_7 D_1 D_3 D_5 D_6 D_7 D_8 D_9 \\ + N_2 N_3 N_6 D_1 D_4 D_5 D_7 D_8 D_9 \end{array}}$$

It can be seen that the necessary and sufficient condition for a type one system has been met since $D_9 = S(S+a)$ can be factored from each term.

Where $G_9 = \frac{N_9}{D_9}$ is of the form: $G_9 = \frac{K}{S(S+a)}$.

VI. Conclusions and Recommendations

6.1 Single Loop

The single loop designed and constructed by Librascope Division of General Precision Corporation will produce satisfactory response without further changes in design. However, by judicious selection of the various input resistors, an improvement is possible of 37.5 percent using settling time as a criteria. It can be seen from the root locus, figure 24 and K versus Real roots, figure 25 that the system is absolutely stable for all values of gain. It can also be seen that the gain can vary appreciably without effecting the response. Should the gain become very low, an appreciable residue will be associated with the root near the zero at S = -2. Tachometer feedback is essential to provide a critically damped system for computation. Integral-damp feedback slows down the response by 26.5 per cent from that obtained without it; however, the damping is required to prevent high frequency oscillations in the gear train during steady state operation. In selecting values of capacitance ($C_3 = C_4 = .25\,\mu f$) in figure 14, the determental effect on response due to the integral-damp feedback is eliminated. The recommended changes improves the response a total of 54.2 per cent over the best obtained by trial and error on the physical system.

6.2 Overall System

The overall system is type zero as designed. This is satisfactory for most applications intended since the error involved is small; however, should large ramp inputs or tracking problems of long duration be encountered, it is possible to generate excessively large errors. The solution to this problem is a modification involving a motor and amplifier in a

feed forward loop. This loop will be physically connected at the error input to the Torpedo Lead Angle and feed forward to the output of Bb6. This is represented in the modified standard block diagram, figure 43.

An alternate method which may be prefered, since the primary function of the loop is to mechanize an equation, is to determine a mean ramp, calculate the various outputs as a function of time, and scale the various loops to reduce or eliminate the resultant error. A check must, of course, be made over the full range of ramps expected, after the scaling has been accomplished, to insure that the error does not become excessive elsewhere.

Measured frequency and transient response indicates that the system operation will be satisfactory with .7 seconds settling time to a unit step, gain margin of 24 db, and phase margin of 72°.

VII. Recommendations for Further Investigation

Should it be deemed desirable to predict accurately the response to a complex multi-loop system utilizing resolvers, it would be advantageous to use the linearizations made herein, consider small pertubations, and determine their accuracies obtained by measurements on the physical system. This would provide a criteria for evaluating future analysis which may be conducted during design work on other systems.

In addition it may be advantageous to consider linearization techniques other than the ones used herein.

If it is required that the overall system be optimized, an analogue computer study is warranted.

REFERENCES AND BIBLIOGRAPHY

1. Technical Information for the Engineer; Kearfott Company, Incorporated, February 1960

2. Truxal, J. G., Control Engineer's Handbook; New York: McGraw-Hill Book Company, Inc., 1958

3. Gardner, M. F., and Barnes, J. L., Transients In Linear Systems, New York: John Wiley and Sons, Inc., 1942

4. Chu, Y., A Generalized Theory of Linear Multi-Loop Automatic Control Systems, Doctoral Dissertation, MIT, 1953

5. Wheeler, R. C. H., Unpublished Lecture Notes and Comments, U. S. Naval Postgraduate School, 1959

6. Thaler, G. J., Unpublished Lecture Notes and Comments, U. S. Naval Postgraduate School, 1959

APPENDIX I

Induction Resolver

An induction resolver is an electromagnetic device employed as a basic element in analog computers, automatic control systems, angle data transmission systems and plan position indicating radars. It is used for performing trigonometric computations.

The induction resolver is essentially a transformer with rotary variable coupling between primary and secondary windings (Figure 1). The windings are distributed in the various stator and rotor slots in such manner as to obtain a true sinusoidal relationship between output voltage and angle of rotation of the rotor. Since the units are used at audio and power frequencies, it is customary to use a high-permeability laminated core similar to that used in an induction motor.

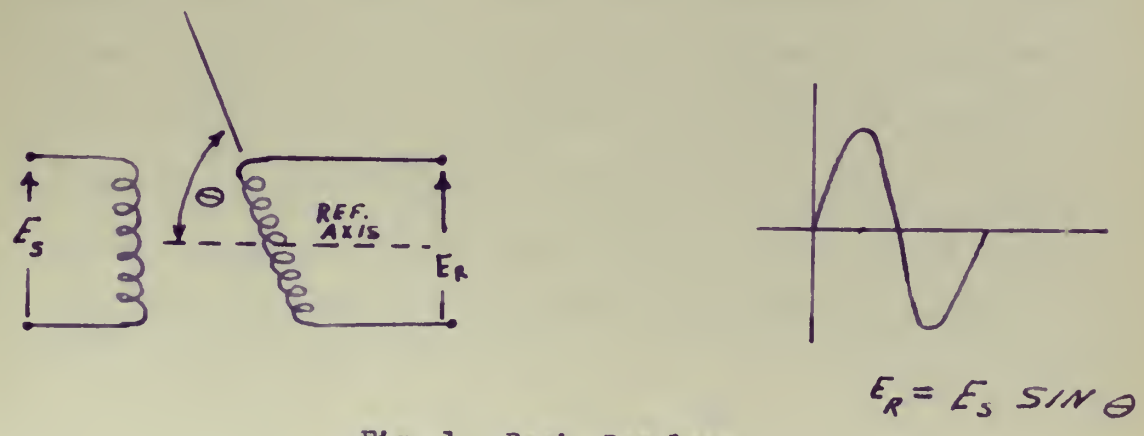

Fig. 1 - Basic Resolver

It is customary to treat the stator winding as the primary or input winding, and the rotor winding as the secondary or output winding. If, as in Figure 2, there are two secondary windings at right angles to each other (in "space quadrature"), one secondary will have induced in it a voltage which is proportional to the sine of the angle of rotation between it and the primary, and the other secondary will have induced in it a voltage which is proportional to the cosine of the angle of rotation between it and the primary.

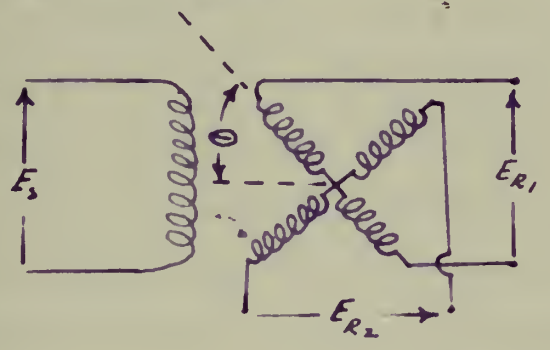

INPUTS	OUTPUTS
E_s	$E_{R_1} = E_s \sin\theta$
θ	$E_{R_2} = E_s \cos\theta$

Fig. 2 - Resolver with two Rotor Windings

To make induction resolvers even more useful, two windings are provided on both the stator and rotor. The pairs of stator windings and rotor windings are located at right angles to each other as shown in Figure 3. This permits computation of cosines as well as sines, and even more complex problems involving both sines and cosines can be solved when both stators are excited. In addition to the resolution of input voltages into sine and cosine components, resolvers can perform the synthesis of resultants from components and the rotation of coordinate systems.

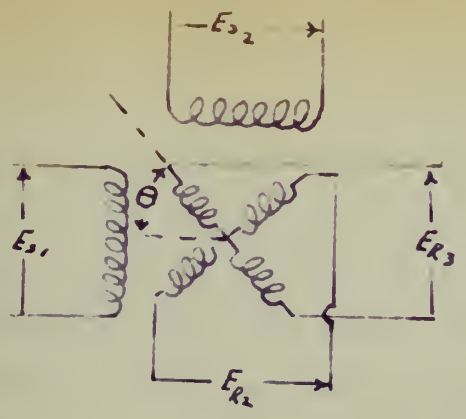

INPUTS

E_{S_1}

E_{S_2}

θ

OUTPUTS

$E_{R_3} = E_{S_2} \cos\theta - E_{S_1} \sin\theta$

$E_{R_2} = E_{S_1} \cos\theta + E_{S_2} \sin\theta$

Fig. 3 - Resolver Input and Output Relationship

As shown in Figure 4, currents in the two stator windings set up magnetic fields at right angles to each other to form a resultant flux vector. This flux vector may assume any angular position, depending upon the amplitudes and polarities of the input currents. Its magnitude and proportional to the vector sum of the instantaneous values of the input currents, and its angular position is equal to the arctangent of the ratio of the two currents. For AC input voltages within the operating frequency range of the resolver, the rotor voltages are proportional to the magnitude of the flux vector and the sine or cosine of the angle of rotation of the rotor winding with respect to the vector. The output voltages may be expressed in terms of the input voltages and the rotor angular position, by the following equations:

$$E_{R_1} = E_{S_2} \cos\theta - E_{S_1} \sin\theta \qquad (1)$$

$$E_{R_2} = E_{S_1} \cos\theta + E_{S_2} \sin\theta \qquad (2)$$

The subscripts refer to the various rotor and stator windings and θ is the rotor angular position.

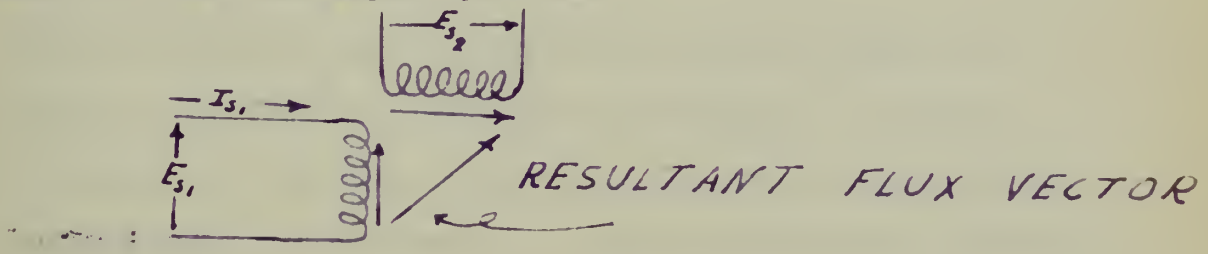

Fig. 4 - Stator Flux Vectors.

While other types of operations are possible with a resolver, its use has been principally with three types of inputs, namely; (1) sine wave voltages of the same electrical phase, (2) sine wave voltages shifted 90 degrees apart, and (3) irregular wave shapes, principally of the sawtooth or square wave variety. For the first type of operation, the output voltages remain fixed in electrical phase shift and their magnitudes vary in accordance with equations (1) and (2). For the second and third types of operation, the output voltages may also be determined by equations (1) and (2) if the instantaneous values of the voltages are taken into consideration. For the case of the resolver with two inputs 90 degrees apart in electrical phase, each of the two rotor output voltages remains constant in amplitude, independent of rotor angular position. However the phase of the voltages varies continuously with rotor angular position. The phase shift between the two output voltages remains fixed at 90 degrees. In this mode of

operation, then, the equations for the output voltages are:

$$E_{R_1} = E_S \angle \theta \qquad (3)$$

$$E_{R_2} = E_S \angle \theta + 90^\circ \qquad (4)$$

For the third case, where irregular wave shapes are used, operation most frequently falls into two categories. In phase, square waves or flat topped sine waves are used in some computing applications. The performance is adequately described by equations (1) and (2) without modification if the two input wave shapes are the same, which is usually the case.

Sawtooth wave shapes are frequently used in radar sweep applications. In the simplest case, a sweep voltage is applied to one stator and the two output voltages from the rotor windings are the same sweep voltage but with an amplitude proportional to the sine or cosine of the rotor angular position. If these two voltages are applied to the "X" and "Y" deflection plates, or coils of a cathode ray tube, they cause a radial trace to be formed. The trace will assume the same angular position as the resolver rotor. This type of operation finds application in plan position indicator types of radar displays.

While the arrangement shown in Figure 5a is suitable for schematic representation of a resolver, the arrangement shown in Figure 5b is more suited for block diagrams and functional schematics.

The diagram, equivalent schematic and equations are shown for clockwise rotation (facing the shaft end) and apply to all standard types of resolvers. Where it is desired to change the direction of rotation of the resolver, it is only necessary to interchange input A with B and output C with D. This can be noted on the block diagram by a negative sign preceding θ.

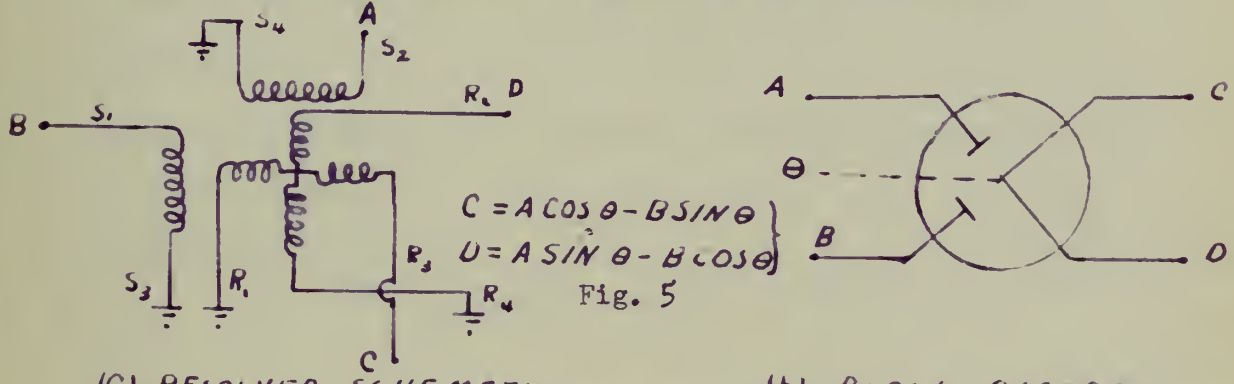

Fig. 5

A resolver used in the simplest form of computation is shown in Figures 6a and b. One stator winding is excited with a voltage proportional to the hypotenuse of a right triangle and the rotor is positioned to the angle θ. The two output voltages are proportional to the two legs of the triangle.

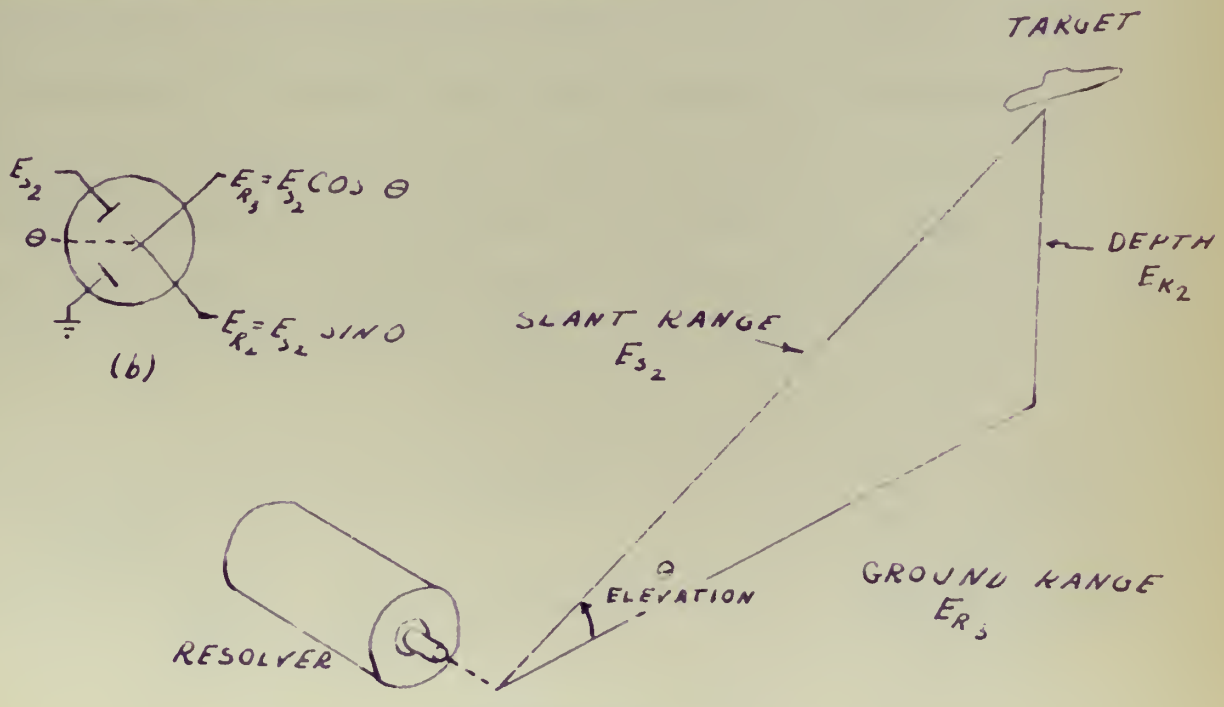

Fig. 6 - Elementary Resolver Application

In Figure 7 the problem is similar, but the hypotenuse and one of the legs, Y are known. A servo amplifier and motor are used to position the resolver rotor until the voltage, E_{R_2}, is delivered by the resolver equals the known voltage Y. The voltage E_{R_3} is then proportional to the length of the other leg of the triangle, and the angle Θ is the angle between the second leg and the hypotenuse. A solution of this type may be used in determining elevation angle and ground range when slant range and depth are known.

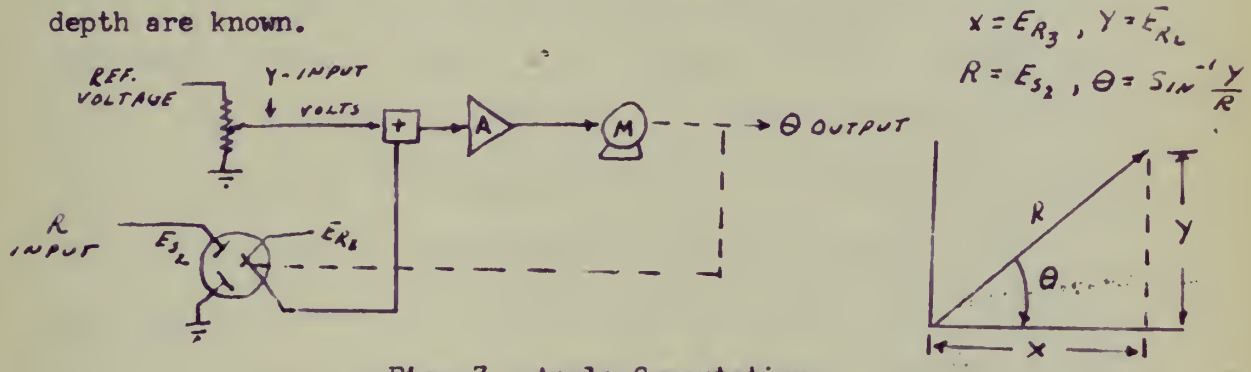

Fig. 7 - Angle Computation

In Figure 8, the inputs are two vectors 90 degrees apart. The servo positions the resolver rotor until one output is zero. At this position the other rotor being 90 degrees away, has maximum coupling with the flux vector formed by the X and Y inputs. Its output is therefore proportional to the vector sum of these two inputs. The rotor angular position is the angle between one leg and the hypotenuse of the triangle.

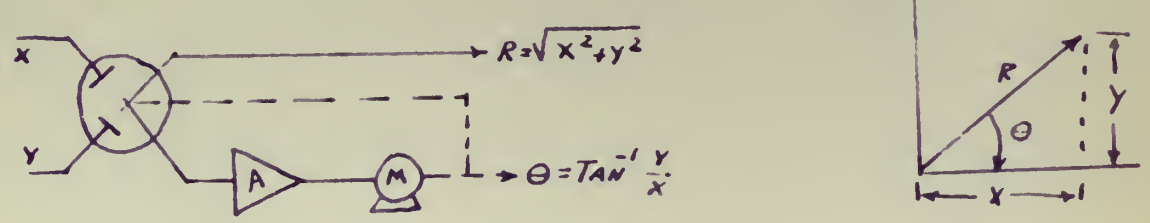

Fig. 8 - Vector Addition

In the rotation of coordinates, both stators and rotors are used. With rectangular coordinates X and Y as inputs to a resolver, as in Figure 9, the outputs are also rectangular coordinates of the same point referenced to a new set of axes rotated with respect to the first. The operation if fully described by the equations in Figure 3 which will be recognized as those required for coordinate rotation.

The actual operation can best be understood by breaking it into two steps. The X-Y coordinates impressed on the two stators form a flux vector in the resolver. This vector is independent of rotor position. Its angular position is the arctangent of Y/X. Each of the rotor windings develops a voltage proportional to the sine or cosine of its angular position with respect to the flux vector (not with respect to zero). If the reference is made with respect to zero then the outputs follow the equations in Figure 9. The rotor voltages are the X', Y' components of the flux vector. The angle between the X', Y' coordinate reference of the inputs is the same as the rotor angular position.

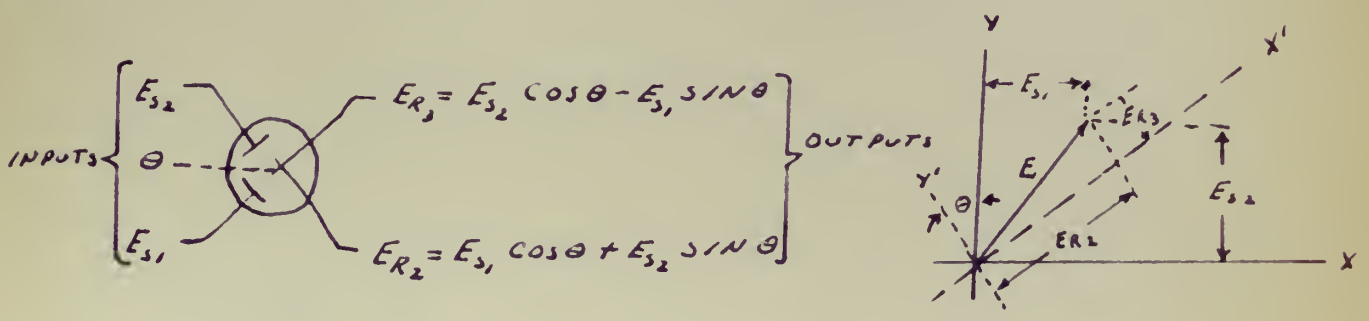

Fig. 9 - Coordinate Rotation

INDUCTION POTENTIOMETER

An induction potentiometer, or linear synchro transmitter, may be considered a special kind of resolver which provides accurate linear indication of shaft rotation about a reference position in the form of a polarized voltage whose magnitude is proportional to angular displacement, and whose phase relationship indicates direction of shaft rotation. The principal difference between a resolver and an induction potentiometer is that the latter's output voltage varies directly as an angle and not as the sine of that angle. Its rotation is usually limited to less than $\pm 90^{\circ}$.

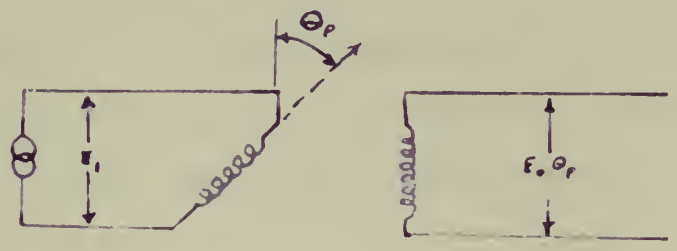

Fig. 1 - Induction Potentiometer Voltage Output

These devices are analogous to resistance potentiometers, but since they are induction type components they have less restraining forces acting upon their rotors, and hence are capable of providing better resolution. Naturally, induction potentiometers do not require sliders such as those used in resistance types. Therefore, circuit interruptions are eliminated, no wear occurs as a result of rubbing parts, and accuracy is consequently continously maintained at the original level throughout the operational life of these types of components. These advantageous features are virtually a necessity in certain applications. For example, in gyroscope systems where low restraining torques and low pick-off angular errors are required, wide use is made of these devices. In general, induction potentiometers find use in applications where resistive potentiometers are impractical, principally because of the following features: (1) induction potentiometers, having no wiping contacts, may be used as gyroscope pick-offs since they contribute less spurious friction torque: (2) input and output are isolated: (3) resolution is infinite: (4) noise level is low: and (5) the total angle of travel is limited to less than 180°

Constructed very much like a resolver, induction potentiometers differ in that their windings and slots are not uniformly distributed, but instead are deliberately modified to produce a linear output. Normally they have only one excitation winding

and one output winding, the former usually carried on the rotor and connected by means of two sliprings and two brushes.

The use of induction potentiometers as linear pick-offs may be considered as a special resolver application in which mutual coupling varies not as $Z_m \sin\theta$, but as $Z_m \theta$. With zero input impedance and infinite output impedance, the voltage gradient,

H, may be defined as $H = \frac{E_o}{E_i \theta}$. Under this condition the transfer function may be expressed as:

$$\frac{E_o}{E_i} = \frac{-H\theta}{1 + \frac{Z_s - H^2 Z_p \theta^2}{Z_L}} + \frac{Z_i}{Z_p}$$

where Z_s = secondary impedance

Z_p = primary impedance

Z_L = load impedance

Z_i = input impedance

thesR73
A transient response analysis of a multi
3 2768 001 00304 9
DUDLEY KNOX LIBRARY